PHYSICS REPORTS (Review Section of Physics Letters) 50, No. 3 (1979) 157–226. NORTH-HOLLAND PUBLISHING COMPANY

DIFFRACTIVE PRODUCTION MECHANISMS

A.B. KAIDALOV

Institute of Theoretical and Experimental Physics, Moscow, USSR

Received 14 July 1978

Contents:

Abstract:

A review of theoretical approaches to the problem of diffractive scattering at high energies is presented. A phenomenological analysis of experimental data on inelastic diffractive processes is carried out and the main properties of diffraction dissociation are discussed.

DIFFRACTIVE PRODUCTION MECHANISMS

A.B. KAIDALOV

Institute of Theoretical and Experimental Physics, Moscow, USSR

NORTH-HOLLAND PUBLISHING COMPANY - AMSTERDAM

0. Introduction

The study of diffractive processes has always been one of the main sources of information on the properties of the strong interactions of hadrons at high energies. The classical example of a diffractive reaction is small angle elastic scattering, which has now been well studied in a wide energy region. In the past few years considerable progress has also been achieved in the field of inelastic diffractive processes.

Clear separation and detailed study of these reactions has become possible due to considerable extension of the energy range, accessible for experiment. Many new interesting experimental results have been obtained. This has stimulated theoretical investigation of the diffractive production of particles. Several different approaches to this problem have been proposed and the results compared with experimental observations.

In this review recent experimental results on inelastic diffractive processes are discussed in terms of the various theoretical approaches to high energy diffractive scattering. The first part of the paper (sections 1 and 2) is devoted to discussion of the theoretical approaches. They can be roughly divided into two categories. The s-channel picture of inelastic diffraction was proposed long ago in the classical papers of Feinberg and Pomeranchuk [1] and of Good and Walker [2]. Diffractive scattering is in this approach the consequence of the absorption of the incident hadronic wave. This is due to the existence at high energies of many open inelastic (nondiffractive) channels. The composite structure of hadrons leads to diffraction dissociation. In this framework the impact parameter representation for diffractive amplitudes provides the basis for the construction of geometrical and optical models. Some bounds on the cross sections of the inelastic diffractive reactions, which follow from s-channel unitarity and the shadow character of diffraction, have been obtained in the past few years [3–6]. These results and their experimental implications are described in section 1. Models for diffraction scattering, based on the quark–gluon picture of hadrons are also discussed in this section.

Another approach to diffractive processes is connected with the t-channel point of view. This is most clearly expressed in terms of Reggeon exchanges. It gives the possibility to consider from a unified point of view both two-body and multiparticle reactions. Applications of Regge theory to inelastic diffractive processes are discussed in detail in section 2. The Drell–Hiida–Deck model is used for the description of dissociation vertices. The predictions of this model for both inclusive and exclusive diffractive reactions are considered. The exchange of several Reggeons in the t-channel, which correspond to Regge-cuts, can be important in diffractive scattering at high energies. The Reggeon calculus method for the evaluation of Regge-cut amplitudes and the eikonal approximation are described in section 2. The problems of Regge-theory in the asymptotic limit $s \to \infty$ and models with the Froissart type asymptotic behaviour of the scattering amplitudes are briefly discussed at the end of this section*. Thus, different theoretical approaches (which, however, need not be in contradition, but rather may complement each other) to diffraction are possible and we can ask what is the proper definition of diffraction? I shall consider the process as diffractive, if it is determined at high energies by the Pomeranchuk singularity at $j = 1$ (which can, in principle, differ from a simple Regge-pole). This definition is sufficiently general and it is valid for both the s-channel and t-channel type models.

It follows from the definition of diffraction, that the main property of the diffractive mechanism, which allows one to separate it from other scattering mechanisms, is a weak energy dependence of the

*A more complete discussion of this subject can be found in reviews [7, 8].

cross sections for these reactions. If $\alpha_P(0) = 1$, then the cross sections of diffractive processes can have only a logarithmic dependence on energy.

It is usually assumed also that the Pomeranchuk singularity has vacuum quantum numbers, positive signature σ, even C-parity and isospin $I = 0$.* The amplitudes of diffractive processes are mainly imaginary at $t = 0$.† This characteristic feature of diffraction follows from the assumption that $\sigma = +1$ and $\alpha_P(0) = 1$.

The second part of the review (section 3) is devoted to experimental information on diffractive processes at high energies. The properties of diffraction, which follow from the analysis of elastic reactions, are briefly discussed. The most complete knowledge of the properties of diffraction dissociation comes from a study of exclusive diffractive reactions. Interesting effects have been observed recently in such processes. The available experimental data on exclusive diffraction dissociation are compared with the predictions of the Deck model with absorption and with factorisation relations. It is pointed out that an approximate factorisation of the cross sections for these processes takes place. Results on the inclusive diffractive production of particles are discussed in the framework of the triple-Regge model. The most important experimental result, which has been obtained from the study of these reactions, is the discovery of the diffractive production of hadronic systems with large masses. This phenomenon is interpreted in terms of the triple-Pomeron interaction. The triple-Regge analysis of the experimental data is carried out and the effective triple-Pomeron coupling constant is determined. This constant plays an important role for the Regge approach to the asymptotic behaviour of strong interactions. The processes of double diffraction dissociation and double Pomeron exchange, which can give new insight into the properties of diffraction, are discussed in section 3‡.

1. Theoretical description of diffractive processes from the s-channel point of view

1.1. Impact parameter representation

Diffractive phenomena at high energies from the s-channel point of view have the shadow character and are due to the strong inelastic interaction of colliding particles (absorption). This approach is based on the unitarity equation in the s-channel

$$S^+S = 1 \tag{1.1}$$

or for the scattering matrix $T(S = I + iT)$

$$\operatorname{Im} T_{ab} = \tfrac{1}{2}\sum_n \int T_{an} \cdot T^*_{bn}\, d\tau_n \tag{1.2}$$

where $d\tau_n = (2\pi)^4\delta(p_a - p_b)\Pi_{i=1}^n d^3p_i/2\omega_i(2\pi)^3$ is the phase space factor.

The well known optical theorem follows directly from the unitarity equation (1.2)

$$\operatorname{Im} T_{aa}(s, 0) = 2p\sqrt{s}\,\sigma^{(tot)}(s) \tag{1.3}$$

where p is the center of mass momentum of the colliding particles, $s = (p_1 + p_2)^2$.

*If the Pomeranchuk singularity is not a pure Regge-pole and moving branch points are also important, then, generally speaking, it does not have definite parity. However the relative contribution of the parity-odd part decreases logarithmically with energy.

†The ratio $\operatorname{Re}T(s, 0)/\operatorname{Im}T(s, 0)$ decreases logarithmically as $s \to \infty$.

‡The field of investigation referred to as diffractive scattering is too vast for us to consider all it's aspects in this review. In particular the diffractive production of particles off nuclei is not discussed here. The reader interested in this subject should refer himself to the review articles [9, 10]. Some questions relevant to diffractive dissociation, which will be only shortly mentioned in this article are discussed in more detail in reviews [10–14].

It is convenient to consider the unitarity equation for each partial-wave amplitudes $f_l(s)$

$$f(s,t)=\frac{T(s,t)}{8\pi\sqrt{s}}=\frac{1}{p}\sum_{l=0}^{\infty}(2l+1)\,f_l(s)\,P_l(\cos\theta_s)$$

$$f_l(s)=\frac{p}{2}\int_{-1}^{1} f(s,z)\,P_l(z)\,\mathrm{d}z; \qquad z=\cos\theta_s. \tag{1.4}$$

Unitarity leads to the following inequalities for the partial-wave amplitudes of elastic scattering

$$\mathrm{Im}f_l(s)\geqslant|f_l(s)|^2, \quad \text{i.e. } |f_l(s)|\leqslant 1. \tag{1.5}$$

The amplitudes $f_l(s)$, which satisfy these inequalities can be written in the form

$$f_l(s)=\frac{1}{2\mathrm{i}}(\mathrm{e}^{2\mathrm{i}\delta_l(s)}-1); \qquad \mathrm{Im}\,\delta_l(s)\geqslant 0. \tag{1.6}$$

At high energies and small scattering angles* large values of l are important, so it is convenient to use an impact parameter $b=(l+\frac{1}{2})/p$-representation

$$T(s,t)=16\,\pi\sum_{l=0}^{\infty}f_l(s)\,P_l(\cos\theta_s)\,2(l+\tfrac{1}{2})$$

$$\simeq 16\,\pi\int_0^{\infty} f_l(s)J_0((l+\tfrac{1}{2})\theta_s)\,\mathrm{d}(l+\tfrac{1}{2})^2=4\pi s\int_0^{\infty} f(b,s)\,J_0(q_\perp b)\,\mathrm{d}b^2. \tag{1.7}$$

Taking into account, that

$$J_0(z)=\frac{1}{2\pi}\int_0^{2\pi}\mathrm{e}^{\mathrm{i}z\cos\varphi}\,\mathrm{d}\varphi$$

we can write the impact parameter representation (1.7) in the following form

$$T(s,t)=8\pi s\int f(s,b)\,\mathrm{e}^{\mathrm{i}\boldsymbol{q}_\perp\boldsymbol{b}}\frac{\mathrm{d}^2b}{2\pi} \tag{1.8}$$

where $\boldsymbol{b}$ is the transverse impact parameter vector, $\mathrm{d}^2b=b\,\mathrm{d}b\,\mathrm{d}\varphi$.

The elastic scattering amplitude, written in the impact parameter space, is given by the expression

$$f(s,b)=\frac{\mathrm{e}^{2\mathrm{i}\delta(s,b)}-1}{2\mathrm{i}}; \qquad \mathrm{Im}\,\delta(s,b)\geqslant 0. \tag{1.9}$$

The function $2\mathrm{i}\delta(s,b)\equiv-\Omega(s,b)$ is the eikonal.

The unitarity equation for the amplitude $f(s,b)$ has a simple form

$$\mathrm{Im}f_{\mathrm{el}}(s,b)=|f_{\mathrm{el}}(s,b)|^2+\sum_n|f_n(s,b)|^2. \tag{1.10}$$

The inelastic overlap function $G_{\mathrm{in}}(s,b)\equiv\Sigma_n|f_n(s,b)|^2$ determines the contribution of inelastic proces-

*In this kinematical region the momentum transfer $q=p_3-p_1$ is perpendicular to the direction of motion of the colliding particles; $q\approx q_\perp$ and $t=(p_3-p_1)^2\approx-q_\perp^2$.

ses to the unitary sum. If we define the partial cross sections $\sigma^{(i)}(b, s)$ by the relation

$$\sigma^{(i)}(s) = \int \sigma^{(i)}(b, s)\, \mathrm{d}^2 b \tag{1.11}$$

then

$$\sigma^{(\mathrm{tot})}(b, s) = 4\mathrm{Im} f_{\mathrm{el}}(b, s); \qquad \sigma^{(\mathrm{el})}(b, s) = 4|f_{\mathrm{el}}(b, s)|^2; \qquad \sigma^{(\mathrm{in})}(b, s) = 4\, G_{\mathrm{in}}(b, s). \tag{1.12}$$

It follows from the unitarity equation (1.10) that

$$\sigma^{(\mathrm{in})}(s, b) = 1 - \mathrm{e}^{\mathrm{Im}\delta(s, b)}. \tag{1.13}$$

The positivity condition for Im $\delta(s, b)$ leads to the inequality $\sigma^{(\mathrm{in})}(s, b) \leqslant 1$ ($G_{\mathrm{in}}(s, b) \leqslant \frac{1}{4}$).

1.2. Geometrical models. Scattering on a black disk and a ring.

The impact parameter representation is often used to provide a geometrical interpretation of high energy scattering. In this section we will consider some models of diffraction, which use such notions of geometrical optics as an opacity and a radius. The simplest model is the scattering on a black disk of radius R. It corresponds to the maximum value for the cross sections for inelastic processes $\sigma^{(\mathrm{in})}(b, s) = 1$ for $b \leqslant R$ (Im $\delta(s, b) \gg 1$, full absorption). The elastic scattering amplitude in b-space (fig. 1.1a) can be written as

$$f(s, b) = \begin{cases} \mathrm{i}/2, & b \leqslant R \\ 0, & b > R \end{cases} \tag{1.14}$$

The scattering amplitude $T(s, t)$ is purely imaginary and is given by the expression

$$T(s, t) = \mathrm{i}4\pi R^2 \frac{J_1(q_\perp R)}{q_\perp R} s; \qquad \sigma^{(\mathrm{el})}(s) = \sigma^{(\mathrm{in})}(s) = \tfrac{1}{2}\sigma^{(\mathrm{tot})}(s) = \pi R^2. \tag{1.15}$$

The differential cross section for elastic scattering shows a sequence of diffractive minima and maxima (fig. 1.2). The width of the diffraction peak is $\sim 1/R^2$. A model with scattering on a black disk with a sharp edge is over simplified and can give only a quantitative idea on the character of elastic diffractive scattering. The realistic amplitude $f(s, b)$ has the form shown in fig. 1.1b with a smooth edge and some "opacity". A natural generalisation of eq. (1.15) for amplitude $T(s, t)$, which takes these effects into account is given by the expression

$$T(s, t) = \mathrm{i}sA(\xi) \frac{J_1(q_\perp R)}{q_\perp R} \exp(-R_1^2 q_\perp^2); \qquad \xi = \ln \frac{s}{s_0}. \tag{1.16}$$

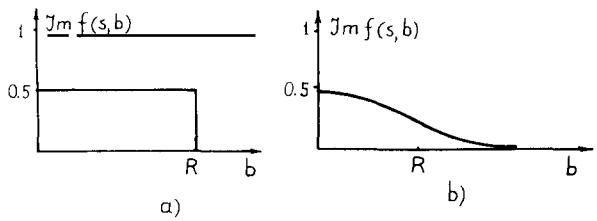

Fig. 1.1. Impact parameter distribution of Im $f(s, b)$, (a) for scattering on a black disk, (b) realistic case.

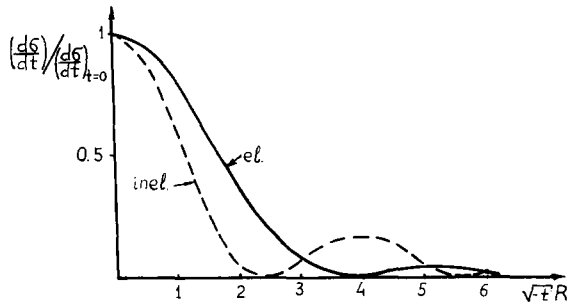

Fig. 1.2. Differential cross sections, as functions of $q_\perp^2$ for elastic scattering on a black disk (full curve) and inelastic diffractive process (dashed curve).

The function $A(\xi)$ depends on the "opacity" of hadrons. The quantity R_1 characterizes the width of the edge. In the limit $R \to 0$, $T(s,t)$ has a gaussian form, which corresponds to $f(b) \sim \exp(-b^2/4R_1^2)$.

If the elastic scattering amplitude is purely imaginary at high energies, then the function $f(s,b)$ can be directly obtained from the experimental data on $d\sigma/dt$. The result of such an analysis [15] of the experimental data on elastic pp-scattering at $\sqrt{s} = 53$ GeV is shown in fig. 1.3. The functions $\sigma^{(tot)}(b)$ and $\sigma^{(el)}(b)$ have approximately gaussian form and differ from the black disk values ($\sigma^{(tot)}(b) = 2$, $\sigma^{(el)}(b) = 1$). On the other hand $\sigma^{(in)}(b)$ for small values of b is rather close to the upper limit ($\sigma^{(in)}(0) = 0.94$) and has a weak energy dependence.

Consider now the geometric picture for inelastic diffractive processes. If the absorption of the incoming wave is strong enough for $b < R$ then inelastic diffraction can arise only from the edge

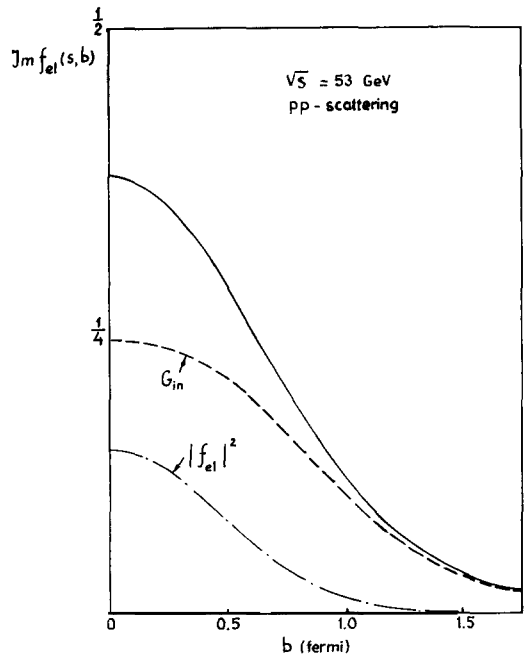

Fig. 1.3. Im $f(s,b)$, $|f(s,b)|^2$ and $G_{in}(s,b)$ for the elastic pp-scattering at $\sqrt{s} = 53$ GeV [15].

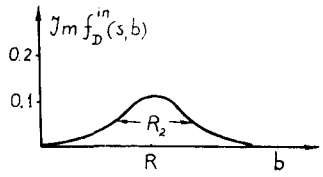

Fig. 1.4. Impact parameter distribution of Im f_D^{in} in the case of strong absorption.

region $b \approx R$ and the amplitude for this reaction as written in b-space has a peripheral form (fig. 1.4). The amplitude $T(s, t)$ can in this case be approximated by the following expression

$$T_D^{(in)}(s, t) = is\, B(\xi)\, J_0(q_\perp R) \exp(-q_\perp^2 R_2^2). \tag{1.17}$$

The value of $R_2 \sim R_1$ is connected with the width of the distribution in b-space (fig. 1.4). In this case the differential cross section for the elastic diffractive processes has the form shown in fig. 1.2 by the dashed line. It shows a first diffraction minimum at a value of $|t|$ which is smaller than for the elastic scattering.

Thus the impact parameter profile in the case of strong absorption (for example for the scattering of hadrons on heavy nuclei) is central for elastic reaction (scattering on a disk) and is peripheral for an inelastic diffractive process (scattering on a ring).

Most of the geometrical and optical models for diffractive scattering at high energies [15–19] are based on these ideas. This approach is simple and physically appealing but it has a serious drawback: the main parameters, which characterise the functions $f(s, b)$ namely the radius of interaction, the opacity and the width of an edge are usually unknown theoretically and are determined from a comparison with experiment. In particular in order to predict the cross section for diffractive processes at high energies it is very important to know the energy depence of the radius. Analyticity and unitarity impose only a rather weak asymptotic bound on the value of the radius $R \leq C \ln(s/s_0)$ [20].

1.3. Bounds on amplitudes for inelastic diffractive processes from s-channel unitarity

The s-channel unitarity equation allows one to derive some bounds on the amplitudes for inelastic diffractive processes. Consider the submatrix of the scattering matrix $f_{mn}(s, b) - iD_{ik}(s, b)$ $(i, k \leq N)$, whose elements describe diffractive transitions. If the amplitudes f_{ik} for diffractive reactions are purely imaginary then D is a real matrix. It's elements can be expressed in terms of the partial cross sections according to eq. (1.12) as follows

$$\sigma^{(tot)}(s, b) = 4D_{11}; \qquad \sigma^{(el)}(s, b) = 4D_{11}^2; \qquad \sigma_D^{(in)}(b, s) = 4\sum_{k=2}^{N} D_{1k}^2;$$

$$\sigma^{(el)}(s, b) + \sigma_D^{(in)}(s, b) = 4\sum_{k=1}^{N} D_{1k}^2 = 4(D^2)_{11}. \tag{1.18}$$

The real and symmetric matrix D can be transformed by an orthogonal matrix Q to the diagonal form F

$$F = Q^T D Q; \qquad F_{ij} = F_i \delta_{ij}$$

$$D = QFQ^T; \qquad Q^T Q = QQ^T = 1. \tag{1.19}$$

The physical diffractive states ψ_i are the linear combinations of the eigenstates φ_k,

$$\psi_i = \sum_k Q_{ik} \varphi_k. \tag{1.20}$$

Only elastic scattering exists for the states φ_k.

Following Good and Walker [2] we can interpret inelastic diffractive scattering in the following way: the initial state ψ_1 is a superposition of the "bare" eigenstates φ_k, which undergo elastic diffractive scattering with amplitudes F_k, which are different, generally speaking, for different φ_k. So after scattering we have another superposition of φ_k and the final state consists not only of the state ψ_1 (elastic scattering), but also of some admixture of other physical states ψ_i $(i = 2, \dots N)$, that corresponds to the inelastic diffractive scattering. From this point of view diffraction dissociation is analogous to the well known phenomenon of $K_L \to K_S$ regeneration, where K^0 and $\bar{K}^0$ are the "bare" eigenstates.

Note that diffraction dissociation arises only because of the difference in values of the eigenamplitudes F_k. If for some values of b full absorption takes place (all $F_k = \frac{1}{2}$), then inelastic diffraction disappears in this b-region. A bound on the cross section for diffractive processes

$$\sigma^{(el)}(b, s) + \sigma_D^{(in)}(b, s) \leq \tfrac{1}{2}\sigma^{(tot)}(b, s) \tag{1.21}$$

based on the assumption, that the eigenamplitudes F_k do not exceed the "black disk limit": $F_k \leq \frac{1}{2}$,* has been derived by Pumplin [3]. It follows directly from eqs. (1.18) and (1.19).

$$\sigma^{(tot)}(b, s) = 4D_{11} = 4\sum_k Q_{1k}^2 F_k; \qquad \sigma^{(el)}(b, s) + \sigma^{(in)}(b, s) = 4(D^2)_{11} = 4\sum_k Q_{1k}^2 F_k^2. \tag{1.22}$$

The Pumplin's bound leads to strong restrictions on the cross sections for inelastic diffractive processes. The upper bound on $\sigma_D^{in}(b)$ for pp collisions at $\sqrt{s} = 53$ GeV have been obtained in ref. [4] fig. 1.5. For the integrated cross section it is about 13 mb. We can see from fig. 1.5 that the bound has a peripheral shape and it is most restrictive at small b.

An elegant interpretation of such relations between $\sigma^{(tot)}(b)$ and $\sigma_D^{(in)}(b)$ has been given in ref. [6]. The quantities Q_{1k}^2 determine the probabilities of finding the eigenstates φ_k in the decomposition of the initial state ψ_1 and we can interpret the total cross section $\sigma^{(tot)}(b)$ as the average value of the eigenamplitudes $4F_k \equiv \sigma_k(b)$ weighted with probabilities $\rho_k = Q_{1k}^2$

$$\sigma^{(tot)}(b, s) = 4\sum_k Q_{1k}^2 F_k = \sum_k \rho_k \sigma_k = \langle \sigma_k \rangle. \tag{1.23}$$

The total inelastic diffractive cross section considered in these terms is obtained as the square of the dispersion of the spectrum of the eigenamplitudes that couple to the corresponding initial state (fig. 1.6)

$$\sigma_D^{(in)}(b, s) = 4\sum_k Q_{1k}^2 F_k^2 - 4\left(\sum_k Q_{1k}^2 F_k\right)^2 = \tfrac{1}{4}[\langle \sigma_k^2 \rangle - \langle \sigma_k \rangle^2] = \tfrac{1}{4}\Sigma^2(b, s). \tag{1.24}$$

If all the eigenamplitudes are equal, so that their spectrum is a δ-peak, then $\Sigma = 0$ and $\sigma_D^{(in)} = 0$. In order to obtain large values of $\sigma_D^{(in)}(b)$ it is necessary to have a large variation of absorption among the different φ_k. The saturation of the Pumplin's bound corresponds to a distribution, which consists of two δ-peaks, one at $\sigma_k = 0$ and another at the maximum value of σ_k (fig. 1.7).

Let us consider in more detail the example of two diffractive channels. In this case the matrix D has the form

$$D = \begin{pmatrix} \sigma^{(1)}(b)/4 & \sqrt{\sigma_{12}(b)}/2 \\ \sqrt{\sigma_{12}(b)}/2 & \sigma^{(2)}(b)/4 \end{pmatrix}$$

*This assumption is satisfied in the multi-channel eikonal models. For unitary models of K-matrix type the inequality $F_k \leq 1/2$ is not in general valid. The exact consequence of unitarity: $F_k \leq 1$ leads to a trivial inequality $\sigma^{(el)}(b, s) + \sigma_D^{(in)}(b, s) \leq \sigma^{(tot)}(b, s)$.

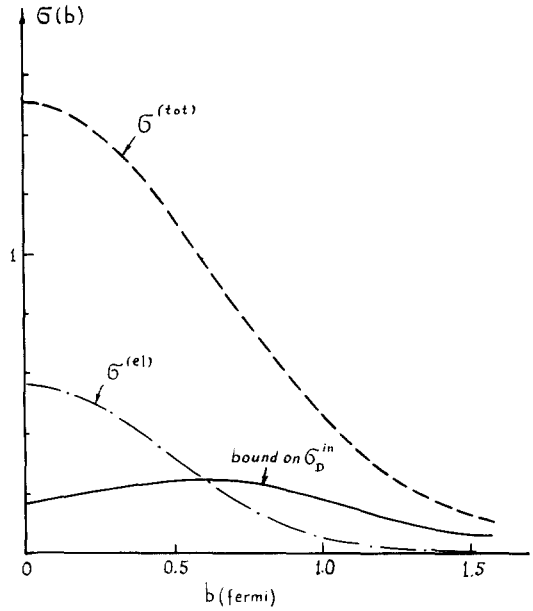

Fig. 1.5. Upper bound from eq. (1.22) for inelastic diffractive cross section versus b for pp-interaction [4].

and the condition $0 \leq F_k \leq \frac{1}{2}$ leads to the inequalities [4]

$$\sigma^{(12)}(b) \leq \sigma^{(1)}(b)\cdot\sigma^{(2)}(b)/4 \qquad \text{(i)}$$

$$\sigma^{(12)}(b) \leq (1-\tfrac{1}{2}\sigma^{(1)}(b))(1-\tfrac{1}{2}\sigma^{(2)}(b)). \qquad \text{(ii)} \tag{1.25}$$

The Pumplin's bound is then saturated if both inequalities (i) and (ii) are simultaneously saturated. This happens, when $\sigma^{(1)}(b)+\sigma^{(2)}(b)=2$ and $F_1=\frac{1}{2}$, $F_2=0$ (maximum dispersion). However in the large b region, where $\sigma^{(k)}(b)$ are small the condition $\sigma^{(1)}(b)+\sigma^{(2)}(b)=2$ cannot be satisfied. The assumption that $\sigma^{(k)}(b)$ is a monotonically decreasing function of b leads to a more stringent bound on $\sigma_D^{(in)}$, [4].

It should be emphasized that while the inequality (1.25i) follows only from the positivity of F_k the inequality (1.25ii) is based on the extra assumption, $F_k \leq \frac{1}{2}$.

Consider now the bounds, which can be derived using only the exact consequence of unitarity and positivity for the eigenamplitudes F_k. If we have only information about the diagonal elements of the matrix $D-\sigma^{(k)}$, then for N diffractive channels this bound is rather weak [5]

$$\sigma_{1D}^{(in)}(b) \leq \tfrac{1}{4}\sigma^{(1)}(b)\sum_{k=2}^{N}\sigma^{(k)}(b). \tag{1.26}$$

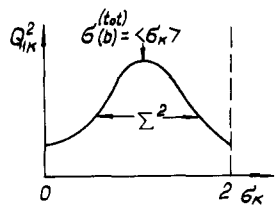

Fig. 1.6. Cross sections and distribution of probabilities Q_{ik}^2 of the eigenamplitudes.

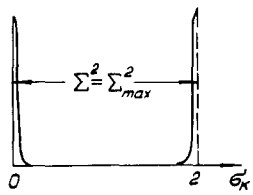

Fig. 1.7. The distribution of Q_{ik}^2, which corresponds to the maximum value of $\sigma_D^{(in)}$.

It is equivalent to a sum of inequalities (1.25i) for the cross sections $\sigma^{(1k)}(b)$ for inelastic diffractive transitions from channel 1 to the channels k.

This bound can be improved if more complete information on the structure of the matrix D is available. The necessary and sufficient condition for the matrix D to have nonnegative eigenvalues ($F_k \geq 0$) is that the determinants of D and it's main submatrices are all nonnegative.

Let us apply this theorem to an interesting class of diffractive processes: the photoproduction of the ρ and ω vector mesons. The three channel (γ, ρ, ω) matrix D has the form

$$4D = \begin{pmatrix} \sigma^{(\gamma)} & 2\sqrt{\sigma^{(\gamma\rho)}} & 2\sqrt{\sigma^{(\gamma\omega)}} \\ 2\sqrt{\sigma^{(\gamma\rho)}} & \sigma^{(\rho)} & 0 \\ 2\sqrt{\sigma^{(\gamma\omega)}} & 0 & \sigma^{(\omega)} \end{pmatrix}.$$

Transitions $\rho \leftrightarrow \omega$ are forbidden by G-parity conservation applied to diffractive processes. The condition that the determinants of D and it's submatrices are nonnegative leads to the following bounds

$$\sigma^{(\gamma\rho)} \leq \sigma^{(\gamma)}\sigma^{(\rho)}/4; \qquad \sigma^{(\gamma\omega)} \leq \sigma^{(\gamma)}\sigma^{(\omega)}/4; \tag{1.27}$$

$$\sigma^{(\gamma\omega)}\sigma^{(\rho)} + \sigma^{(\gamma\rho)}\sigma^{(\omega)} \leq \sigma^{(\gamma)}\sigma^{(\rho)}\sigma^{(\omega)}/4. \tag{1.28}$$

For $\sigma^{(\rho)} = \sigma^{(\omega)}$ the bound of eq. (1.28)

$$(\sigma^{(\gamma\omega)}(b) + \sigma^{(\gamma\rho)}(b) \leq \sigma^{(\gamma)}(b)\sigma^{(\rho)}(b)/4 \tag{1.29}$$

is twice stronger than the sum of bounds (1.27), which is equivalent to eq. (1.26). Taking into account the inequality

$$\left(\int \sqrt{\sigma^{(\gamma)}(b)}\sqrt{\sigma^{(\rho)}(b)}\,\mathrm{d}^2b\right)^2 \leq \int \sigma^{(\gamma)}(b)\,\mathrm{d}^2b \int \sigma^{(\rho)}(b)\,\mathrm{d}^2b$$

and using eq. (1.29) we find a bound on the differential cross sections for the reactions $\gamma p \to \omega p$ and $\gamma p \to \rho^0 p$ at $t = 0$

$$\left[\frac{\mathrm{d}\sigma}{\mathrm{d}t}(\gamma p \to \omega p) + \frac{\mathrm{d}\sigma}{\mathrm{d}t}(\gamma p \to \rho^0 p)\right]\Big|_{t=0} \leq \frac{1}{16\pi}\sigma^{(\mathrm{tot})}_{(\gamma p)}\sigma^{(\mathrm{tot})}_{(\rho^0 p)}. \tag{1.30}$$

Experimental data on photoproduction of vector mesons show that this bound is nearly saturated for $\sigma^{(\mathrm{tot})}_{(\rho^0 p)} = \sigma^{(\mathrm{tot})}_{(\pi^0 p)}$ (fig. 1.8).

Saturation for eq. (1.28) means that one of the eigenvalues of matrix D is equal to zero and that the states ρ, ω and γ are related as follows

$$|\gamma\rangle = \gamma_\rho|\rho\rangle + \gamma_\omega|\omega\rangle. \tag{1.31}$$

The elements of the D-matrix are also connected

$$D_{\gamma\rho} = \gamma_\rho D_{\rho\rho} = \gamma_\rho \frac{\sigma^{(\rho)}}{4}; \qquad D_{\gamma\omega} = \gamma_\omega D_{\omega\omega} = \gamma_\omega \frac{\sigma^{(\omega)}}{4}; \qquad \sigma^{(\gamma)} = \gamma_\rho^2\sigma^{(\rho)} + \gamma_\omega^2\sigma^{(\omega)}. \tag{1.32}$$

The relations (1.32) are the same as these obtained in the vector dominance model.

Inequalities of the type (1.27)–(1.30) can be considered as bounds for the total cross sections of interaction of an unstable particle (ρ, ω) with a proton. This method can also be used in order to derive a bound for the total cross sections for the photoproduction of charm.

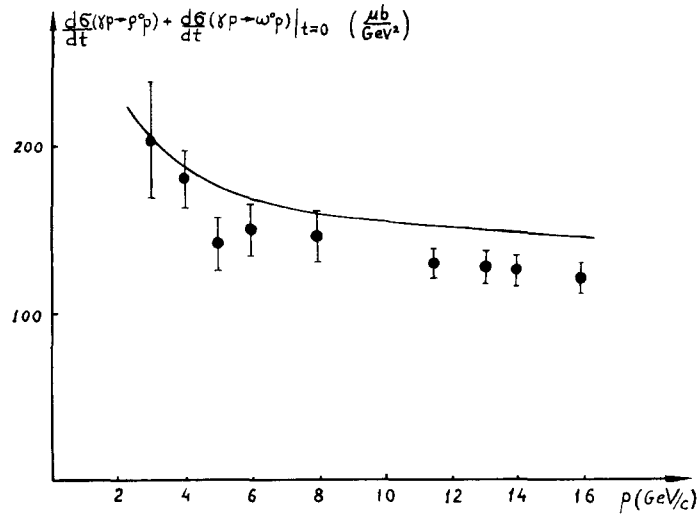

Fig. 1.8. Comparison of the bound (1.30) with experimental data,

Assuming that the imaginary parts of the amplitudes for ψ-meson photoproduction and ψN-elastic scattering are determined by those intermediate states, which includes charmed quarks C and $\bar{C}$, we obtain the following bound

$$\sigma_{\gamma N\to C\bar{C}X} \geqslant \frac{16\pi}{1+\alpha_\psi^2}\frac{d\sigma}{dt}(\gamma N\to \psi N)|_{t=0}/\sigma_{\psi N}^{(tot)} \tag{1.33}$$

where $\alpha_\psi = \mathrm{Re}\, T_{\gamma N\to\psi N}(s,0)/\mathrm{Im}\, T_{\gamma N\to\psi N}(s,0)$.

$\sigma_{\psi N}^{(tot)}$ is the total cross section for ψ-nucleon interaction. Using experimental data on the values of $(d\sigma/dt)(\gamma N\to\psi N)|_{t=0}$ [21] and $\sigma_{\psi N}^{(tot)}$ [22] and assuming, that for $E_L \geqslant 100$ GeV $\alpha_\psi^2 \ll 1$, we find a rather strong bound, $-\sigma_{\gamma N\to C\bar{C}X} \geqslant 250$ nb.

Analogous inequality connects the cross section for photoproduction of strange particles with φ-meson photoproduction (if we assume that the φ-meson consists of strange (λ) quarks). This reads

$$\sigma_{\gamma N\to\lambda\bar{\lambda}X} \geqslant \frac{16\pi}{1+\alpha_\varphi^2}\frac{d\sigma}{dt}(\gamma N\to\varphi N)|_{t=0}/\sigma_{\varphi N}^{(tot)}. \tag{1.34}$$

Experiment shows that the bound (1.34) is approximately saturated.

Analysis of experimental data on inelastic diffraction for purely hadronic processes indicates that also for these reactions some of the F_k's are close to zero. So it is very interesting to understand the dynamical mechanism which leads to a saturation of unitarity bounds.

1.4. Quarks, gluons and diffractive scattering

A simple geometrical picture of diffractive scattering is closely connected with the constituent structure of hadrons. The space-time description of high energy scattering allows one to express the amplitudes in terms of parton distributions inside hadrons. The best candidate for a dynamical description of strong interaction is the theory of quarks and gluons, i.e. quantum chromodynamics. This theory has asymptotic freedom and is most adequate for the description of processes with large

momentum transfer. Application of this theory to hadronic processes with small transverse momenta faces the serious problem of quark and gluon confinement. This problem is not solved yet though some ideas as how to obtain colour confinement have been proposed. So semiphenomenological approaches are usually used for the description of high energy scattering in terms of quarks and gluons. The additive quark model [23, 24] is the most simple and widespread one. In the framework of this model it is assumed that bosons consist of quark q and antiquark $\bar{q}$ and that baryons are bound states of three quarks. These quarks are on the average far from each other ($R \sim 1$ fm), while the radius of interactions for two quarks is comparatively small (at present energies $r_{\text{int}} \sim 0.2$ fm). The amplitudes for hadronic scattering are expressed in terms of the qq($q\bar{q}$) scattering amplitudes and the wave functions of hadrons. The simplest diagram, which corresponds to a single scattering of quarks is shown in fig. 1.9a. The addivity assumption for quark scattering leads to a number of relations between amplitudes for different hadronic processes [23]. One of the most well known relations of this type is [23]

$$\bar{\sigma}(\pi N) = \tfrac{2}{3}\bar{\sigma}(NN) \qquad (\bar{\sigma}(aN) = \tfrac{1}{2}(\sigma_{aN} + \sigma_{\bar{a}N})) \tag{1.35}$$

which is in a reasonable agreement with experiment.

In the framework of this model, which considers a hadron as a loosely bound system of almost free quarks, it is possible to explain the increase of the total cross section for pp-interaction at high energies and to describe the structure of differential cross sections for elastic reactions [24]. In particular the minimum in $d\sigma/dt$ for elastic pp-scattering at high energies is connected with the double scattering of quarks (fig. 1.9b).

An interesting quark–glue model, where gluons inside hadrons play an active role in processes with small momentum transfer has been proposed in refs. [25–27]. We have seen in a previous section that the large value for the cross section for inelastic diffractive processes indicates a strong variation in the opacity of the eigenamplitudes F_k. This behaviour is difficult to understand in the framework of the standard quark model, in which all eigenstates correspond to the same configuration of valence quarks and should have opacities of the same order. In the quark–glue model this property of the eigenamplitudes is connected with the variation of the glue parameters in the incident hadrons (gluons inside hadrons have some distributions in longitudinal momenta and in impact parameters). In this approach diffractive scattering can be considered as the shadow of gluon scattering. The authors of ref. [26] are led to the conclusion that it is necessary to have full absorption for the glue–glue interaction at small impact parameters in order to obtain the correct value of $\sigma_D^{(in)}$. In the framework of this model it is possible to describe the differential cross section for elastic pp-scattering in a wide t-range [27].

The connection between the Pomeron and gluon exchanges in the t-channel has been discussed in papers [28, 29]. It has been argued in the framework of QCD that gluon exchanges lead to a positive signature singularity with $j \approx 1$ at $t = 0$. If the Pomeranchuk singularity is indeed related to the

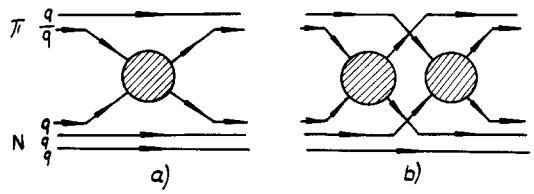

Fig. 1.9. Additive quark model diagram (a) for the amplitude of elastic πN-scattering; (b) double rescattering of quarks.

structure of the gluon interaction, the study of diffractive processes at high energies may then provide important information on the gluon structure of hadrons and on the properties of gluon–gluon interaction [30].

2. t-channel models of diffraction. Regge approach

2.1. Regge-pole model

The complex angular momentum method (Regge theory) [31] has a solid theoretical basis and is widely used in the phenomenological description of hadronic processes at high energies. In the framework of this method scattering amplitudes are expressed in terms of singularities in the complex j-plane of the t-channel partial wave amplitudes $\varphi(j, t)$. The simplest singularity in the j-plane is a moving pole $\alpha(t)$ (Regge pole) [32]. Regge pole exchange in the t-channel (fig. 2.1) is a natural generalization of single particle exchange. It leads to a scattering amplitude of the form

$$\frac{T^{(1)}(s,t)}{8\pi s_0} = \gamma(t)\,\eta(\alpha(t))\left(\frac{s}{s_0}\right)^{\alpha(t)} \tag{2.1}$$

where $\eta(\alpha(t)) = -\{1+\sigma\exp(-i\pi\alpha(t))\}/\sin\pi\alpha(t)$ is the signature factor, $\sigma = \pm 1$ is the signature of the pole, $\gamma(t) = g_{ac}(t)\,g_{bd}(t)$ is the factorized residue, s_0 is a constant scale factor ($s_0 = 1\,\mathrm{GeV}^2$). We will also use the amplitude

$$M(s,t) = T(s,t)/8\pi s; \qquad M^{(1)}(s,t) = \gamma(t)\,\eta(\alpha(t))\,(s/s_0)^{\alpha(t)-1}. \tag{2.2}$$

In the same way as ordinary particles, Regge poles have definite conserved quantum numbers, parity, isospin, strangeness etc.

The connection of Regge poles with particles and resonances for positive t allows one to determine the parameters of Regge trajectories from information on the spectrum of hadrons. The leading meson trajectories ρ, A_2, ω, f have $\alpha_i(0) \approx 0.5$ and $\alpha_i' \approx 1\,\mathrm{GeV}^{-2}$. The π-Regge pole with $\alpha_\pi(0) \approx 0$ is also important for a phenomenological description of binary processes. The Pomeranchuk pole α_P plays a specially important role in Reggeon theory. It has been introduced in the theory in order to provide an approximate constancy of the total cross sections. Scattering amplitudes for an exchange of the Pomeranchuk pole with $\alpha_P(0) = 1$ are purely imaginary at $t = 0$ and total cross sections are energy independent. Thus in the Regge pole model diffractive reactions are described by P-pole exchange in t-channel.

Let us consider now the impact parameter picture of scattering in the Regge pole model and calculate the amplitude $f(s, b)$

$$f(s,b) = \int M(s,t)\,e^{-iq_\perp b}\,\frac{d^2q}{2\pi}. \tag{2.3}$$

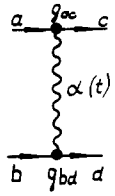

Fig. 2.1. Graph of a Regge-pole exchange in the t-channel.

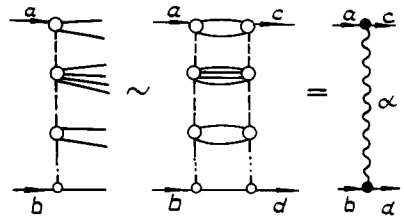

Fig. 2.2. Multiperipheral diagrams and their contribution to a two-body process amplitude.

In the small t-region, the contribution of a Regge pole to the scattering amplitude $M(s,t)$ can be parametrized in the form

$$M^{(1)}(s,t) = \gamma(0)\,\eta(\alpha(0))\,(s/s_0)^{(\alpha(0)-1)}\cdot\exp(\lambda(s)t) \tag{2.4}$$

where $\lambda(s) = R^2 + \alpha'(\ln(s/s_0) - \frac{1}{2}i\pi)$, $\alpha(t) = \alpha(0) + \alpha'\cdot t$. The parameter R^2 characterizes the t-dependence of the product of residue functions and of the factor $1/\sin(\pi\alpha(t)/2)$ ($\sigma = \pm 1$) or $1/\cos(\pi\alpha(t)/2)$ ($\sigma = -1$).

We find from eqs. (2.3), (2.4) that the amplitude $f(s,b)$ has a gaussian form

$$f^{(1)}(s,b) = \frac{\gamma(0)\,\eta(\alpha(0))}{2\lambda(s)}\left(\frac{s}{s_0}\right)^{(\alpha(0)-1)}\exp\left(-\frac{b^2}{4\lambda(s)}\right). \tag{2.5}$$

It follows from eq. (2.5) that, for P-pole exchange (with $\alpha_P(0) = 1$), the amplitude $f(s,b)$ decreases logarithmically at $b^2 \ll \lambda(s)$ and the effective radius of interaction increases asymptotically as $\sqrt{\alpha'\ln(s/s_0)}$. So the Regge pole model gives definite predictions for the energy dependence of the opacity and of the radius.

From the point of view of s-channel unitarity this picture of interaction corresponds to the multiperipheral mechanism of multiparticle production [33]. The imaginary part of the Regge pole amplitude for a two body process is connected with the contribution of the multiperipheral intermediate states in the s-channel unitarity equation, fig. 2.2. Experimental studies of the multiple production of particles have confirmed the main predictions of the multiperipheral approach, i.e. the logarithmic increase with energy of the average multiplicities of particles, the small and practically energy independent values for the mean transverse momenta, the scaling behaviour of inclusive spectra, the flat rapidity distributions in the central region of spectra, important short range correlations (see, for example, the review papers listed under ref. [34]).

Therefore it seems reasonable to assume that at present energies diffractive scattering can be described in a first approximation by the exchange of a simple Pomeranchuk pole with $\alpha_P(0) \approx 1$. Complications due to the possible existence of Regge cuts will be discussed in subsection 2.5.

2.2. *Drell–Hiida–Deck model*

Multiperipheral models can be successfully used not only for the explanation of the general properties of the multiparticle production but also for a detailed description of the exclusive processes. One of the models, widely used for this purpose, because of it's predictive power, is the OPE-model. It takes into account the exchange of the lightest particle in the t-channel namely the π-meson, figs. 2.4, 2.5. The diagrams of the OPE-model include amplitudes for $\pi\pi$ and πN-scattering and the $\pi N\bar{N}$ coupling constant, which can be obtained from the experimental data. The only

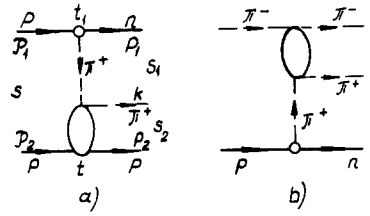

Fig. 2.3. OPE-model diagrams for the reactions $pp \to pn\pi^+$ (a) and $\pi^-p \to \pi^-\pi^+n$ (b).

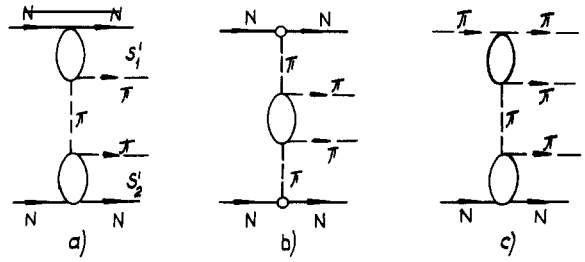

Fig. 2.4. OPE-model diagrams for the reactions $NN \to NN\pi\pi$ (a) and (b), $\pi N \to \pi\pi\pi N$ (c).

arbitrariness of the model is connected with the off-mass shell dependence of the amplitudes. The off-mass shell effects are usually described by phenomenological form-factors [36] and (or) reggeization of π-exchange [37, 38]. The π-exchange model with a small number of free parameters gives a good description of experimental data on both exclusive and inclusive processes in NN, $\bar{N}N$, πN and KN interactions [38, 39].

How does diffraction dissociation emerge in this model? Consider for example the process $pp \to (n\pi^+)p$ (fig. 2.3a). At intermediate energies $s = (\mathcal{P}_1 + \mathcal{P}_2)^2 \lesssim 10\,\text{GeV}^2$ the mass of the system $p\pi^+$ $s_2 = (p_2 + k)^2$ is rather small and resonances are important in the blob associated with π^+p scattering, which is a part of the OPE diagram. As the energy s increases the effective values of s_2 increase also and diffractive scattering becomes important for elastic π^+p-scattering. If we approximate diffractive scattering by P-pole exchange, the diagram of fig. 2.3a can then be represented in the region of large s, s_2 by the diagram of fig. 2.6a. So the OPE-diagrams of fig. 2.3, 2.4 contain both resonance production and diffractive dissociation. Resonance production is important at low and intermediate energies, while diffraction dissociation is the dominant mechanism at high energies. This change of regime is clearly seen in fig. 2.5, where experimental mass distributions for the π^+p-system observed in the

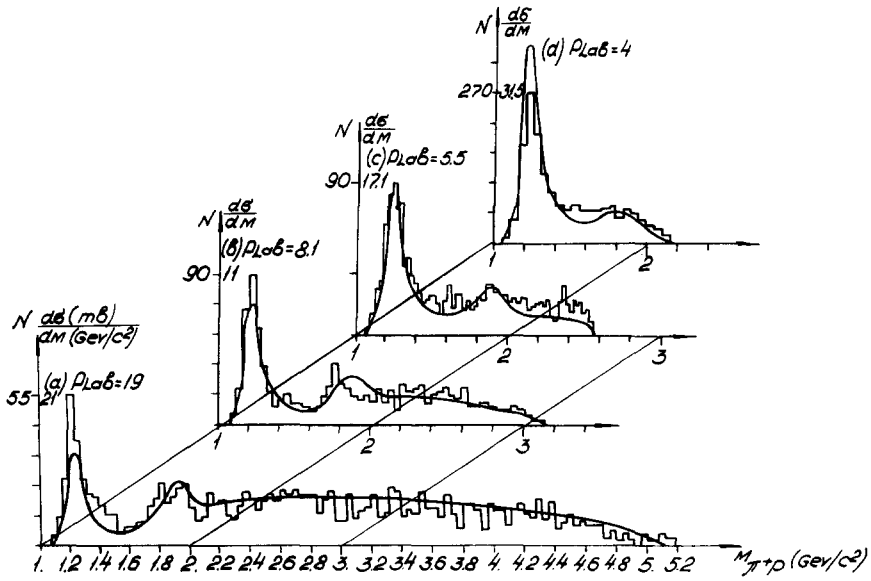

Fig. 2.5. Distribution in mass M_{π^+p} for the reaction $pp \to pn\pi^+$ at different energies. Full curves are the predictions of OPER-model [38].

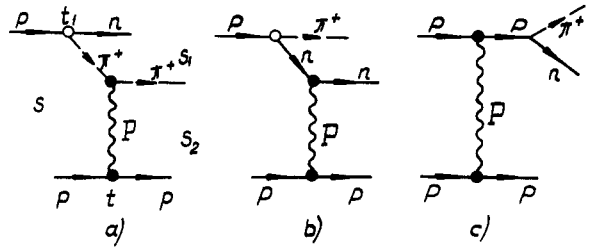

Fig. 2.6. DHD-model graphs for the $n\pi^+$-system diffractive production in pp-collisions.

reaction $pp \to n\pi^+ p$ for different energies are compared with the predictions of the reggeized pion exchange model (OPER) [38]. The model provides a description of exclusive reactions in a wide region of energy. A comparison of the OPER-model predictions (in absolute normalization) [38] with the total cross sections for some exclusive processes is shown in fig. 2.7.

Diffractive excitation of an incident particle can be interpreted in the framework of the OPE-model (fig. 2.5a) in a somewhat different way: the incident nucleon dissociates first into two particles (N, π) and the virtual pion then diffractively scatters on the target-nucleon. From this point of view it is natural also to take into account the other pole graphs (fig. 2.6b, c), which correspond to the elastic diffractive scattering of the produced nucleon (fig. 2.6b) and of the incident nucleon before dissociation (fig. 2.6c). The diagrams of fig. 2.6 describe diffraction dissociation in the Drell–Hiida–Deck model [40]. At high energies and small t the diagrams of fig. 2.6b and fig. 2.6c give contributions to the amplitudes, which have different signs and are close in magnitude. Therefore these diagrams are mutually canceled as $t \to 0$ and the diagram with π-exchange, fig. 2.6a gives the main contribution to the cross section for this process. However the diagrams of fig. 2.6 (b and c) can still be important in certain kinematical regions.

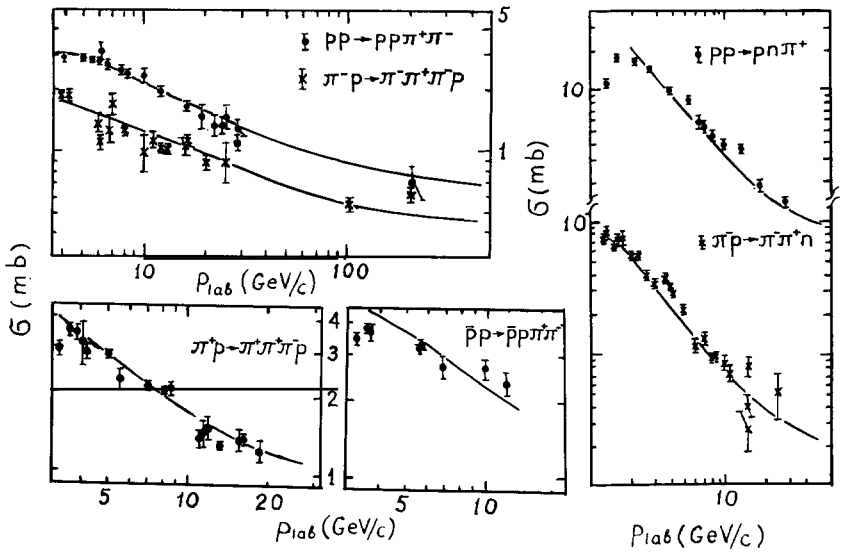

Fig. 2.7. Cross sections for the reactions $pp \to pn\pi^+$, $pp \to \Delta^{++} n$, $\pi^\pm p \to \pi^\pm\pi^+\pi^- p$, $pp \to pp\pi^+\pi^-$, $\bar{p}p \to \bar{p}p\pi^+\pi^-$ as functions of incident laboratory momentum. The curves are the predictions of the OPER-model [38].

The contribution to the amplitude of the diagram of fig. 2.6a has the form

$$T = G\sqrt{2}\,\bar{u}_n\gamma_5 u_p \frac{1}{t-\mu^2}\, T_{\pi^+p}(s_2, t)\, F(t_1) \tag{2.6}$$

where G is the pion–nucleon coupling constant ($G^2/4\pi = 14.6$). $F(t_1)$ is a form-factor, which takes into acount off-mass shell effects. $T_{\pi^+p}(s_2, t)$ is the amplitude for π^+p elastic scattering on mass shell, which, for large values of s_2, is described by Pomeron exchange

$$T_{\pi^+p}(s_2, t) = i\gamma_P(0)\,(s_2/s_0)\exp(\lambda_P(s_2)t).$$

In the double-Regge region s_2, $s_1 \gg m^2$ the following kinematical relation holds*

$$s_1 \cdot s_2 \simeq s(\mu^2 + k_T^2) \tag{2.7}$$

where $\boldsymbol{k}_T$ is the transverse momentum of the produced pion. Therefore at fixed energy s, the amplitude T decreases with s_1 as $1/s_1$. The differential cross section $d^2\sigma/dt\,ds_1$ is concentrated in the region of small masses $s_1 \sim m^2$ and decreases as $1/s_1^3$ for large values of s_1. A rapid decrease of $d^2\sigma/dt\,ds_1$ as s_1 increases also takes place for all the diagrams of fig. 2.6.

Let us now briefly discuss how to reggeize the pion exchange contribution to multiparticle reactions amplitudes. The simplest way to do that [38] is to replace the product of pion propagator and form-factor $F(t)/(t-\mu^2)$ in eq. (2.6) by the function

$$\frac{\pi\alpha'_\pi}{2}\,\eta(\alpha_\pi(t_1))\,F(t_1, s_2, k_T^2)$$

where

$$F(t_1, s_2, k_T^2) = \exp\left[\left(R_\pi^2 + \alpha'_\pi \ln\frac{s(k_T^2+\mu^2)}{s_0 s_2}\right)(t_1-\mu^2)\right]. \tag{2.8}$$

This expression satisfies to the following natural requirements

i) $\frac{\pi\alpha'_\pi}{2}\,\eta(\alpha_\pi(t)_1))\,F(t_1, s_2, k_1^2) \to \frac{1}{t_1-\mu^2}$ as $t_1 \to \mu^2$.

ii) A double Regge behaviour $T \sim (s_1/s_0)^{\alpha_\pi(t_1)}\,(s_2/s_0)^{\alpha_P(t)}$ exists for $s_2 \gg m^2$, $s_1 \gg m^2$.

iii) In the region $s_2 \sim m^2$, $s_1 \gg m^2$ the amplitude has a usual single Regge behaviour $T \sim (s/s_0)^{\alpha_\pi(t_1)}$. (This region of phase space corresponds to the quasi two-body processes induced by the π-Regge pole.)

Equation (2.8) can be considered as an interpolation formula which gives a reasonable description of the amplitude both for large and small values of s_2. The quantity R_1^2 is the only free parameter of the model.

The same procedure has been used [38] for the construction of amplitudes for reactions with more particles in the final state (of the type shown in fig. 2.4).

2.3. *Diffractive production of particles. Triple-Regge approach*

Regge theory is formulated for both exclusive and inclusive diffractive processes. Study of inclusive diffractive production gives important information on the properties of high-energy scattering.

*This relation is approximately valid even for not too large masses of the diffractively produced system.

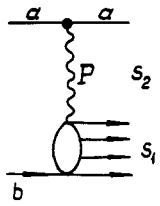

Fig. 2.8. Graph of diffraction dissociation of particle b.

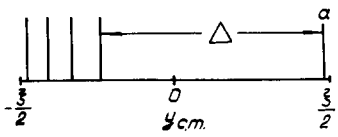

Fig. 2.9. Rapidity distribution for diffractive production of particles.

The inclusive process for single diffractive dissociation to a state with effective mass $M_X = \sqrt{s_1}$, namely $a + b \to a' + X$ is described by the P-pole exchange diagram shown in fig. 2.8. If the value of s_1 is large ($s_1 \gg m^2$) then the invariant s_2, which defines the energy for diffractive scattering is smaller than s. For the multiperipheral configuration of the diffractively produced final state the kinematics is analogous to the case of single pion production, considered above and, according to eq. (2.7), $s_2 \sim s/s_1$. The Regge pole description is valid for $s_2 \gg m^2$ or $s_2/s_1 \gg 1$.

The convenient variables for the inclusive reactions are $x = p^{\parallel}_{a'}/p_a$ and $(p^{\perp}_{a'})^2 \equiv p^2_{\perp}$. At high energies and small t the following relations hold

$$1 - x \simeq \frac{s_1 - m^2 - t}{s}; \qquad t = -\frac{p^2_{\perp}}{x} - (1-x)\left(\frac{m^2_{a'}}{x} - m^2_a\right). \tag{2.9}$$

The Regge approach can be used in the kinematical region $(1-x) \ll 1$, $t \simeq -p^2_{\perp} \lesssim m^2$. The rapidity variable

$$y = \tfrac{1}{2} \ln \frac{E + p^{\parallel}}{E - p^{\parallel}} = \ln \frac{E + p^{\parallel}}{m_{\perp}} \qquad (m_{\perp} = \sqrt{m^2 + p^2_{\perp}})$$

is also widely used for a description of inelastic reactions. The rapidity distribution of particles in diffractive process is shown in fig. 2.9. A large value of s_2 (or $(1-x) \ll 1$) corresponds to a large rapidity gap Δ between the rapidity of the particle a' and that of the other particles. Although the values of s_2 and Δ are not directly connected to the inclusive variable x their mean values (after averaging over the momenta k_i of the produced pions) in the region of large s_2 are related*

$$s_2 - m^2 \approx \overline{\mu^2_{\perp}} \frac{s}{s_1} \approx \overline{\mu^2_{\perp}} \frac{1}{1-x}; \qquad \overline{\mu^2_{\perp}} = \mu^2 + \overline{k^2_{\perp}} \approx (0.1\text{–}0.2)\ \mathrm{GeV}^2;$$

$$\Delta \approx \ln \frac{s_2 - m^2}{m_{a'} \bar{\mu}_{\perp}} \approx \ln \frac{1}{1-x} + C; \qquad C = \ln \frac{\bar{\mu}_{\perp}}{m_{a'}}. \tag{2.10}$$

The amplitude, which corresponds to the diagrams of fig. 2.8, can be written in the same form as done for a binary reaction†

$$\frac{1}{8\pi s_0} T(s, s_1, t, \tau_n) = g^{P}_{aa'}(t) v_n(s_1, t, \tau_n)(s/s_1)^{\alpha_P(t)} \eta(\alpha_P(t)) \tag{2.11}$$

*Equation (2.10) is written for the case $s_1 \gg m^2$.

†Here and in following the normalization used in papers [7, 8, 41] is also used.

where $v_n(s_1, t, \tau_n)$ is the vertex for n-particle production in Pomeron-particle interaction, τ_n are the variables, which characterize the diffractively produced system of particles.

The differential cross section for the inclusive diffractive process has the form

$$\frac{d^2\sigma}{ds_1\,dt} = \frac{x}{s}\frac{d^2\sigma}{dx\,dp_\perp^2} = \frac{\pi}{s}\frac{d^2\sigma}{dy\,d^2p_\perp} = \frac{\pi E}{s}\frac{d^3\sigma}{d^3p}$$
$$= \tfrac{1}{2}(g^{P}_{aa'}(t))^2\left(\frac{s}{s_1}\right)^{2(\alpha_P(t)-1)}\frac{|\eta(\alpha_P(t))|^2}{s_1}\frac{1}{2s_1}\sum_n\int d\tau_n\,|\tilde{T}_{Pb\to n}(s_1, t, \tau_n)|^2 \tag{2.12}$$

where $\tilde{T}_{Pb\to n}(s_1, t, \tau_n) \equiv \sqrt{8}s_0\, v_n(s_1, \tau_n, t)$ is the amplitude for the transition from Pomeron-particle b to n-particles.

The last factor in eq. (2.12) can be interpreted as the total cross section for interaction between the Pomeron and particle b (fig. 2.10).

$$\sigma^{(tot)}_{Pb}(s_1, t) = \frac{1}{2s_1}\sum_n\int d\tau_n\,|\tilde{T}_{Pb\to n}(s_1, t, \tau_n)|^2. \tag{2.13}$$

The differential cross section can then be written as

$$\frac{d^2\sigma}{d\xi_1\,dt} = \tfrac{1}{2}(g^{P}_{aa'}(t))^2\,|G_P(\xi', t)|^2\,\sigma^{(tot)}_{Pb}(\xi_1, t) \tag{2.14}$$

where $\xi_1 = \ln(s_1/m^2)$, $\xi' = \ln(s/s_1)$

$$G_P(\xi', t) = (s/s_1)^{\alpha_P(t)-1}\cdot\eta(\alpha_P(t)) \approx \exp(-\alpha'_P\xi' p_\perp^2)\,\eta(\alpha_P(t)).$$

It should be noted that the Pomeron–particle cross section contrary to the total cross section of interaction for usual particles cannot be directly measured experimentally. The function $\sigma^{(tot)}_{Pb}$ is connected with the physical quantity $d^2\sigma/d\xi_1\,dt$ by eq. (2.14), which determines it's normalization. The definition of $\sigma^{(tot)}_{Pb}$ by eq. (2.13) is convenient because $\sigma^{(tot)}_{Pb}$ has a usual Regge form in the region of large s_1, namely;

$$\sigma^{(tot)}_{Pb}(s_1, t) = 8\pi\sum_k g^{\alpha_k}_{bb}(0)\,r^{\alpha_k}_{PP}(t)\left(\frac{s_1}{s_0}\right)^{\alpha_k(0)-1} \tag{2.15}$$

where $r^{\alpha_k}_{PP}(t)$ is the two Pomeron-reggeon k vertex (in particular $r^{P}_{PP}(t)$ is the triple-Pomeron vertex).

Diffraction dissociation into a state with large mass is thus described by the following triple-Regge formula [42–44]

$$\frac{d\sigma}{d\xi_1\,dt} = 4\pi\sum_k g^{\alpha_k}_{bb}(0)(g^{P}_{aa'}(t))^2 r^{\alpha_k}_{PP}(t)|\eta(\alpha_P(t))|^2\left(\frac{s}{s_1}\right)^{2(\alpha_P(t)-1)}\cdot\left(\frac{s_1}{s_0}\right)^{\alpha_k(0)-1}. \tag{2.16}$$

It corresponds to the diagrams of fig. 2.11.

It should be emphasized that eq. (2.16) is valid only in the region $s_1 \gg m^2$, $s \gg s_1$ or $m^2/s \ll (1-x) \ll$

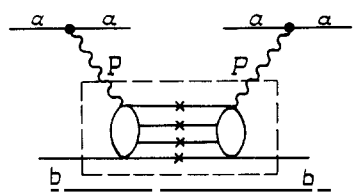

Fig. 2.10. Representation of the differential cross section for the diffractive process and for the Pomeron-particle total cross section (part indicated by a dashed line).

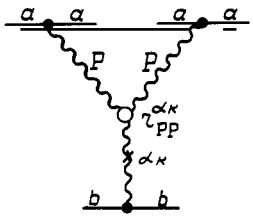

Fig. 2.11. PPα_k for an inclusive cross section. A cross on a line means that the discontinuity of the corresponding Green function should be taken.

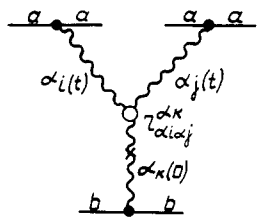

Fig. 2.12. Triple-Regge diagram.

1. This kinematical region of inclusive spectra is usually called the triple-Regge region. It exists at sufficiently high energies $s \geq 10^2\ \mathrm{GeV}^2$.

For a phenomenological description of inclusive spectra in the triple-Regge region it is necessary to take also into account the nondiffractive background, which is connected with the contributions of secondary (f, ω, ρ, A_2, π) poles. Formula (2.16) can be easily generalized to this case and the invariant inclusive cross section $f = E\,d^3\sigma/d^3p$ can be written in the form

$$f = \sum_{ijk} G_{ijk}(t)\,(1-x)^{\alpha_k(0)-\alpha_i(t)-\alpha_j(t)}\cdot(s/s_0)^{\alpha_k(0)-1} \tag{2.17}$$

where $G_{ijk}(t) = 4s_0 g_{aa'}^{\alpha_i}(t)\, g_{aa'}^{\alpha_j}(t)\, g_{bb}^{\alpha_k}(0)\, r_{\alpha_i\alpha_j}^{\alpha_k}(t)\, \eta(\alpha_i(t))\, \eta^*(\alpha_j(t))$. In the limit $s \to \infty$ at fixed x only the terms with $\alpha_k(0) = \alpha_P(0) = 1$ survive in eq. (2.17) and lead to a scaling behaviour of f. It is a remarkable property of eq. (2.17) that the x dependence of cross sections is uniquely determined by trajectories of Regge poles, which are well determined from the analysis of the two-body reactions. The behaviour at $t = 0$ of some triple Regge terms, which are usually used for a description of inclusive spectra, is given in table 1. The summary contribution of the secondary trajectories (f, ω, ρ, A_2) with $\alpha_i(0) = 0.5$ is denoted by R. The triple-Pomeron term is the only scaling term which rapidly increases as $x \to 1$. It corresponds to the diffractive production of large mass states. The triple Pomeron vertex plays an important role in Regge theory at high energies.

The OPE-model, discussed in subsection 2.2, allows one to calculate inclusive processes at high energies [38, 45]. In particular it predicts the values of the triple-Regge vertices $r_{\alpha_i\alpha_j}^{\alpha_k}$. Consider, for example, the inclusive process $pp \to pX$. The production of fast protons in this reaction is described by the diagrams shown in fig. 2.13. All the particles, which are not emitted at the upper blob of the multiperipheral diagram, can be considered together and, after integration over their variables and summation, their role is simply summarized in terms of the total cross section for πN interaction. The diagram 2.13b corresponds to the $\pi\pi P$-term in terms of the triple-Regge model (fig. 2.14b). The value

Table 1
Dependence on s and x of the triple-Regge contributions to the invariant inclusive cross section

Triple-Regge terms	s-dependence (fixed x)	x-dependence (fixed s)
PPP	const.	$1/(1-x)$
PPR	$1/\sqrt{s}$	$1/(\sqrt{(1-x)})^3$
RRP	const.	const.
RRR	$1/\sqrt{s}$	$1/\sqrt{(1-x)}$

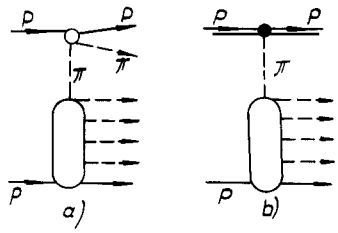

Fig. 2.13. OPE-model diagrams for the inclusive reaction pp→pX.

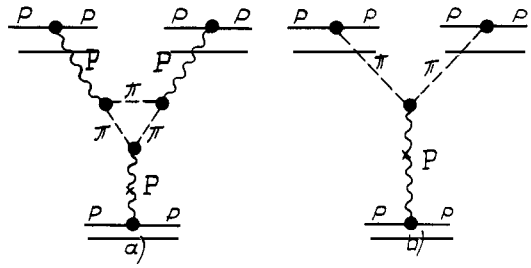

Fig. 2.14. Diagrams of OPE-model for triple Regge terms PPP (a) and $\pi\pi$P (b).

of $s_{\pi p}$ in fig. 2.13, is large as $x \to 1$ ($s_{\pi p} \sim \bar{\mu}_T^2/(1-x) \gg m^2$) and the elastic diffractive πp-scattering amplitude at the upper blob of the diagram 2.13a leads to the triple-Pomeron graph of fig. 2.14a. The value of the triple-Pomeron vertex is uniquely determined by the $\pi\pi$P-residue and the parameters of the form-factor for a virtual pion. These parameters are fixed from the description of the exclusive processes in the OPE-model. This model allows one also to define in a more quantitative way the range in $1-x$, where the triple-Regge description is reasonable. The analysis shows [38], that the triple-Regge region corresponds to $1-x \leqslant 0.05$. In the region $1-x > 0.05$ the spectra of protons are determined mainly by the resonance region of the πp-amplitudes (the Δ-isobar production and subsequent decay is especially important).

Let us calculate now the total cross section for the diffractive production of high mass state ($s_1 \geqslant \bar{s}$, $\xi_1 \geqslant \xi_0 = \ln(\bar{s}/m^2)$). If the vertex $r^P_{PP}(t)$ does not tend to zero as $t \to 0$, we can parametrize $G_{PPP}(t)$ for small values of t in terms of an exponential form, $G_{PPP}(0)\exp(R_P^2 t)$ and, for the contribution of the PPP-term to the cross section, we have [46]

$$\sigma_1 \equiv \sigma^P_{PP} = 4\pi (g^P_{aa'}(0))^2 g^P_{bb}(0)\, r^P_{PP}(0) \int_{-\infty}^{t_{min}} dt \int_{\bar{s}}^{\beta s} \frac{ds_1}{s_1} \exp\left[\left(R_P^2 + 2\alpha'_P \ln\frac{s}{s_1}\right)t\right]$$

$$= \frac{2\pi}{\alpha'_P}(g^P_{aa'}(0))^2\, g^P_{bb}(0)\, r^P_{PP}(0) \ln\frac{R_P^2 + 2\alpha'_P(\xi - \xi_0)}{R_P^2 + 2\alpha'_P \Delta_0} \tag{2.18}$$

where $\beta \ll 1$ determines the boundary of the region where the Regge approach is valid, $\Delta_0 = \ln(1/\beta) \approx 2$–3.

This cross section increases slowly (as $\ln \xi$) as $s \to \infty$. It will be shown in the next subsection that the cross sections for diffractive production of several high mass states rise more rapidly with energy.

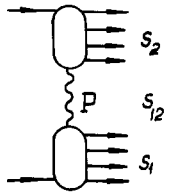

Fig. 2.15. Graph of double diffractive dissociation.

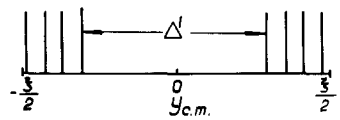

Fig. 2.16. Rapidity distribution for double diffractive dissociation.

2.4. *Production of several showers of particles. Multipomeron exchanges*

We have considered the simplest diffractive process, single diffraction dissociation, where only one of the colliding particles is excited. It is clear that double diffraction dissociation, where both of the initial particles are excited, is possible (fig. 2.15). The rapidity distribution, which corresponds to this reaction is shown in fig. 2.16. It has a large gap Δ' between the two groups of produced particles. Pomeron exchange gives a dominant contribution to the amplitude for this process for large values of $\xi' = \ln(sm^2/s_1 s_2) = \xi - \xi_1 - \xi_2 \approx \Delta' - 2C \qquad (\xi_i = \ln(s_i/m^2))$.

If the Pomeron is a pole and the amplitude has a factorized form, then the differential cross section for double diffraction dissociation is connected with the cross sections for single diffraction excitation and that for elastic scattering by the relation

$$\frac{d\sigma_{DD}(ab \to X_1X_2)}{ds_1\, ds_2\, dt} = \frac{d\sigma_D(ab \to aX_1)}{ds_1\, dt}\,\frac{d\sigma_D(ab \to X_2b)}{ds_2\, dt}\Big/\frac{d\sigma_{el}(ab)}{dt}. \tag{2.19}$$

The differential cross section for the diffractive production of two states with large masses $s_1, s_2 \geqslant \bar{s}$ is described by the diagram of fig. 2.17 and has the form

$$\frac{d\sigma}{d\xi_1\, d\xi_2\, dt} = 4\pi g^P_{aa}(0)\, g^P_{bb}(0)\, (r^P_{PP}(t))^2\, |G_P(\xi', t)|^2. \tag{2.20}$$

The total cross section for this process has the following energy dependence (for $\xi > 2\xi_0 + \Delta_0$)

$$\sigma_2 = \frac{2\pi}{\alpha'_P} g^P_{aa}(0)\, g^P_{bb}(0)(r^P_{PP}(0))^2 \int_{\xi_0}^{\xi-\Delta_0-\xi_0} d\xi_1 \int_{\xi_0}^{\xi-\Delta_0-\xi_1} \frac{d\xi_2}{\xi - \xi_1 - \xi_2}$$

$$= \frac{2\pi}{\alpha'_P} g^P_{aa}(0)\, g^P_{bb}(0)\, (r^P_{PP}(0))^2 \left[(\xi - 2\xi_0)\ln\frac{(\xi - 2\xi_0)}{\Delta_0 e} + \Delta_0\right]. \tag{2.21}$$

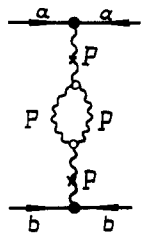

Fig. 2.17. Graph corresponding to diffractive production of two high mass states.

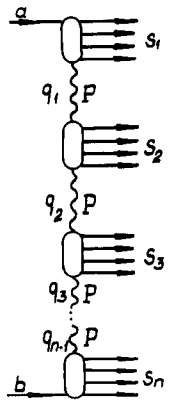

Fig. 2.18. Multipomeron production of particles.

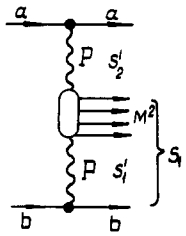

Fig. 2.19. Diagram for the contribution of double-Pomeron exchange to the cross section of the reaction ab→aXb.

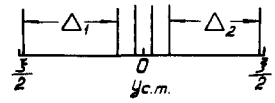

Fig. 2.20. Rapidity distribution in double-Pomeron exchange.

In eq. (2.21) we have neglected the t-dependence of r_{PP}^{P}. Experimental data show that r_{PP}^{P} is practically t-independent (see section 3). The cross section σ_2 increases with energy faster than σ_1, but at present energies, $s \lesssim 3 \times 10^3\ \mathrm{GeV}^2$, it is small $\sigma_2 \lesssim 0.1$ mb.

Let us note that the factorisation condition (2.19) is valid only for differential cross sections at fixed values of s_1, s_2 and t. Cross sections, integrated over phase space, are not factorizable in general, because of differences in t-dependences and in the limits of the ξ_i integrations (compare, for example, eq. (2.18) for σ_1, eq. (2.21) for σ_2 and $\sigma_{el} = 2\pi g_{aa}^{P}(0)\, g_{bb}^{P}(0)/(R^2 + \alpha_P' \xi)$).

Up to now we discussed the processes of diffraction dissociation of incident particles, which correspond to a single Pomeron exchange. In the framework of Regge theory the processes of multipomeron production of particles, fig. 2.18 must also exist [47–49]. These processes correspond to configurations in rapidity space which have several large rapidity gaps between groups of final particles. One such example is the double Pomeron exchange (DPE) process in the reaction ab→a′Xb′, fig. 2.19. The rapidity distribution, which corresponds to this process is shown in fig. 2.20. The existence of a DPE-mechanism for particle production can be easily understood from the point of view of the OPE-model. Consider, for example, the reaction corresponding to two-pion production in NN-collisions, which is described by the diagrams of fig. 2.4. For large masses s_1', s_2' of the πN-systems in the diagram 2.4a (this corresponds to large rapidity intervals) Pomeron exchange describes the amplitudes for πN-elastic scattering and we are led to the DPE-diagram of fig. 2.21. It is analogous to the well known double-photon exchange diagram of QED.

The kinematics for the DPE process fig. 2.16, is similar to that discussed in the case of a single P-exchange, eq. (2.9)

$$(s_2/s) \approx (1 - x_{b'}); \qquad (s_1/s) \approx (1 - x_{a'})$$

$$M_\perp^2 = M_X^2 + p_\perp^2 \approx \frac{s_1 \cdot s_2}{s} = s(1 - x_{a'})(1 - x_{b'}) \tag{2.22}$$

where M_X is the effective mass of the central cluster of particles, $p_\perp$ is it's transverse momentum.

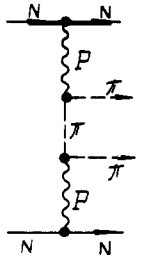

Fig. 2.21. Diagram of the OPE-model for the double-Pomeron contribution to the reaction NN→N$\pi\pi$N.

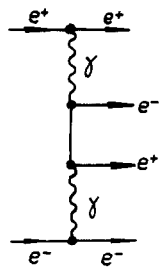

Fig. 2.22. Double photon exchange in the reaction $e^+e^- \to e^+(e^+e^-)e^-$.

There are simple relations analogous to eq. (2.10) between the average values of s_1', s_2', Δ_1', Δ_2' and the variables $1-x_{a'}$, and $1-x_{b'}$. They read:

$$s_1' - m^2 \approx \frac{\overline{\mu_\perp^2}}{1-x_{b'}}; \qquad s_2' - m^2 \approx \frac{\overline{\mu_\perp^2}}{1-x_{a'}}$$

$$\Delta_1 \approx \ln \frac{1}{1-x_{a'}} + C; \qquad \Delta_2 \approx \ln \frac{1}{1-x_{b'}} + C. \tag{2.23}$$

The fact that the rapidity gaps Δ_1, Δ_2 differ by a constant ≈ -1 from $\ln 1/(1-x_{a'(b')})$ should be taken into account when comparing theoretical predictions with experimental results where DPE candidate events are isolated out using cuts in rapidity.

The rapidity interval over which to find the produced particles, is

$$\Delta_\pi \approx \ln \frac{M_\perp^2}{\overline{\mu_\perp^2}} \approx \ln \frac{M_\perp^2}{m^2} - 2C = \xi - \Delta_1 - \Delta_2. \tag{2.24}$$

The region of validity for DPE is determined by the conditions s_1', $s_2' \gg m^2$ or Δ_1, $\Delta_2 \gg 1$. In terms of the variables $x_{a'}$, $x_{b'}$ this means

$$m^2/s \ll 1 - x_i \ll 1 \qquad (i = a', b'). \tag{2.25}$$

Conditions (2.25) can be satisfied only at sufficiently high energies. For example, it follows from eq. (2.22) that if we take $(1-x_i) < 0.1$, then it is possible to study the region $M^2 \sim 1\,\mathrm{GeV}^2$ at $s > 100\,\mathrm{GeV}^2$ only.

The amplitude for the DPE process of fig. 2.16 can be written in the form

$$T(s, s_1, s_2, q_1, q_2, \tau_n) = g^{\mathrm{P}}_{aa'}(q_1^2)\, g^{\mathrm{P}}_{bb'}(q_2^2)\, (s/s_1)^{\alpha_{\mathrm{P}}(q_1^2)} \eta(\alpha_{\mathrm{P}}(q_1^2))$$
$$\times (s/s_2)^{\alpha_{\mathrm{P}}(q_2^2)} \eta(\alpha_{\mathrm{P}}(q_2^2))\, V_n(q_1, q_2, M_{\mathrm{X}}^2, \tau_n) \tag{2.26}$$

where $q_1 \equiv p_{\perp a'}$, $q_2 \equiv p_{\perp b'}$; $q_1^2 \approx -t_1$, $q_2^2 \approx -t_2$, $V_n(q_1, q_2, M_{\mathrm{X}}^2, \tau_n)$ is the vertex for $\mathrm{PP} \to n$-particles transition, τ_n are the variables which characterize the particles in the central cluster.

The differential cross section for the DPE process is given by the formula

$$\frac{\mathrm{d}\sigma}{\mathrm{d}\xi_1'\,\mathrm{d}\xi_2'\,\mathrm{d}^2q_1\,\mathrm{d}^2q_2} = (1-x_{a'})(1-x_{b'})\frac{\mathrm{d}\sigma}{\mathrm{d}x_{a'}\,\mathrm{d}x_{b'}\,\mathrm{d}^2q_1\,\mathrm{d}^2q_2} = \frac{M_\perp^2 E_{a'} E_{b'}}{s}\frac{\mathrm{d}\sigma}{\mathrm{d}^3p_{a'}\,\mathrm{d}^3p_{b'}}$$
$$= \frac{1}{(2\pi)^2}(g^{\mathrm{P}}_{aa'}(q_1^2)\, g^{\mathrm{P}}_{bb'}(q_2^2))^2\, |G_{\mathrm{P}}(\xi_1', q_1^2)\, G_{\mathrm{P}}(\xi_2', q_2^2)|^2\, \sigma^{(\mathrm{tot})}_{\mathrm{PP}}(\xi_{\mathrm{M}}, q_1, q_2) \tag{2.27}$$

where $\xi_1' = \ln(s/s_1) = \ln 1/(1-x_{a'})$; $\xi_2' = \ln(s/s_2) = \ln 1/(1-x_{b'})$; $\xi_{\mathrm{M}} = \xi - \xi_1' - \xi_2'$. The quantity

$$\sigma^{(\mathrm{tot})}_{\mathrm{PP}}(\xi_{\mathrm{M}}, q_1, q_2) = \frac{1}{2M_\perp^2}\sum_n \int \mathrm{d}\tau_n\, |\tilde{T}_{\mathrm{PP}\to n}(\xi_{\mathrm{M}}, q_1, q_2, \tau_n)|^2$$
$$(\tilde{T}_{\mathrm{PP}\to n}(\xi_{\mathrm{M}}, q_1, q_2, \tau_n) = 8 s_0^2 V_n(\xi_{\mathrm{M}}, q_1, q_2, \tau_n)) \tag{2.28}$$

is the "total cross section" for PP-interaction. It should be noted that the dependence of the differential cross section on ξ_1', ξ_2' is connected not only with the usual Regge-factors $G_{\mathrm{P}}(\xi_i', q_i^2)$ but also with the ξ_{M} dependence of $\sigma(\xi_{\mathrm{M}})$, because $\xi_{\mathrm{M}} = \xi - \xi_1' - \xi_2'$. So the DPE behaviour of the cross section should be tested at fixed values of M_{T}^2.

The situation simplifies in the region of large M_{X}^2, where the dependence of σ_{PP} on M_{X}^2 can be

described in the framework of the Regge pole model by a formula

$$\sigma_{PP}^{(tot)}(\xi_M, q_1, q_2) = \frac{(\sigma_{Pb}^{(tot)})^2}{\sigma_{bb}^{(tot)}} = 8\pi \sum_k r_{PP}^{\alpha_k}(t_1)\, r_{PP}^{\alpha_k}(t_2) \exp\left[(\alpha_k(0)-1)\xi_M\right]. \tag{2.29}$$

Inserting this expression for σ_{PP} into eq. (2.27) we obtain

$$\frac{d\sigma}{d\xi_1' d\xi_2' d^2q_1 d^2q_2} = \frac{2}{\pi}\sum_k (g_{aa'}^{P}(t_1)\, g_{bb'}^{P}(t_2))^2 |\eta(\alpha_P(t_1))\eta(\alpha_P(t_2))|^2$$
$$\times r_{PP}^{\alpha_k}(t_1)\, r_{PP}^{\alpha_k}(t_2) \exp[(\alpha_k(0)-1)\xi + (2\alpha_P(t_1) - \alpha_k(0) - 1)\xi_1' + (2\alpha_P(t_2) - \alpha_k(0) - 1)\xi_2']. \tag{2.30}$$

This cross section corresponds to the "beetle diagram", shown in fig. 2.23a.

For arbitrary reggeon exchanges i, j (fig. 2.23b) eq. (2.30) can be generalized as follows

$$\frac{d\sigma}{d\xi_1' d\xi_2' d^2q_1 d^2q_2} = \sum_{ijklm} F_{ijklm}(t_1, t_2)$$
$$\times \exp[(\alpha_k(0)-1)\xi + (\alpha_i(t_1) + \alpha_j(t_1) - \alpha_k(0) - 1)\xi_1' + (\alpha_l(t_2) + \alpha_m(t_2) - \alpha_k(0) - 1)\xi_2']$$
$$= \sum_{ijklm} F_{ijklm}(t_1, t_2) \exp[(\alpha_k(0)-1)\xi_M + (\alpha_i(t_1) + \alpha_j(t_1) - 2)\xi_1' + (\alpha_l(t_2) + \alpha_m(t_2) - 2)\xi_2'] \tag{2.31}$$

where

$$F_{ijklm}(t_1, t_2) = \frac{2}{\pi}\, g_{aa'}^{\alpha_i}(t_1) g_{aa'}^{\alpha_j}(t_1) g_{bb'}^{\alpha_l}(t_2) g_{bb'}^{\alpha_m}(t_2) r_{\alpha_j\alpha_j}^{\alpha_k}(t_1) r_{\alpha_l\alpha_m}^{\alpha_k}(t_2) \eta(\alpha_i(t_1))\, \eta^*(\alpha_j(t_1))\, \eta(\alpha_l(t_2))\, \eta^*(\alpha_m(t_2)).$$

For large enough M^2 ($\xi_M \gg 1$) only P-pole can be kept in the sum over k and the differential cross section has the form

$$\frac{d\sigma}{d\xi_1' d\xi_2' d^2q_1 d^2q_2} = \sum_{ijlm} F_{ijPlm}(t_1, t_2) \exp[(\alpha_i(t_1) + \alpha_j(t_1) - 2)\xi_1' + (\alpha_l(t_2) + \alpha_m(t_2) - 2)\xi_2']. \tag{2.32}$$

Comparing this expression with eq. (2.17) for the single particle inclusive spectrum (for $k = P$)

$$\frac{d\sigma}{d\xi' d^2q_1} = \sum_{ij} 4 g_{aa'}^{\alpha_i}(t_1)\, g_{aa'}^{\alpha_j}(t_1)\, g_{bb}^{P}(0)\, r_{\alpha_i\alpha_j}^{P}(t_1)\, \eta(\alpha_i(t_1))\, \eta^*(\alpha_j(t_1)) \exp[(\alpha_i(t_1) + \alpha_j(t_1) - 2)\xi'] \tag{2.33}$$

we see that the following factorization relation exists

$$\frac{d\sigma}{d\xi_1' d\xi_2' d^2q_1 d^2q_2} = \frac{1}{\sigma_{ab}^{(tot)}} \frac{d\sigma}{d\xi_1' d^2q_1} \frac{d\sigma}{d\xi_2' d^2q_2}. \tag{2.34}$$

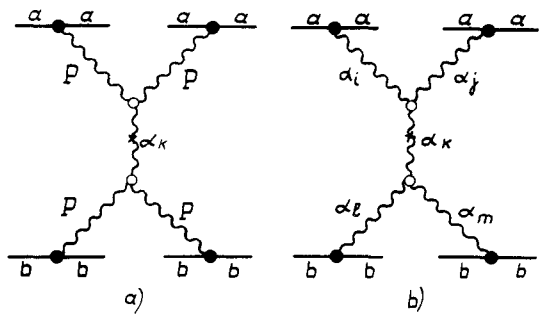

Fig. 2.23. Graph for the cross section of double-Pomeron production of high mass state.

Thus the double-Pomeron production of a state with large mass is given by the formula

$$\frac{d\sigma}{d\xi_1' d\xi_2' d^2q_1 d^2q_2} = \frac{2}{\pi}(g^P_{aa'}(t_1)\, g^P_{bb'}(t_2))^2 |\eta(\alpha_P(t_1))\, \eta(\alpha_P(t_2))|^2$$
$$\times r^P_{PP}(t_1)\, r^P_{PP}(t_2) \exp[2(\alpha_P(t_1)-1)\xi_1' + 2(\alpha_P(t_2)-1)\xi_2']. \tag{2.35}$$

The contribution of the large mass region ($\xi_M \geq \xi_0$) to the total cross section of DPE has the form

$$\sigma_{12} = 2\pi(g^P_{aa'}(0)\, g^P_{bb'}(0)\, r^P_{PP}(0))^2 \int_{\Delta_0}^{\xi-\Delta_0-\xi_0} d\xi_1' \int_{\Delta_0}^{\xi-\Delta_0-\xi_1'} d\xi_2' \frac{1}{(R_a^2+2\alpha_P'\xi_1')(R_b^2+2\alpha_P'\xi_2')}$$
$$= \frac{\pi}{\alpha_P'}(g^P_{aa'}(0)\, g^P_{bb'}(0)\, r^P_{PP}(0))^2 \int_{\Delta_0}^{\xi-\Delta_0-\xi_0} \frac{d\xi_1'}{R_a^2+2\alpha_P'\xi_1'} \ln\frac{R_b^2+2\alpha_P'(\xi-\xi_1'-\xi_0)}{R_b^2+2\alpha_P'\Delta_0}. \tag{2.36}$$

For present energies $s \leq 3\times 10^3\ \mathrm{GeV}^2$ we have $2\alpha_P'(\xi-\xi_{min}) < R^2_{a(b)}$, where $\xi_{min} = 2\Delta_0 + \xi_0$ is a threshold for the process. In this energy region σ_{12} can be approximately written in the form

$$\sigma_{12} \approx \frac{2\pi(g^P_{aa'}(0)\ g^P_{bb'}(0)\, r^P_{PP}(0))^2}{(R_a^2+2\alpha_P'\Delta_0)\,(R_b^2+2\alpha_P'\Delta_0)}(\xi-\xi_{min})^2. \tag{2.37}$$

In the practically inaccessible limit of ultra-high energies, where $2\alpha_P'(\xi-\xi_{min}) \gg R^2_{a(b)}$ we obtain

$$\sigma_{12} = \frac{\pi}{(2\alpha_P')^2}(g^P_{aa'}(0)\, g^P_{bb'}(0)\, r^P_{PP}(0)\ln\xi)^2. \tag{2.38}$$

In the small mass region for the produced system $M_X^2 \leq 1\ \mathrm{GeV}^2$, eqs. (2.29), (2.31), based on the triple-Regge model are not valid. For small values of M the central cluster decays however mainly into two pions, i.e. the exclusive processes $ab \to a'\pi\pi b'$ give the main contribution to the inclusive cross section. The OPE-model is then usually used in order to describe the DPE in these reactions [41, 53–56]. In the framework of this model the reaction amplitude is described by the diagrams shown in fig. 2.21. The differential cross section has the especially simple form for $q_1 \approx q_2 \approx 0$

$$\frac{d\sigma}{d\xi_1' d\xi_2' d^2q_1 d^2q_2} = \frac{3(g^P_{aa'}(0)\, g^P_{bb'}(0))}{\pi^3(M_X^2)^2}(g^P_{\pi\pi}(0))^4 \int_0^{\kappa_{max}} F_\pi(\kappa^2)(\mu^2+\kappa^2)^2\, d\kappa^2 \tag{2.39}$$

where $F_\pi(\kappa^2)$ is the form-factor (see eq. (2.6)), κ is the transverse momentum of the produced pion. The factor 3 in eq. (2.39) is due to the three possible types of π meson exchanges (π^+, π^-, π^0). The interference between the different π-exchange graphs has been neglected in eq. (2.39). More accurate calculations of the DPE cross sections in the OPE-model, which take into account the interference of the diagrams, absorption effects and final state interactions among the produced pions, have been performed in refs.[55, 56].

It follows from eq. (2.39) that the differential cross section of the exclusive reaction rapidly decreases with M_X for large M_X^2. It has a maximum in the region $M_X \approx 400$–500 MeV. Besides this "kinematical" maximum the DPE cross section may have the maxima, which correspond to the DPE production of resonances, with the isospin $I = 0$ and positive G-parity, such as f, f′ etc. Investigation of the DPE-production of resonances can give an important information on the internal characteristics of the Pomeron, such as it's SU(3)-structure.

We have discussed the production of particles for the two-Pomeron exchange interactions.

Iteration of this process in the t-channel leads to the multipomeron production of particles, shown in fig. 2.18. The multipomeron production of small mass states has been studied first in refs. [47, 48]. In the limit $\xi \to \infty$ the cross sections for these reactions behave as $\sigma_k \sim (\ln \xi)^{k-1}/\xi$ (where k is the number of exchanged Pomerons) and their sum grows with energy [48, 49]. The multipomeron production of showers with large masses leads to a more rapid increase of cross sections. According to the rules formulated above, the amplitude for the multipomeron production of N clusters, shown in fig. 2.18 can be written in the form

$$T(\xi, \xi_i, \xi'_i, \boldsymbol{q}_i) = v^{\mathrm{a}}_{n_1}(\xi_1, q_1^2, \tau_{n_1})\; V_{n_2}(\xi_2, \boldsymbol{q}_1, \boldsymbol{q}_2, \tau_{n_2}) \ldots V_{n_{N-1}}(\xi_{N-1}, \boldsymbol{q}_{N-2}, \boldsymbol{q}_{N-1}, \tau_{N-1})$$
$$\times v^{\mathrm{b}}_{n_N}(\xi_N, q^2_{N-1}, \tau_{n_N}) \exp(\alpha_{\mathrm{P}}(t_1)\xi'_1 + \ldots + \alpha_{\mathrm{P}}(t_{N-1})\xi'_{N-1})(8\pi s_0)^{N-1}\eta_{\mathrm{P}}(t_1) \ldots \eta_{\mathrm{P}}(t_{N-1}) \tag{2.40}$$

where $\xi_i = \ln(s_i/m^2)$ (for $s_1 \gg m^2$ ξ_i is the rapidity interval occupied by the particles of ith cluster), $\xi'_i \gg 1$ are the rapidity gaps between the clusters i and $i+1$ ($\xi = \Sigma_{i=1}^{N}\xi_i + \Sigma_{i=1}^{N-1}\xi'_1$), $\boldsymbol{q}_i^2 = -t_i$ is the square of the transverse momenta in the i-th part of the multipomeron chain. The vertices $v_n^{\mathrm{a(b)}}$ and V_n are determined by eqs. (2.11), (2.26).

The differential cross section for an n-clusters production can be expressed in terms of the total cross sections for Pomeron–particle and Pomeron–Pomeron interactions

$$\frac{\mathrm{d}\sigma}{\mathrm{d}\xi_1 \ldots \mathrm{d}\xi_N\, \mathrm{d}\xi'_1 \ldots \mathrm{d}\xi'_{N-1}\, \mathrm{d}^2q_1 \ldots \mathrm{d}^2q_{N-1}} = \frac{1}{(4\pi)^{2(N-1)}}\sigma_{\mathrm{aP}}(\xi_1, q_1^2)\, \sigma_{\mathrm{bP}}(\xi_N, q^2_{N-1}) \tag{2.41}$$
$$\times \sigma_{\mathrm{PP}}(\xi_2, \boldsymbol{q}_1, \boldsymbol{q}_2) \ldots \sigma_{\mathrm{PP}}(\xi_{N-1}, \boldsymbol{q}_{N-2}, \boldsymbol{q}_{N-1})\, |G_{\mathrm{P}}(t_1, \xi'_1) \ldots G_{\mathrm{P}}(t_{N-1}, \xi'_{N-1})|^2 \delta\Big(\xi - \sum_{i=1}^{N}\xi_i - \sum_{i=1}^{N-1}\xi'_i\Big).$$

Using the Regge-asymptotic forms (2.15), (2.29) for these total cross section in the regions $\xi_i \gg 1$ we obtain the following form for the differential cross section of N large mass showers production

$$\frac{\mathrm{d}\sigma}{\mathrm{d}\xi_1 \ldots \mathrm{d}\xi_N\, \mathrm{d}\xi'_1 \ldots \mathrm{d}\xi'_{N-1}\, \mathrm{d}^2q_1 \ldots \mathrm{d}^2q_{N-1}} = 8\pi g^{\mathrm{P}}_{\mathrm{aa}}(0)\, g^{\mathrm{P}}_{\mathrm{bb}}(0)$$
$$\times \left(\frac{r^{\mathrm{P}}_{\mathrm{PP}}(0)}{2\pi}\right)^{N-1} |G_{\mathrm{P}}(t_1, \xi'_1) \ldots G_{\mathrm{P}}(t_{N-1}, \xi'_{N-1})|^2\, \sigma\Big(\xi - \sum_{i=1}^{N}\xi_i - \sum_{i=1}^{N-1}\xi'_i\Big). \tag{2.42}$$

For the diffractive production of two heavy clusters eq. (2.42) coincides with (2.20).

The total cross sections for the diffractive production of N-heavy clusters ($\xi_i \geq \xi_0, \xi'_i \geq \Delta_0$) in the limit of ultrahigh energies $\xi \gg N\xi_0 + (N-1)\Delta_0$ have the following energy dependence*

$$\sigma_N = 8\pi g^{\mathrm{P}}_{\mathrm{aa}}(0)\, g^{\mathrm{P}}_{\mathrm{bb}}(0) \left(\frac{r^{\mathrm{P}}_{\mathrm{PP}}(0)}{4\alpha'_{\mathrm{P}}}\right)^{N-1} \frac{(\xi \ln \xi)^{N-1}}{(N-1)!}. \tag{2.43}$$

In the framework of the Regge pole model this rapid increase of the multipomeron cross sections as $\xi \to \infty$ leads to an inconsistency, since it contradicts to the assumption that the total cross section is asymptotically constant (for $\alpha_{\mathrm{P}}(0) = 1$). Note that the energy dependence of σ_N (2.43) leads even to a violation of the Froissart bound ($\sigma^{(\mathrm{tot})} \leq \xi^2$), which is a consequence of analyticity and unitarity. So it should be changed (at least in the limit $\xi \to \infty$) in any realistic theory. The simplest way out of this difficulty is to assume, that $r^{\mathrm{P}}_{\mathrm{PP}}(q^2) \to 0$ as $q^2 \to 0$ (for example $r^{\mathrm{P}}_{\mathrm{PP}}(q^2) = Aq^2$ as $q^2 \to 0$). In this case (the so-called weak coupling theory) the diffractive production of large mass states leads only to the renormalization of the "bare" Pomeron pole and the theory can be consistent with the asymptotically

*These cross sections are very small at energies $s \leq 10^3$ GeV^2 due to strong kinematical limitations and the smallness of triple Pomeron vertex (see section 3).

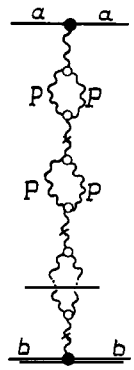

Fig. 2.24. Graph for the cross section of diffractive production of high mass states.

constant total cross section [57, 58]. More detailed analysis of the weak coupling theory [58, 59] shows that in order to satisfy s-channel unitarity and the t-channel constraints, all the inelastic Pomeron vertices should be zero at very small transverse momenta. The differential cross sections for inelastic diffractive processes should vanish at $q_\perp \to 0$. This theory has been interpreted in terms of the parton model [58] and it has been shown that in this approach all the total cross sections $\sigma^{(\mathrm{tot})}$ should be equal in the asymptotic limit $s \to \infty$. Experimental data on diffractive processes do not confirm the predictions of this approach at present energies and it can be consistent with experiment only if large corrections due to Regge cuts are taken into account [60].

The versions of Regge theory, where $r^{\mathrm{P}}_{\mathrm{PP}}$ and other Pomeron vertices are different from zero at $q_\perp = 0$ are in a better agreement with experiment. The role of Regge cuts is very important for such theories in order to obtain the self-consistent asymptotic solutions.

2.5. *Regge cuts and eikonal models*

Regge poles are not the only singularities in the j-plane. There are moving branch points, which are connected with the exchange of several Reggeons in the t-channel (fig. 2.25). A Regge pole can be interpreted as corresponding to single scattering while Regge cuts correspond to multiple scatterings on constituents of hadrons. The positions of the branch points, which is connected with the exchange in the t-channel of n Pomeranchuk poles $\alpha_{\mathrm{P}}(t)$ is given by the formula

$$\alpha_{n\mathrm{P}}(t) = n\alpha_{\mathrm{P}}(t/n^2) - n + 1. \tag{2.44}$$

The location of these branch points at $t = 0$ is the same as that of the pole (for $\alpha_{\mathrm{P}}(0) = 1$), and they are to the right of the pole for $t < 0$. So the contributions of the branch points to scattering amplitudes are important at very high energies.

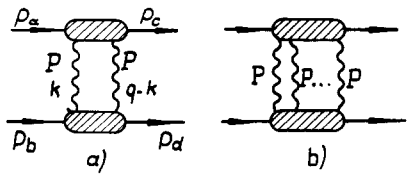

Fig. 2.25. Graphs corresponding to Regge-cuts.

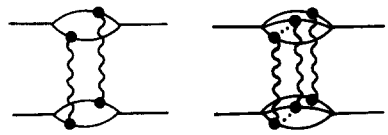

Fig. 2.26. Regge-cut amplitudes and rescattering on constituents of hadrons.

A general method for the evaluation of Regge cut contributions has been proposed by Gribov [63]. Though a certain class of Feynman diagrams has been used for the derivation of the Reggeon calculus method [63] the rules of the Reggeon calculus are neither sensitive to the details of the underlying field theory nor to the details of the hadronic internal structure.

Let us illustrate this method using as an example the two Reggeon exchange amplitude, shown in fig. 2.25a.*

The set of all the Feynman graphs, which corresponds to the two-Reggeon exchange diagram of fig. 2.25a, can be written using the usual Feynman rules in the form

$$T^{(2)}(s,t)=\frac{(-\mathrm{i})}{2!(2\pi)^4}\int \mathrm{d}^4k\,\eta_{\mathrm{P}}(k^2)\,\eta_{\mathrm{P}}((q-k)^2)\left(\frac{s}{s_0}\right)^{\alpha_{\mathrm{P}}(k^2)+\alpha_{\mathrm{P}}((q-k)^2)}\cdot(8\pi s_0)^2\cdot T_{\mathrm{a}}^{(2)}\cdot T_{\mathrm{b}}^{(2)} \tag{2.45}$$

where $T_{\mathrm{a(b)}}^{(2)}$ is the Pomeron-particle scattering amplitude†. The "Green-function" of the Pomeron-$(s/s_0)^{\alpha_{\mathrm{P}}(k_i^2)}\eta(\alpha_{\mathrm{P}}(k_i^2))\,8\pi s_0$ is associated with each Pomeron line of momentum $k_i (k_2 = q - k_1,\ q = p_{\mathrm{c}} - p_{\mathrm{a}})$. The factor 2! in eq. (2.45) appears because of the identity of the two exchanged Pomerons.

It is useful to change from the integration variables k_0, k_z to the variables s_{a}, s_{b}, which are the energies of the P-particle scattering amplitudes at the upper and lower blobs of the diagram 2.25a

$$s_{\mathrm{a}}=(p_{\mathrm{a}}+k)^2=m_{\mathrm{a}}^2+k^2+\sqrt{s}(k_0-k_z),\qquad s_{\mathrm{b}}=(p_{\mathrm{b}}-k)^2=m_{\mathrm{b}}^2+k^2-\sqrt{s}(k_0+k_z). \tag{2.46}$$

Eq. (2.45) can be written as follows

$$T^{(2)}(s,t)\frac{(-\mathrm{i})(8\pi s_0)^2}{2!2s(2\pi)^4}\int \mathrm{d}^2k_\perp\,\mathrm{d}s_{\mathrm{a}}\mathrm{d}s_{\mathrm{b}}\,\eta_{\mathrm{P}}(k^2)\,\eta_{\mathrm{P}}((q-k)^2)\left(\frac{s}{s_0}\right)^{\alpha_{\mathrm{P}}(k^2)+\alpha_{\mathrm{P}}((q-k)^2)}\cdot T_{\mathrm{a}}^{(2)}\cdot T_{\mathrm{b}}^{(2)}. \tag{2.47}$$

The integration contour C over the variables s_i in eq. (2.47) is shown in fig. 2.27. The amplitudes $T_{\mathrm{a(b)}}^{(2)}$ have the usual singularities in the s_i-plane, poles and branch points on a real axis, connected with the real intermediate states in the corresponding channel.

If the functions $T_{\mathrm{a(b)}}^{(2)}$ decrease sufficiently fast at large s_i, then the integration contour C can be deformed into a contour C′ (fig. 2.27), which enclose the right-hand singularities of $T_{\mathrm{a(b)}}^{(2)}$. In this case we obtain the following expression for the two Reggeon exchange amplitude

$$\frac{T^{(2)}(s,t)}{8\pi s}=M^{(2)}(s,t)=\frac{\mathrm{i}}{2!}\int\frac{\mathrm{d}^2k_\perp}{\pi}\,\eta_{\mathrm{P}}(k_\perp^2)\,\eta_{\mathrm{P}}((k_\perp-q)^2)\left(\frac{s}{s_0}\right)^{\alpha_{\mathrm{P}}(k_\perp^2)+\alpha_{\mathrm{P}}((q-k_\perp)^2)-2} N_{\mathrm{a}}^{(2)}(k_\perp,q)\,N_{\mathrm{b}}^{(2)}(k_\perp,q) \tag{2.48}$$

*A detailed discussion of the Reggeon calculus can be found in reviews [7, 8].

†These amplitudes are connected with the functions $F_{\mathrm{a(b)}}^{(2)}$ introduced in ref. [7] by the relation $T_{\mathrm{a(b)}}^{(2)}=F_{\mathrm{a(b)}}^{(2)}/s_{\mathrm{a(b)}}$.

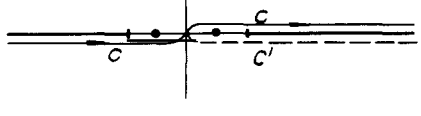

Fig. 2.27. Contour of integration in eq. (2.47).

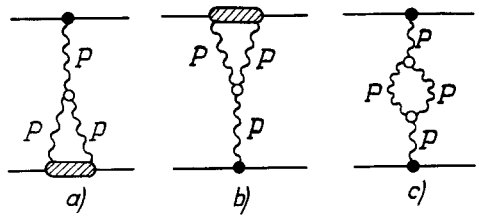

Fig. 2.28. Some "enhanced" graphs for the two-Pomeron exchange amplitude.

where

$$N^{(2)}_{a(b)} = \frac{1}{2\pi i}\int_{C'} ds_{a(b)}\, T^{(2)}_{a(b)}. \tag{2.49}$$

At large values of s_i the amplitudes $T^{(2)}_{a(b)}$ are proportional to $(s_i/s_0)^{\alpha_k(q^2)-\alpha_P(k^2)-\alpha_P((q-k)^2)}$ where $\alpha_k(q^2)$ is the position of the rightmost singularity of the amplitude $T^{(2)}_{a(b)}$ in the j-plane. For $\alpha_k = \alpha_P(t)$ and small q, k the decrease of the amplitudes $T^{(2)}_{a(b)}$ is not fast enough in order to consider only the contribution of the finite s_i-region. The contributions of the regions of large $s_i \sim \epsilon s$ ($\epsilon \ll 1$) correspond to the "enhanced" diagrams, shown in fig. 2.28.

In this subsection we will be interested mainly in the contributions of the "nonenhanced" diagrams, which correspond to finite s_i and are described by eqs. (2.48), (2.49).

The unitarity equation is valid for the Reggeon–particle scattering amplitudes

$$\delta_{s_a} T^{(2)}_a = \mathrm{Im} T^{(2)}_a = \frac{1}{2}\sum_n \int T_{aP\to n}(s_a, k_\perp^2, \tau_n)\, T^*_{cP\to n}(s_a, (q-k_\perp)^2, \tau_n)\, d\tau_n. \tag{2.50}$$

The amplitudes $T_{a(c)P\to n}(s_a, k_i^2, \tau_n)$, which describe the Pomeron–particle transition to n-particles, are connected with the vertices v_n, introduced earlier in eq. (2.11) by the following relation

$$T_{aP\to n}(s_a, k_\perp^2, \tau_n) = (s_0/s_a)^{\alpha_P(k_\perp^2)}\, v^a_n(s_a, k_\perp^2, \tau_n). \tag{2.51}$$

Thus the quantities $N^{(2)}_{a(b)}$ can be expressed according to eqs. (2.49), (2.50) as a sum of contributions from the real intermediate states. Isolating the single particle (pole) contribution we have

$$N^{(2)}_a = g^P_{aa}(k_\perp^2)\, g^P_{ac}((q-k_\perp)^2) + \Delta N^{(2)}_a, \tag{2.52}$$

where $\Delta N^{(2)}_a$ corresponds to the multiparticle intermediate states*. An analogous formula is valid for $N^{(2)}_b$. Inserting eq. (2.52) into eq. (2.48) we can express $T^{(2)}$ as a sum of elastic and inelastic diffractive rescattering in the s-channel (fig. 2.29). The contribution of the pole term in eq. (2.52), which corresponds to elastic rescattering, has an especially simple form

$$M^2(s,t) = \frac{1}{2!}\int M^{(1)}_{ab\to ab}(s, k_\perp^2)\, M^{(1)}_{ab\to cd}(s, (q-k_\perp)^2)\, \frac{d^2k_\perp}{\pi} \tag{2.53}$$

*The contribution of the particle c-state (for $c \neq a$) is included in $\Delta N^{(2)}_a$.

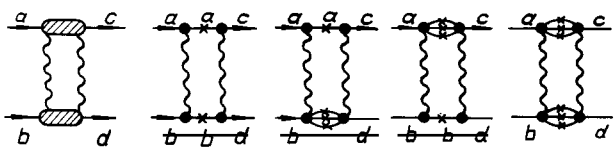

Fig. 2.29. Rescattering graphs which determine the value of the two-Reggeon exchange amplitude.

where $M^{(1)}$ is the Regge pole term $M^{(1)}_{ab\to cd} = g_{ac}\cdot g_{bd}(s/s_0)^{\alpha_P-1}$. The approximation of $N^{(2)}_{a(b)}$ by the pole term contribution, which leads to eq. (2.53), is equivalent to the well known absorption model [64–66].

For the case of elastic scattering (a = c, b = d) at $t = 0$ the expression for $\mathrm{Im}\,T^{(2)}(s,0)/s$, differs only by sign from the total cross section of diffractive processes (including elastic scattering), calculated in the Regge pole approximation. This can be seen if we take into account that $\eta_P \approx i$ and compare the expression for $\mathrm{Im}\,T^{(2)}(s,0)/s$, eqs. (2.48)–(2.52) with the diffractive cross sections

$$\sigma^{(1)}_{ab\to ab}(s) = 4\pi\int (g^P_{aa}(k_\perp^2)\, g^P_{bb}(k_\perp^2))^2 \left(\frac{s}{s_0}\right)^{2(\alpha_P(k_\perp^2)-1)} \cdot|\eta_P(k_\perp^2)|^2 \frac{d^2k_\perp}{\pi},$$

$$\sigma^{(1)}_{ab\to aX} = 4\pi\int \frac{d^2k_\perp}{\pi}(g^P_{aa}(k_\perp^2))^2 \left(\frac{s}{s_0}\right)^{2(\alpha_P(k_\perp^2)-1)} |\eta_P(k_\perp^2)|^2 \frac{1}{\pi}\int ds_b \frac{1}{2}\sum_n |T_{bP\to n}(s_b, k_\perp^2, \tau_n|^2\, d\tau_n \qquad (2.54)$$

$$= 4\pi\int \frac{d^2k_\perp}{\pi}(g^P_{aa}(k_\perp^2))^2 \left(\frac{s}{s_0}\right)^{2(\alpha_P(k_\perp^2)-1)} \cdot|\eta_P(k_\perp^2)|^2\, \Delta N^{(2)}_b(k_\perp^2),$$

$$\sigma^{(1)}_{ab\to X_1X_2}(s) = 4\pi\int \frac{d^2k_\perp}{\pi}\left(\frac{s}{s_0}\right)^{2(\alpha_P(k_\perp^2)-1)} \cdot|\eta_P(k_\perp^2)|^2\, \Delta N^{(2)}_a\cdot\Delta N^{(2)}_b.$$

Thus the value of the two Reggeon exchange amplitude for elastic scattering at $t = 0$ is determined by the cross section of diffractive processes. Diffractive production of large mass states s_a, $s_b \gg m^2$ corresponds to the enhanced diagrams of fig. 2.28.

The n-Pomeron exchange amplitudes have a structure analogous to that in eqs. (2.48), (2.49) [7, 8]

$$M^{(n)}(s,t) = \frac{(i)^{n-1}}{n!}\int N^{(n)}_a(q_{i\perp})\, N^{(n)}_b(q_{i\perp})\left(\frac{s}{s_0}\right)^{\alpha_1+\ldots+\alpha_n-n} \cdot\eta_{P_1}\ldots\eta_{P_n}\frac{d^2q_{1\perp}}{\pi}\ldots\frac{d^2q_{n-1\perp}}{\pi}, \qquad (2.55)$$

$$N^{(n)}_a(q_{i\perp}) = \int_C \ldots\int T^{(n)}_a(q_{i\perp}, s_{a1}, \ldots, s_{a(n-1)})\frac{ds_{a1}}{2\pi i}\ldots\frac{ds_{a(n-1)}}{2\pi i} \qquad (2.56)$$

where $\alpha_i \equiv \alpha_P(q^2_{i\perp})$, $q_{i\perp}$ is the transverse momentum of the ith Pomeron.

The integration contours over s_{ai} in eq. (2.56) are of the same type as in eq. (2.47). Deformation of contours C_i into C_i' in order to enclose the right-hand singularities of $T^{(n)}_a$ leads to the formula

$$N^{(n)}_a(q_{i\perp}) = \int \frac{ds_{a1}}{\pi}\ldots\frac{ds_{a(n-1)}}{\pi}\,\delta^{(n-1)}_{s_{a1}\ldots s_{a(n-1)}}\, T^{(n)}_a(q_{i\perp}, s_{a1}, \ldots s_{a(n-1)}) \qquad (2.57)$$

where $\delta^{(n-1)}_{s_{a1}\ldots s_{a(n-1)}} T^{(n)}_a(q_{i\perp}, s_{a1}, \ldots, s_{a(n-1)})$ is the multiple discontinuity of the function $T^{(n)}_a$ on the right hand cuts.

If only the pole contributions to these discontinuities are taken into account, one has

$$N^{(n)}_a\cdot N^{(n)}_b = \gamma_P(q^2_{1\perp})\ldots\gamma_P(q^2_{n\perp}). \qquad (2.58)$$

The n-Pomeron exchange amplitude can then be written in the "eikonal"form [67]

$$M^{(n)}(s,t) = \frac{(i)^{n-1}}{n!}\int M^{(1)}_P(s, q^2_{i\perp})\ldots M^{(1)}_P(s, q^2_{n\perp})\frac{d^2q_{1\perp}}{\pi}\ldots\frac{d^2q_{(n-1)\perp}}{\pi}$$

$$= \frac{(2i)^{n-1}}{n!}\int M^{(1)}_P(s, q^2_{1\perp})\ldots M^{(1)}_P(s, q^2_{n\perp})\frac{d^2q_{1\perp}\ldots d^2q_{n\perp}}{(2\pi)^{n-1}}\,\delta\Big(q - \sum_{i=1}^{n} q_{i\perp}\Big). \qquad (2.59)$$

It was noted above that the P-pole contribution to elastic scattering amplitude is connected with a multiperipheral inelastic process in the s-channel (fig. 2.2). In other words this means that the unitarity

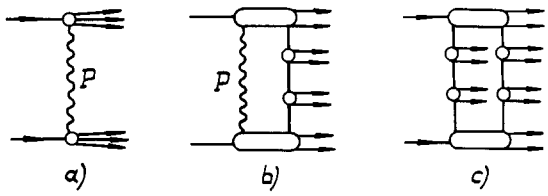

Fig. 2.30. Diagrams corresponding to the unitarity cuts of the two Reggeon exchange amplitude.

cut of the Regge-pole graph corresponds to the multiperipheral structure of the inelastic intermediate state. Consider now the unitarity cuts of the n-Pomeron exchange amplitudes of fig. 2.21. The total imaginary part of the Feynman diagram is equal to a sum over all the possible cuttings of this diagram in the s-channel. The graphs for the physical processes, which correspond to the unitarity cuts of the two Pomeron exchange amplitude of fig. 2.21, are shown in fig. 2.30. These are the diffractive processes, fig. 2.30a (which are connected with the cutting of the diagram 2.21a between the Pomeron lines), the effects of absorption (screening) for the multiperipheral processes (cutting of one of the Pomerons), fig. 2.30b and the production of two multiperipheral showers (simultaneous cutting of both Pomerons) respectively. According to the rules, formulated by Abramovskii, Gribov and Kancheli [68] the contribution of the corresponding cuttings to the total cross section $\mathrm{Im}\, T_{ab}(s,0)/s$ are determined by the following relations:

$$\sigma_A = \sigma_{Dif.} = -\sigma^{(2)}; \qquad \sigma_B = 4\sigma^{(2)}; \qquad \sigma_C = -2\sigma^{(2)} \tag{2.60}$$

where $\sigma^{(2)} = \mathrm{Im}\, T^{(2)}(s,0)/s$ is the contribution of the two Pomeron exchange to the total cross section.

The quantities σ_A and σ_C determine cross sections for physical processes and hence are positive, whereas σ_B characterizes an interference effect, the decrease of the multiperipheral cross section due to absorption. The total contribution of the two Pomeron exchange to the total cross section $\sigma^{(2)}$ is negative and, as we have seen before, it's modulus is equal to the P-pole contribution to σ_{diff}.

Cuttings of the n-Pomeron exchange diagrams of fig. 2.25b lead in particular to the graphs of fig. 2.31, which correspond to absorption corrections to amplitudes for inelastic diffractive processes.

Thus the AGK-cutting rules allows one to find a connection between the Reggeon calculus diagrams and s-channel unitarity.

Let us now estimate the contributions of the n-Pomeron exchange terms to scattering amplitudes. We can use eqs. (2.53), (2.59) in order to understand the structure and the main properties of the n-Pomeron exchange amplitudes. These expressions correspond to elastic rescattering, but for $s \to \infty$ they differ from the more general formulae (2.48), (2.55) only by the coefficients $C^{(n)}(q^2)$, which take into account inelastic intermediate states. Using the parametrization (2.4) for the Regge pole contribution and performing the integration over the transverse momenta of Reggeons in eqs. (2.53), (2.59) we obtain the following expressions for the two Pomeron exchange amplitude

$$M^{(2)}(s,q^2) = \frac{i}{2}(\gamma_P(0))^2 \frac{\eta^2(\alpha_P(0))\epsilon_P^2}{2\lambda_P(s)} \exp\left(-\frac{\lambda_P(s)q^2}{2}\right) \tag{2.61}$$

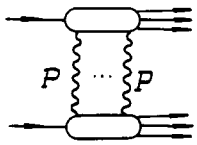

Fig. 2.31. Exchange of several Pomerons in amplitudes for inelastic diffractive reactions.

where

$$\epsilon_P = \left(\frac{s}{s_0}\right)^{\alpha_P(0)-1}, \quad \lambda_P(s) = R_P^2 + \alpha_P'(0)\left(\ln\frac{s}{s_0} - i\frac{\pi}{2}\right)$$

and for the n-Pomeron exchange amplitude

$$M^{(n)}(s, q^2) = \frac{(i)^{n-1}}{n!} \frac{(\gamma_P(0)\, \eta(\alpha_P(0))\, \epsilon_P)^n}{n\lambda_P^{n-1}} \exp\left(-\frac{\lambda_P q^2}{n}\right). \tag{2.62}$$

Consider the properties of the two-Pomeron exchange amplitude. It follows from eq. (2.61) that (for $\alpha_P(0) = 1$)

i) The P-pole and PP-cut contributions differ by a sign at $t = 0$ (because $\eta(\alpha_P(0)) = i$);

ii) The two Pomeron exchange amplitude decreases logarithmically with s at $t = 0$;

iii) The amplitude $M^{(2)}$ falls less rapidly with q^2, than the pole contribution $M^{(1)}$;

iv) The relative value of the PP-cut contribution is determined by the factor $\gamma_P(0)/4\lambda_P$, which is $\approx 1/4$ at present energies.

In the weak coupling theory the total cross sections tend to the asymptotic limit from below due to the decrease of the negative PP-exchange contribution [57].

Note that the n-Pomeron exchange amplitudes as well as the P-pole have positive signature and positive G-parity, an isotopic spin equal to zero, but contrary to the P-pole they do not have, generally speaking, definite parity.

The sum of the n-Pomeron exchange amplitudes in the eikonal approximation, eqs. (2.59), (2.62), can be written in a closed form, using an impact parameter representation

$$f^{(n)}(s, b) = \int M^{(n)}(s, q^2)\, e^{-iqb} \frac{d^2q}{2\pi} = \frac{(2i\delta(s, b))^n}{2in!} \tag{2.63}$$

where

$$\delta(s, b) = \int M^{(1)}(s, q^2)\, e^{-iqb} \frac{d^2q}{2\pi} = f^{(1)}(s, b).$$

Thus

$$f(s, b) = \sum_{n=1}^{\infty} f^{(n)}(s, b) = \frac{e^{2i\delta(s, b)} - 1}{2i}. \tag{2.64}$$

The total nonenhanced part of the two Pomeron exchange amplitude differs from the eikonal approximation $-\delta^2(s, b)/i$ by the factor $C_P^{(1)}(0) = 1 + \sigma_D^{(1)in}/\sigma^{(1)el}$,* where $\sigma_D^{(1)in}$ and $\sigma^{(1)el}$ are the P-pole contributions to the cross section for inelastic and elastic diffractive processes respectively, eq. (2.54); $\sigma_D^{(1)in}$ corresponds to the diffractive production of not too large masses (large mass diffraction production is accounted for by the enhanced diagrams). The assumption that $C_P^{(n)}(q^2) = (C_P^{(1)}(0))^{n-1}$ for the n-Pomeron cuts leads to a "quasieikonal" approximation for the elastic scattering amplitude [69]:

$$f(s, b) = \frac{\exp\{2iC_P^{(1)}(0)\, \delta(s, b)\} - 1}{2iC_P^{(1)}(0)}. \tag{2.65}$$

Let us discuss now the effects of the Pomeron cuts for the amplitudes of inelastic diffractive processes. The Reggeon calculus and the AGK-cutting rules let one to describe elastic and inelastic

*It has been assumed that $C(q^2) = C(0)$.

diffractive processes from a single point of view and show that these reactions are closely connected. Consider for example the two-channel model, where the diffractive inelastic states are approximated by a resonance a* (for simplicity we take a = b). The diagrams which correspond to this model are shown in fig. 2.32.

They contain the vertices g_{aa^*}, g_{aa}, $g_{a^*a^*}$ which can be written in the matrix form

$$\hat{g}_a = \begin{pmatrix} g_{aa} & g_{aa^*} \\ g_{a^*a} & g_{a^*a^*} \end{pmatrix} = g_0 \begin{pmatrix} 1+\alpha & \beta \\ \beta & 1-\alpha \end{pmatrix} \tag{2.66}$$

where $\beta = 2g_{aa^*}/(g_{aa} + g_{a^*a^*})$, $\alpha = (g_{aa} - g_{a^*a^*})/(g_{aa} + g_{a^*a^*})$; $g_0 = \frac{1}{2}(g_{aa} + g_{a^*a^*})$. The amplitude $f(s, b)$ is also a matrix and has the eikonal form

$$\hat{f}(s, b) = \frac{e^{2i\hat{\delta}(s,b)} - 1}{2i} \tag{2.67}$$

where

$$\hat{\delta}(s, b) = \frac{\hat{g}_a^u \cdot \hat{g}_a^l \cdot \eta(\alpha_P)\, \epsilon_P}{2\lambda_P} \exp\left(-\frac{b^2}{4\lambda_P}\right). \tag{2.68}$$

The matrices of the residues $\hat{g}_a^u$ and $\hat{g}_a^l$ in eq. (2.68) correspond to the upper and lower particles in fig. 2.32. Equations (2.67), (2.68) have been obtained under the assumption that all residues have the same t-dependence. (A difference in t-dependence among residues can be taken into account [8], but the resulting formulae are more complicated.)

The matrix elements of $\hat{f}$ can be evaluated [8] and the elastic scattering amplitude has the form

$$f_{aa\to aa}(s, b) = \frac{1}{2i}\left[\left(\frac{1+\alpha/\gamma}{2}\right)^2 \exp\{(1+\gamma)^2 2i\delta_0\} + \left(\frac{1-\alpha/\gamma}{2}\right)^2 \exp\{(1-\gamma)^2 2i\delta_0\} + \frac{\gamma^2 - \alpha^2}{2\gamma^2} \exp\{(1-\gamma^2)2i\delta_0\} - 1\right]. \tag{2.69}$$

For the single diffraction dissociation amplitude we have

$$f_{aa\to aa^*}(s, b) = \frac{\beta}{4i\gamma}\left[\frac{(1+\alpha/\gamma)}{2} \exp\{(1+\gamma)^2 2i\delta_0\} - \frac{(1-\alpha/\gamma)}{2} \exp\{(1-\gamma)^2 2i\delta_0\} - \frac{\alpha}{\gamma} \exp\{(1-\gamma^2)2i\delta_0\}\right]. \tag{2.70}$$

The double diffraction dissociation amplitude is written in the form

$$f_{aa\to a^*a^*}(s, b) = \frac{1}{2i}\left(\frac{\beta}{2\gamma}\right)^2 [\exp\{(1+\gamma)^2 2i\delta_0\} + \exp\{(1-\gamma)^2 2i\delta_0\} - 2\exp\{(1-\gamma^2)2i\delta_0\}] \tag{2.71}$$

where $\gamma = \sqrt{\alpha^2 + \beta^2}$; $\delta_0 = \{g_0^2 \eta(\alpha_P)\epsilon_P/2\lambda_P\} \exp(-b^2/4\lambda_P)$. Formulae (2.69)–(2.71) can be generalized to the multichannel case, and also for $a \neq b$ [8]. Let us note that the quasieikonal approximation, eq.

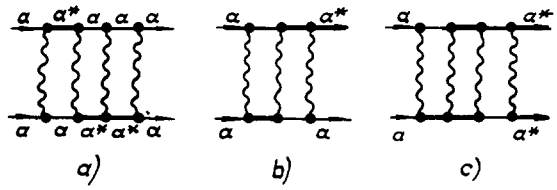

Fig. 2.32. Diagrammatic representation of eqs. (2.67), (2.68).

(2.65), corresponds to a special choice of the vertices g_{ik}, which satisfy the relation $g_{aa}g_{a^*a^*} = g^2_{aa^*}(\gamma = 1)$. This leads to a saturation of the unitarity bound (1.25 i). The amplitudes for diffractive processes have in this case a simple form

$$f_{aa\to aa}(s,b) = \frac{e^{C\chi_0}-1}{2iC}; \qquad f_{aa\to aa^*}(s,b) = \sqrt{\frac{1-\alpha}{1+\alpha}}\frac{e^{C\chi_0}-1}{2iC}; \qquad f_{aa\to a^*a^*}(s,b) = \frac{1-\alpha}{1+\alpha}\frac{e^{C\chi_0}-1}{2iC} \tag{2.72}$$

where

$$\chi_0 = 2i\delta_{aa} = 2i(1+\alpha)^2\delta_0; \qquad C = \left(\frac{2}{1+\alpha}\right)^2 = 1 + \sigma_D^{(in)}/\sigma^{(el)}.$$

Note that in this special case the amplitudes for all diffractive processes have the same b-dependence and satisfy the factorization relation $(f_{aa\to aa^*}(s,b))^2 = f_{aa\to aa}(s,b)\,f_{aa\to a^*a^*}(s,b)$. The situation, where β and α are $\ll 1$, i.e. the cross section for the diffractive production of resonance is much smaller than the cross sections for elastic aa and a*a scattering and $\sigma^{(tot)}_{aa} \approx \sigma^{(tot)}_{a^*a}$, seems to be more realistic. Then (for $\alpha = 0$, $\beta \ll 1$, $\gamma = \beta$) we have

$$f_{aa\to aa}(s,b) \approx \frac{1}{2i}(e^{2i\delta_0}-1), \qquad f_{aa\to aa^*}(s,b) \approx \delta_{aa\to aa^*}(s,b)\cdot e^{2i\delta_0}, \qquad f_{aa\to a^*a^*}(s,b) \approx \delta_{aa\to a^*a^*}(s,b)\cdot e^{2i\delta_0} \tag{2.73}$$

where $\delta_{aa\to aa^*}(s,b) = \beta\delta_0$, $\delta_{aa\to a^*a^*}(s,b) = \beta^2\delta_0$.

Expressions (2.73) are equivalent to the formulae of the absorption model.

If absorption is important, $-\mathrm{Im}\,\delta_0(s,b) \geq 1$ in a region $b^2 \geq 4\lambda_P$, then the amplitudes for inelastic diffraction will be strongly suppressed for these values of b. This is due to the factor $\exp\{-2\mathrm{Im}\,\delta_0\}$ in eq. (2.73). In this model the amplitudes for inelastic diffractive processes contrary to the amplitude for elastic scattering have a peripheral form in b-space. Thus the n-Pomeron exchanges leads to important effects in diffractive processes, if $\mathrm{Im}\,\delta_0 \geq 1$. In particular factorisation is violated.* At present energies $\delta_0(s,0) \approx 0.7$ to 0.8.

The method of evaluation of the n-Pomeron exchange amplitude for the nonresonance diffractive production of particles (fig. 2.31) does not differ in principle from the one we have already discussed above. But in this case we must deal with more complicated objects, amplitudes for n-Pomeron–m-particles transitions, fig. 2.33. Consider for example the process of one pion production in NN-collisions. Taking into account only the pole contributions to these amplitudes, in accordance with the prescription shown in figs. 2.34, 2.35, we obtain the diagrammatic representation of the two-Pomeron exchange amplitude, shown in fig. 2.36. Expressions analogous to eq. (2.53) correspond to these diagrams. The sum of the diagrams 2.36a and 2.36b, which are the same, can be expressed in the form

$$M^{(2)} = i\int M^{(1)}_{pp\to pp}(s,k^2)\,M^{(1)}_{pp\to p(n\pi^+)}(s,s_1,k_1^2,k_2^2)\frac{d^2k}{\pi} \tag{2.74}$$

*It should be taken into account however, that in some cases the observed deviations from the factorization relations can be numerically small [70, 71].

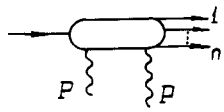

Fig. 2.33. Graph representing the two-Pomeron–n-particle transition amplitude.

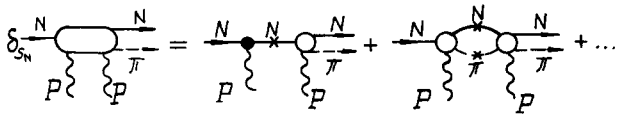

Fig. 2.34. Graphs for the discontinuity of the amplitude $PN \to PN\pi$.

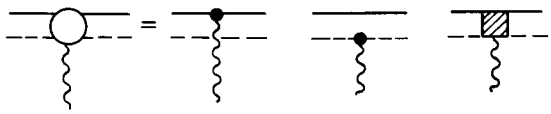

Fig. 2.35. Graphs for the coupling of the Pomeron to an $N\pi$-system.

where

$$k_2 = q_2 - k; \qquad k_1 = q_1 + k; \qquad q_1 = p_n - p_{p1}; \qquad q_2 = p_{p3} - p_{p2}.$$

Using the impact parameter representation

$$f_{pp\to p(n\pi^+)}(s, s_1, b_1, b_2) = \int M_{pp\to p(n\pi^+)}(s, s_1, q_1, q_2) \exp\{-iq_1b_1 - iq_2b_2\} \frac{d^2q_1}{2\pi} \frac{d^2q_2}{\pi} \tag{2.75}$$

we obtain the simple expression for the function $f^{(2)}(s, s_1, b_1, b_2)$

$$f^{(2)}_{pp\to p(n\pi^+)}(s, s_1, b_1, b_2) = \delta_{pp\to p(n\pi^+)}(s, s_1, b_1, b_2)(2i\delta_{pp\to pp}(s, b^2)) \tag{2.76}$$

where $b = b_1 + b_2$; functions δ_i are the Fourier transforms, eqs. (2.63), (2.75) of the corresponding Regge pole amplitudes.

The summation of all the graphs with elastic rescatterings of nucleons in the initial and final states leads to the expression

$$f_{pp\to p(n\pi^+)}(s, s_1, b_1, b_2) = \delta_{pp\to p(n\pi^+)}(s, s_1, b_1, b_2) \exp\{2i\delta_{pp\to pp}(s, b^2)\}, \tag{2.77}$$

is analogous to eq. (2.73) written for the diffractive production of resonance.

In the framework of the OPE-model for diffraction dissociation vertices, diagrams with rescatterings of the final pion can be also described by eq. (2.77), but the function $\delta_{pp\to p(n\pi^+)}$ should now be considered as the Fourier transform of the amplitude of fig. 2.3a with $T_{\pi N}$ calculated in the eikonal approximation (2.64).

Expressions of the type (2.77) are usually used for practical calculations of rescattering effects in inelastic diffractive processes [72–74]. This approximation is rather simple and may be useful for estimates of absorption in diffractive scattering but it should be noted that it's accuracy is unknown theoretically and contributions from inelastic intermediate states to the amplitudes $N^{(n)}$ can be important.

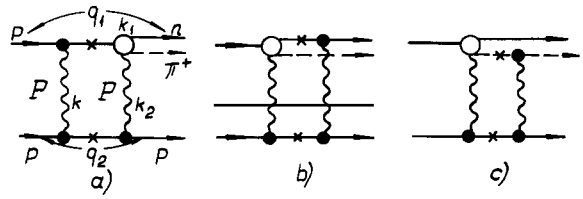

Fig. 2.36. Diagrams for two-Pomeron exchange in the reaction $pp \to pn\pi^+$, in the eikonal approximation.

2.6. *The problems of Reggeon theory at $s \to \infty$. Models with Froissart type asymptotic behaviour for amplitudes*

In the previous subsection we have discussed the rescattering effects which are connected with diffractive excitations of small mass, $s_i \sim m^2$ and have neglected the enhanced diagrams (of the type shown in fig. 2.28), which are proportional (at $t = 0$) to the cross sections for large mass excitations. This can be a reasonable procedure at present energies, because the enhanced diagrams are rather small for $\xi \leqslant 10$ due to the smallness of the triple Pomeron vertex $r^{\mathrm{P}}_{\mathrm{PP}}$ (see section 3). However in the limit $\xi \to \infty$ the contributions of the enhanced diagrams, which take into account the interaction of Pomerons (figs. 2.28, 2.37, 2.38), are very important. Summation of all the diagrams of Reggeon field theory is a very difficult problem. However it can be solved in some special cases. I shall discuss only the main properties and physical consequences of these solutions (the method of calculations and the results of recent developments in Reggeon field theory are discussed in detail in reviews [7, 8, 75, 76]).

One of the most significant parameters of Reggeon theory is the value of the intercept of the "bare" Pomeranchuk pole (P-pole without selfinteraction of the type, shown in fig. 2.28c). If the value $\Delta \equiv \alpha^{\mathrm{P}}_0(0) - 1$ is less than $\Delta_{\mathrm{crit}} = \{(r^{\mathrm{P}}_{\mathrm{PP}})^2/4\alpha'_{\mathrm{P}}\} \ln\{4\alpha'_{\mathrm{P}}/(r^{\mathrm{P}}_{\mathrm{PP}})^2\}$, then the renormalized pole $\alpha_{\mathrm{P}}(0)$ is to the left of unity in the j-plane, Regge cuts are unimportant asymptotically and $\sigma^{(\mathrm{tot})}$ decreases as $s^{\alpha_{\mathrm{P}}(0)-1}$ as $s \to \infty$. This asymptotic behaviour is difficult to reconcile with the observed rise of $\sigma^{(\mathrm{tot})}$. The case where $\Delta = \Delta_{\mathrm{crit}}$ and the renormalized Pomeron intercept $\alpha_{\mathrm{P}}(0) = 1$ is more interesting. This "critical" Pomeron theory was first studied in refs. [77, 78]. The diagrams with triple Pomeron interactions play a main role in this case. The equations of Reggeon field theory have a scale invariant solution with anomalous dimensions. Total cross sections then rise $\sim \xi^{\eta}$ as $\xi \to \infty$. The quantity η can be estimated using the method of ϵ-expansion and is found to be $\approx 1/6$ [77, 78]. The interaction of Pomerons leads to screening effects for inelastic Pomeron vertices and allows one to solve the problems of Regge pole models with the too fast increase of the inelastic diffractive cross sections [77, 79]. The relative contribution to the total cross section of the multipomeron kinematical region of phase space is unimportant asymptotically [77, 79] and the main contribution to exclusive diffractive processes comes from configurations of final particles with only one large rapidity gap $\Delta \sim \xi$ [79]. Cross sections for such diffractive processes have the same energy dependence as $\sigma^{(\mathrm{el})}$, they decrease as $1/\xi^{\alpha}$ (with $\alpha \approx \frac{5}{6}$) due to the shrinking of the diffractive cone. It can be shown [77, 80] that absorption effects, connected with the enhanced diagrams, remove the inconsistencies of the Regge pole model also for inclusive diffractive reactions. Thus the "critical" Pomeron theory with $\alpha_{\mathrm{P}}(0) = 1$ is consistent with the s-channel unitarity [77–80].

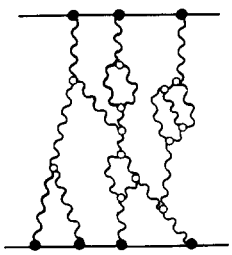

Fig. 2.37. Graphs of Reggeon calculus with triple-Pomeron interactions.

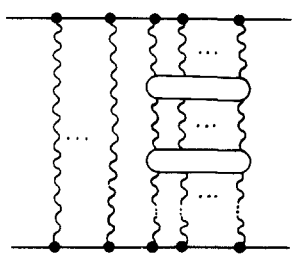

Fig. 2.38. Graphs with multi-Pomeron interactions.

Versions of Reggeon theory with $\Delta > \Delta_{crit}$ were studied recently in many papers [81–87]. The interest to the case $\Delta > \Delta_{crit}$ is connected mainly with two reasons:

1) There are at present no theoretical arguments for $\alpha_0^P(0)$ to be exactly at the critical value (for example in the framework of the multiperipheral model the bare Pomeron intercept $\alpha_0^P(0)$ depends on the number of exchanged particles and the strength of their interactions in the low energy (resonance) region and can have any value).

2) Estimates of $r_{PP}^P(0)$ from the triple-Regge analysis of diffractive processes give for Δ_{crit} the value $\sim 10^{-2}$. This shift of the bare pole is too small to explain the observed rise of the total cross sections in the framework of the standard Reggeon calculus approach. It should be noted however that a reasonable modification of the formulae of Reggeon theory, which takes into account the influence of the "threshold" effects at present energies [89] allows one to explain the behaviour of $\sigma^{(tot)}$ even for $\Delta = \Delta_{crit}$.

If $\Delta > \Delta_{crit}$ then the renormalized pole is to the right of unity in the j-plane ($\alpha_P(0) > 1$) and all the diagrams of Reggeon field theory should be taken into account.

The hypothesis that the intercept of the Pomeranchuk pole is larger than unity has been proposed several years ago by Cheng and Wu [90]. These authors have also assumed that unitarity in the s-channel is restored by an eikonalization (2.64) of the pole contribution*

$$T(s,t) = 8\pi s \int \frac{e^{2i\delta(s,b)} - 1}{2i} e^{iqb} \frac{d^2b}{2\pi}; \qquad \delta(s,b) = \frac{\gamma_P(0)\,\eta_P(0)(s/s_0)^{\alpha_P(0)-1}}{16\pi\lambda_P(s)} \exp\left(-\frac{b^2}{4\lambda_P(s)}\right). \tag{2.78}$$

This leads to a Froissart type asymptotic behaviour of the elastic scattering amplitudes. The amplitude $f(s,b)$ is equal to i/2 at $s \to \infty$ in the region of b, where $\mathrm{Im}\,\delta(s,b) \gg 1$, i.e. for $b^2 < R_0^2\xi^2$, where $R_0^2 = 4\alpha_P'(0)\Delta$.† For larger values of b the amplitude decreases exponentially with b and the width of the edge is $\sim\sqrt{\alpha_P'/\Delta}$, fig. 2.39a. Thus in the limit $\xi \to \infty$ the impact parameter distribution is the same as for scattering by a black disk of expanding radius $R_0\xi$ with a sharp edge (fig. 1.1). In this case the total cross sections $\sigma^{(tot)} = 8\pi\alpha'\Delta\cdot\xi^2$ and the slopes of the diffraction cone

$$B = \frac{d}{dt}\ln\frac{d\sigma}{dt}\bigg|_{t=0} \sim \alpha_P'(0)\Delta\xi^2$$

are universal for all hadronic processes.

*In the Cheng and Wu model [90] the t-dependence of $\alpha_P(t)$ has been neglected ($\lambda_P = \mathrm{const}$).

†For a linear form of the P-pole trajectory ($\alpha_P(t) = \alpha_P(0) + \alpha_P' \cdot t$) and a gaussian parametrisation of the residue function, Im $\delta(s,b)$ becomes ~ 1 according to eq. (2.78) at somewhat smaller values of b: $b^2 = 4\alpha_P'(\Delta\xi^2 - \xi\ln\xi)$.

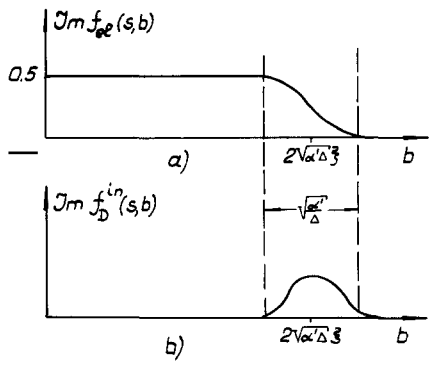

Fig. 2.39. Impact parameter distributions in theories with $\alpha_P(0) > 1$; (a) for elastic scattering, (b) for inelastic diffractive processes.

The amplitudes for inelastic diffractive processes in the same eikonal approximation (eqs. (2.73, 2.77)) are peripheral in b-space and are concentrated only in the edge-region due to the full absorption for $b < R$. The cross section for diffractive excitation at a fixed mass varies as $\sigma_D^{(in)} \approx \xi$.

We have discussed so far only eikonal graphs, but generally speaking there are no reasons to neglect diagrams with Pomeron interactions of the type, shown in figs. 2.37, 2.38. The theory of interacting Pomerons with $\Delta > \Delta_{crit.}$ has been studied in refs. [81–87]. Reggeon field theory with triple Pomeron interaction has been studied in several papers [82]. It has been found [82] that the solution corresponds to the Froissart asymptotic behaviour for scattering amplitudes. However all the n-Pomeron interactions are equally important in the case $\Delta > \Delta_{crit.}$. So it is natural to ask the following questions: a) whether the same solution is valid in the general case for arbitrary interactions of Pomerons? and b) is the solution consistent with t-channel and s-channel unitarity? These questions have been studied in refs. [84] under the assumption that the vertices for the transition from n-Pomeron to m-Pomerons are analytic functions of the variables n and m. This approach to Reggeon field theory with $\alpha_P(0) > 1$ has been proposed by Cardy [81]. The main object (initial element) in the approach is the sum of eikonal type rescatterings in the s-channel, "Froissarton" [84]. General set of Reggeon graphs can be written in terms of the Froissarton graphs. The Froissarton contribution is factorizable [81] and the multi-Froissarton contributions are determined by the usual rules of Reggeon calculus.

It has been shown in refs. [84, 85] that the sum of all the diagrams of Reggeon field theory leads to the Froissart type asymptotic behaviour and does not violate t-channel and s-channel unitarity equations. A consistent solution can be obtained only if the singularity of the Pomeranchuk trajectory $\alpha_P(t)$ at the point $t = 4\mu^2 \equiv t_0$ is taken into account [85]. This effect has been usually neglected, because, in the versions of Regge theory with $\alpha_P(0) \leqslant 1$, the impact parameter region $b^2 \sim \xi$ is important and the threshold singularity of $\alpha_P(t)$ has no influence on the amplitudes in this region. However, in the case $\alpha_P(0) > 1$ the region $b^2 \sim \xi^2$ is very important and the behaviour of the pole amplitude $\delta(s, b)$ depends crucially on the singularity of $\alpha_P(t)$ at $t = 4\mu^2$. For example if the Pomeron trajectory is parametrized in the form $\alpha_P(t) = 1 + \Delta_0 + \alpha_P' t + \epsilon(t_0 - t)^\gamma$, then the function $\delta(s, b)$ in the region $b < 2\alpha' t_0 \xi$ is given by eq. (2.78), but for $b > 2\alpha' t_0 \xi$ and $\Delta_0 > \alpha_P' t_0$ it has another representation [85]

$$\delta(s, b) = B \cdot \xi \frac{\exp[\kappa(R_0 \xi - b)]}{\sqrt{b}(b - 2\alpha_P' \kappa \xi)^{\gamma+1}} \tag{2.79}$$

where

$$B = 2\gamma(0)\left(\frac{s}{s_0}\right)^{\alpha_P(0)-1} \cdot \frac{\sin \pi\gamma}{\sqrt{\pi}} (2\kappa)^{\gamma+1/2} \Gamma(\gamma + 1); \qquad \kappa \equiv \sqrt{t_0} = 2\mu.$$

The most important consequence of the eq. (2.79) for the pole contribution is the change in the behaviour of the scattering amplitude in the edge region of b. The effective radius of interaction in this case

$$R = 2\sqrt{\alpha_P' \Delta}\,\xi - \frac{(\gamma + \frac{1}{2})}{\kappa} \ln \xi \tag{2.80}$$

is less than that for the usual representation (2.78). In the region of very large b, where $|\delta(s, b)| \approx |f(s, b)| \ll 1$ the scattering amplitude $f(s, b)$ decreases now as $\exp(-\kappa b)$. The partial amplitude in the t-channel as a function of $\omega = j - 1$ and $k = \sqrt{-t}$ has a singularity of the type $(\omega \pm iR_0 k)^{-\nu}$ at $\omega \to \pm iR_0 k$ and for $t \geqslant t_0$ the power ν is negative (the singularity is "soft") due to the influence of the $(t_0 - t)^\gamma$ term in the Pomeron trajectory [85]. This allows one to preserve t-channel unitarity.

Let us now discuss the inclusive diffractive production of large mass states and the multipomeron processes in Reggeon theory with $\alpha_P(0) > 1$ [86, 87]. Exclusive multipomeron reactions have been studied in ref. [86] in the framework of Reggeon field theory with triple Pomeron interaction and it has been found that due to absorption effects the total cross section for inelastic diffractive processes is consistent with s-channel unitarity. The "Froissarton" approach gives the satisfactory solution for the cross sections for large mass diffractive excitations only if the threshold singularity is introduced in the Pomeron trajectory. Consider for example the exclusive process of 2π-production in the double Pomeron region of phase space. The Pomeron-poles are replaced by the Froissarton lines in the diagrams shown in fig. 2.40. The simplest graph of fig. 2.40a gives a rapid increase with energy $\sim \xi^5$ for the cross section for this reaction and violates the unitarity condition. However on account of the absorption due to the graph 2.40b changes the situation completely. The sum of the diagrams 2.40a and 2.40b can be written in b-space in a form analogous to eq. (2.77)

$$f_{pp\to pp\pi^+\pi^-}(\xi, y_1, \boldsymbol{b}_1, \boldsymbol{b}_2, M^2) = \sigma_{pp\to pp\pi^+\pi^-}(\xi, y_1, \boldsymbol{b}_1, \boldsymbol{b}_2, M^2)\, e^{2i\delta(\xi, b^2)} \tag{2.81}$$

where $\delta_{pp\to pp\pi^+\pi^-}(\xi, y_1, \boldsymbol{b}_1, \boldsymbol{b}_2, M^2)$ is the impact parameter representation for the double-Froissarton exchange diagram of fig. 2.40a, $\delta(\xi, b^2)$ is the b-space amplitude for Pomeron exchange, it is given by eqs. (2.78), (2.79). M^2 is the mass of the 2π-system, y_1 is the rapidity interval, which corresponds to one of the Froissartons ($y_2 = \xi - y_1$), $\boldsymbol{b} = \boldsymbol{b}_1 + \boldsymbol{b}_2$.

The quantity $\exp\{2i\delta(\xi, b^2)\} = 1 - 2|f_{el}|$, where f_{el} has the Froissarton impact parameter distribution of fig. 2.39a, is equal to zero asymptotically in the region $b < R(\xi)$.

If we approximate the Froissarton amplitudes by the distributions with a sharp edge at $b = R(\xi) = R_0\xi - \beta \ln\xi$, then the function $\delta(\xi, y_1, \boldsymbol{b}_1, \boldsymbol{b}_2, M^2)$ in eq. (2.81) is different from zero in the regions $|\boldsymbol{b}_1| \leq R(y_1)$, $|\boldsymbol{b}_2| \leq R(\xi - y_1)$, $|\boldsymbol{b}| \leq |\boldsymbol{b}_1| + |\boldsymbol{b}_2| \leq R(y_1) + R(\xi - y_1) < R(\xi)$ and it follows from eq. (2.81) that the amplitude for inelastic diffraction vanishes because the function $\exp\{2i\delta(\xi, b^2)\}$ is equal to zero in this b-region. Therefore it is necessary to take into account the width of an edge and the amplitudes for the inelastic diffractive processes are concentrated in the edge region $b \approx R(\xi)$ (fig. 2.39b). The energy dependence of the cross sections in this region depends critically on the parameter β ($R(\xi) - R_0 \cdot \xi = \beta \ln\xi$) and the form of the elastic impact parameter distribution. For example in the case, where $\delta(\xi, b^2)$ has the form (2.78) (linear parametrization of $\alpha_P(t)$) the cross section of the reaction considered above after an integration over the variables b_1, y_1 increases indefinitely in the region $b \approx R(\xi)$ as $\xi \to \infty$. This contradicts the unitarity equation (1.10). On the other hand if the singularity of $\alpha_P(t)$ is taken into account using the expression (2.79) for $b > 2\alpha' t_0 \xi$ then for the values of $\gamma > 1$* the diffractive production of states with more than one large rapidity gap is small in the region $b \approx R(\xi)$ and s-channel unitarity is not violated.

It should be noted that the Froissart type asymptotic behaviour of amplitudes in theories with

*This condition seems to be reasonable, because in the usual Regge pole model $\gamma = \alpha_P(t_0) + \frac{1}{2} > 1.5$.

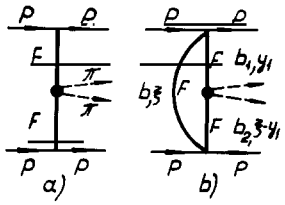

Fig. 2.40. Double-Froissarton production of particles (a) and graph, corresponding to absorption (b).

$\alpha_P(0) > 1$ is set at super higher energies, where $\Delta \cdot \xi \gg 1$. Estimates of Δ give the value ≈ 0.1, so the the relevant energy region, $\xi \gg 10$, is unaccessible for experimental investigation.

Concluding this section let us discuss briefly the theory of "heavy" Pomeron, which has been proposed by Gribov [91]. It has been assumed that $\alpha'_P \to 0$ and at present energies $R^2 = \alpha'_P \xi \ll R_0^2$, where $R_0 \sim 1/2\mu$ is the radius of the usual hadronic interactions. The Pomeron is "heavy" because in Reggeon field theory the quantity $1/\alpha'_P$ plays the role of the "mass". In this approach the nonenhanced cuts are small ($1/\xi^2$) even in the preasymptotic energy region $1 < \xi < R_0^2/\alpha'_P$ and the behaviour of scattering amplitudes is determined mainly by the pole and the enhanced cuts. The general properties of this solution are similar to the ones for the strong coupling solution of the "critical" Pomeron ($\Delta = \Delta_{crit}$). This scheme leads to the following experimental consequences:

a) The physical picture for elastic scattering is analogous to the scattering on a black disk with slowly increasing radius $R \sim \ln\xi$. Thus the total cross section rises with energy as $(\ln\xi)^2$ and the ratio σ_{el}/σ_{tot} is constant.

b) An approximate factorization is valid for elastic and inelastic cross sections.

c) The effective triple Pomeron vertex is small $\sim \alpha'_P$.

This picture is in a qualitative agreement with experimental data. However it is not clear whether the energy region, where this approach can be used exists? Analysis of experimental data shows that at present energies $\alpha'_P \xi \sim R_0^2$.

3. Experimental information on the properties of diffraction

3.1. Elastic scattering and $\sigma^{(tot)}$

Investigation of elastic scattering and total cross sections $\sigma^{(tot)}(s)$ at high energies gives important information on the characteristic features of diffraction. It has been pointed out above, that elastic and inelastic diffractive processes are closely connected, so only the study of all the diffractive phenomena allows us to find out the main properties and the actual mechanism of diffraction.

Let us enumerate some important results of the experimental study of $\sigma^{(tot)}$ and elastic reactions.

a) Total cross sections for hadron–hadron interactions $\sigma^{(tot)}$ rise with energy at $E \geq 100$ GeV (fig. 3.1). This rise is probably a universal feature of all hadronic interactions, but the energy where it starts depends on the type of colliding particles. An early rise of $\sigma^{(tot)}$ (at energies ~ 20 GeV) is seen in K^+p-interaction. The total cross section for pp-interaction, which is investigated in the widest energy range increases by $\approx 10\%$ from $E \sim 10^2$ GeV to $E = 2 \times 10^3$ GeV. Let us note that all the differences between particles and antiparticle total cross sections $\Delta\sigma^{(tot)}$ have a power low decrease with energy which starts at relatively small energies. This behaviour corresponds to the Pomeranchuk theorem and the predictions of Regge theory.

b) The ratio $\alpha = \mathrm{Re}T(s,0)/\mathrm{Im}T(s,0)$ of the real to the imaginary part of the forward elastic scattering amplitude is small at high energies for all the investigated processes. But the behaviour of α at large s does not correspond to a monotonic decrease with energy, which would be characteristic of a pure Regge-pole model. For many elastic reactions (pp, K^+p, $\pi^\pm p$) the function $\alpha(s)$ actually changes sign at energies ~ 100 GeV (fig. 3.2).

Such a behaviour of the real parts of the elastic amplitudes is in agreement with the predictions of dispersion relations. It follows from the simple relation,

$$\bar{\alpha} \underset{s\to\infty}{\simeq} \frac{1}{\bar{\sigma}^{(tot)}(\xi)} \frac{\pi}{2} \frac{d}{d\xi} \bar{\sigma}^{(tot)}(\xi) \tag{3.1}$$

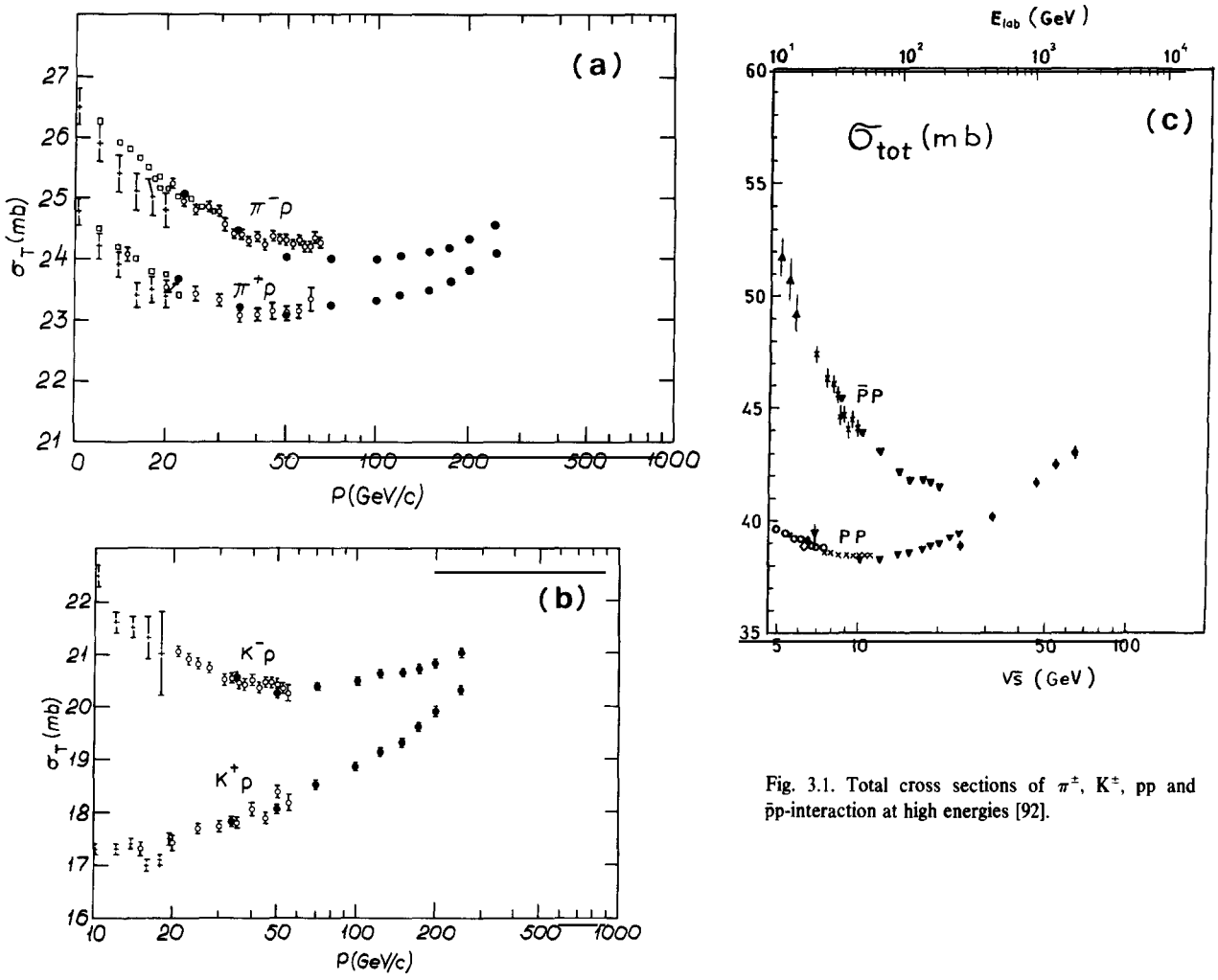

Fig. 3.1. Total cross sections of $\pi^{\pm}$, $K^{\pm}$, pp and $\bar{p}p$-interaction at high energies [92].

where

$$\bar{\alpha} = \alpha(ab) + \alpha(\bar{a}b); \quad \bar{\sigma} = \sigma(ab) + \sigma(\bar{a}b)$$

which is a consequence of analiticity and crossing. The change of the sign for the function $\bar{\alpha}$ takes place at energies, where $\bar{\sigma}^{(tot)}$ has the minimum. The positive values of $\bar{\alpha}$ at very high energies are closely connected with the rise of $\sigma^{(tot)}$. The accurate measurements of $\alpha_{pp}(s)$ at ISR [94] point out that the rise of $\sigma_{pp}^{(tot)}$ continues up to the energies of $\sim 10^5$ GeV.

c) The slope of the diffraction cone $B = (d/dt)(\ln(d\sigma/dt))$ increases with energy. The dependence of B on s for pp-scattering is shown in fig. 3.3. At energies $\gtrsim 50$ GeV this dependence is approximately logarithmic

$$B(s) = B_0 + 2\alpha'_P \ln(s/s_0).$$

The value of α'_P or the effective slope of the Pomeranchuk trajectory is equal to $(0.278 \pm 0.024)\,\text{GeV}^2$ (at $|t| < 0.1\,\text{GeV}^2$) [96]. Let us note, that the values of B and α'_P depend on t. For example at

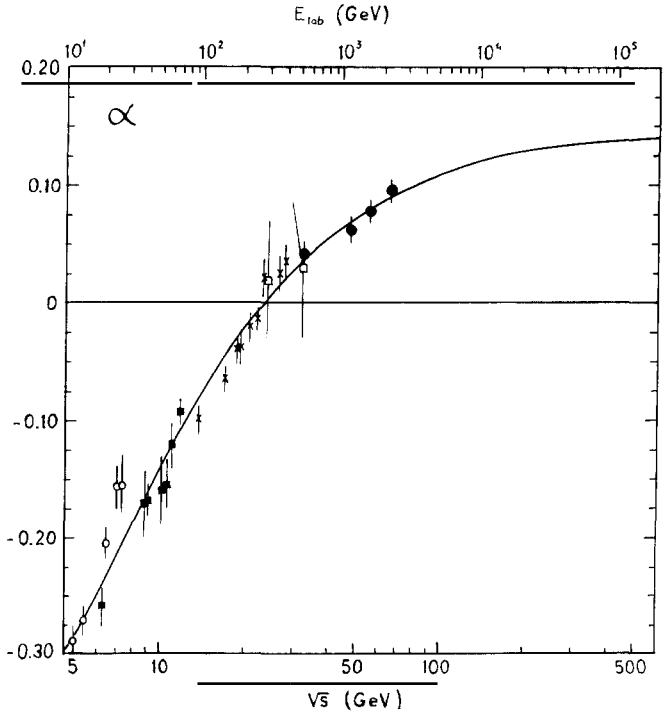

Fig. 3.2. $\alpha = \mathrm{Re}T(s,0)/\mathrm{Im}T(s,0)$ for elastic pp-scattering [93, 94].

$t \approx -0.2\,\mathrm{GeV}^2$ $\alpha'_{\mathrm{P}} = 0.13 \pm 0.02$ GeV^2 [97]. Experimental data on other elastic reactions do not contradict the assumption that the dependence of B on s is universal at energies $\geqslant 50$ GeV.

d) Both the total cross sections and the diffraction slopes rise with energy at large s, but their ratios $\sigma^{(\mathrm{tot})}(s)/B(s)$ are practically energy independent. Experimental data on $\sigma^{(\mathrm{tot})}(s)$ and $B(s)$ for all elastic reactions are in agreement (see fig. 3.4) with the relation [70]

$$\frac{2p}{\sqrt{s}}\frac{\sigma^{(\mathrm{tot})}(s)}{B(s)}C_{\mathrm{P}} = 4\pi \tag{3.2}$$

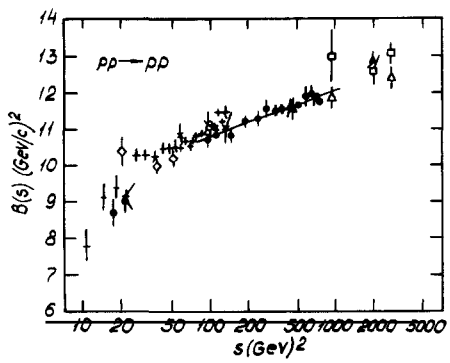

Fig. 3.3. Energy dependence of the diffraction slope for elastic pp-scattering at $(-t) < 0.1$ (GeV/c)^2 [95–97].

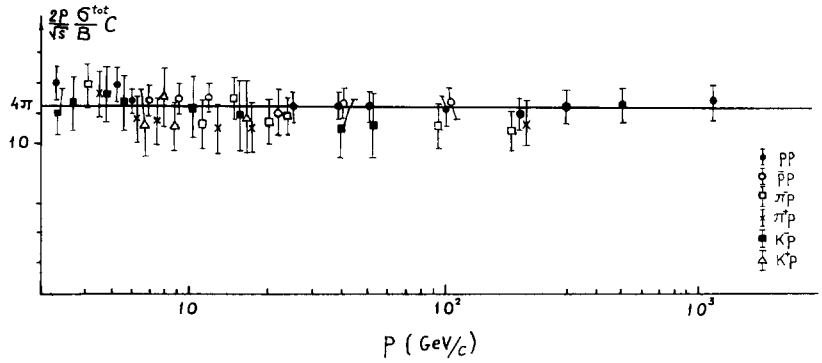

Fig. 3.4. Comparison of the relation (3.2) with experimental data.

where the quantity $C_P = 1 + \sigma_D^{(in)}(s)/\sigma^{(el)}(s)$ (see section 2.5) does not depend on energy at $E \geq 50$ GeV. It can be determined from the analysis of inelastic diffractive processes and it has been found that $C_P(\infty)$ is equal to 1.4 ± 0.1 for NN scattering, 1.6 ± 0.2 for πN and 1.7 ± 0.3 for KN-scattering [70] (C is the same for scattering of particles and antiparticles).

Taking into account, that $\sigma^{(tot)}(s) \sim \text{Im}\, f(b, s)|_{b \ll R} \cdot R^2(s)$ and $B(s) \sim R^2(s)$, where $R(s)$ is an effective radius of interaction, we can conclude from the abovementioned properties of elastic scattering, that $\text{Im}\, f(b, s)|_{b \ll R}$ does not depend on energy. From the geometrical point of view this means that at high energies the radius of interaction increases with energy, but that the opacity is energy independent and is nearly equal for ab and $\bar{a}b$ interactions (but it is different for the πN, KN and NN-interactions). The value of the opacity is probably connected with the cross section for inelastic diffractive processes.

These properties of elastic scattering can be described by the model of "geometrical scaling" [98–100]. In the framework of this model the amplitude $f(s, b)$ is written in the form

$$f(s, b) = \frac{e^{2i\delta(s, b)} - 1}{2i}, \qquad \delta(s, b) = \gamma \cdot F\left(\frac{b}{R(s)}\right), \qquad F(0) = 1 \tag{3.3}$$

where γ is a constant, which depends on the type of reaction considered.
In this case

$$T(s, t) = T(s, 0)\, \tilde{F}(R^2(s)t), \qquad \frac{d\sigma}{dt} = \frac{(\sigma^{(tot)}(s))^2}{16\pi} \bar{f}(x) \tag{3.4}$$

where $x = \sigma^{(tot)}(s) \cdot t$.

Such a behaviour of differential cross sections, the dependence of $\{1/(\sigma^{(tot)})^2\}\, d\sigma/dt$ on the variable x is in agreement with experimental data on elastic pp-scattering in a wide region of t [98], including $|t| \sim (1$ to 2) GeV^2, where $d\sigma_{pp}/dt$ has a characteristic structure with a minimum and a secondary maximum. The assumption that the amplitudes for πN, KN and NN scattering differ only by the value of the constant γ in (3.3) and that the function $F(b/R(s))$ is universal leads to a good description of the data on πN and KN-scattering at energies ≥ 100 GeV [101].

So, the investigation of elastic reactions at very high energies leads to an important conclusion in favour of the "geometrical" character of elastic diffractive scattering.

Let us now discuss the properties of elastic scattering from the point of view of the theoretical approaches to diffraction. In a Regge theory with $\alpha_P(0) = 1$ the rise of $\sigma^{(tot)}(s)$ is usually connected with

the logarithmic decrease of the PP-cut contribution. But detailed calculations in the framework of the eikonal approach [69, 88] (with due account of inelastic intermediate states) leads to too slow an increase of $\sigma^{(\mathrm{tot})}(s)$, which contradicts experimental data*. That is why models with $\alpha_{\mathrm{P}}(0) > 1$ were used recently for the description of the data on $\sigma^{(\mathrm{tot})}$ and differential cross sections for elastic reactions [88, 102, 103]. These models have the Froissart type asymptotic behaviour, but at present energies the pole term is still a dominant contribution. The asymptotic regime sets in at extremely high energies $\xi\Delta \gg 1$ ($\Delta = \alpha_{\mathrm{P}}(0) - 1 \approx 0.1$) and the present situation is very far from the asymptotic one.

Note that in the framework of the existing theoretical models geometrical scaling can be valid only approximately and must break down at higher energies. For example in the eikonal model with $\alpha_{\mathrm{P}}(0) > 1$ (2.78) the opacity or $\delta(s, b)$ at $b^2 \ll R^2(s)$ is approximately constant at present energies because

$$\delta(s, 0) \sim \left(\frac{s}{s_0}\right)^{\Delta} \Big/ \left(R_0^2 + \alpha'_{\mathrm{P}} \ln \frac{s}{s_0}\right) \approx \frac{1 + \Delta \ln(s/s_0)}{R_0^2(1 + (\alpha'_{\mathrm{P}}/R_0^2)\ln(s/s_0))} \approx \frac{1}{R_0^2}$$

for realistic values of $R_0^2 \approx \alpha'_{\mathrm{P}}/\Delta$. So the interesting question is whether the geometrical scaling is "accidental" and will disappear at higher energies† or is it a fundamental property of diffractive scattering, which is not yet understood theoretically?

3.2. *Exclusive diffractive processes*

From the theoretical point of view any process with fixed number of particles in the final state should correspond to a diffractive mechanism at $s \to \infty$. Exceptions are those reactions, where the contribution of the Pomeranchuk singularity is forbidden by quantum numbers conservation (for example $\pi^- \mathrm{p} \to \pi^0 \mathrm{n}$, $\bar{\mathrm{p}}\mathrm{p} \to \bar{\mathrm{n}}\mathrm{n}$). The range of energy $\bar{s}$, where scattering starts to show a diffractive character, depends on the number of particles n in the final state and on the mass M of the diffractively produced system. It moves to higher energies as n or M grows.

In recent years information on the properties of exclusive diffractive processes was greatly improved due to a considerable extension of the energy range, accesible for the experimental study and to the high accuracy of the data. The results of investigation of exclusive reactions with a small number of particles in the final state, $-\mathrm{NN} \to \mathrm{N}(\mathrm{N}\pi)$, $\pi\mathrm{N} \to \pi(\mathrm{N}\pi)$, $\mathrm{KN} \to \mathrm{K}(\mathrm{N}\pi)$, $\pi^{\pm}\mathrm{p} \to \pi^{\pm}\pi^+\pi^-\mathrm{p}$, $\mathrm{pp} \to \mathrm{pp}\pi^+\pi^-$, $\mathrm{K}^{\pm}\mathrm{p} \to \mathrm{K}^{\pm}\pi^+\pi^-\mathrm{p}$ etc. give a rather complete picture of the properties of diffraction dissociation:

a) The cross sections for these reactions (both total and differential) have a weak energy dependence at $E_{\mathrm{L}} \geq 50\,\mathrm{GeV}$ (figs. 2.7, 3.5, 3.6). Note, that at energies $\leq 30\,\mathrm{GeV}$ these cross sections decrease with energy and this dependence is much more pronounced than for elastic reactions. In Regge theory this decrease of the cross sections is connected with the contributions of secondary trajectories P', ρ, ω, π etc. It would be very interesting to study whether the rise of $(\mathrm{d}\sigma/\mathrm{d}t)|_{t\approx 0}$, seen in elastic reactions, takes place also for inelastic diffractive processes. It has been noted in section 2, that models with a Froissart-type behaviour for elastic amplitudes lead also to a logarithmic rise of inelastic diffractive amplitudes and $(\mathrm{d}^2\sigma/\mathrm{d}t\,\mathrm{d}M^2)_{t\approx 0} \sim \ln^2(s/s_0)$ as $s \to \infty$. At the same time models with asymptotically constant total cross sections predict the decrease of $\mathrm{d}^2\sigma/\mathrm{d}t\,\mathrm{d}M^2$ at small t with energy, because for such models $\mathrm{d}^2\sigma/\mathrm{d}t\,\mathrm{d}M^2 \sim t$ as $t \to 0$ and $s \to \infty$. So the detailed study of the energy dependence of differential cross sections for inelastic diffractive processes can give important

*It is possible to describe the rise of $\sigma^{(\mathrm{tot})}$ with $\alpha_{\mathrm{P}}(0) = 1$ if the threshold effects (see section 2.6) are taken into account [89].

†In the theory with $\alpha_{\mathrm{P}}(0) > 1$ geometrical scaling is restored again at practically inaccesible energies $\xi \sim 100$ (when $\xi\Delta \gg 1$).

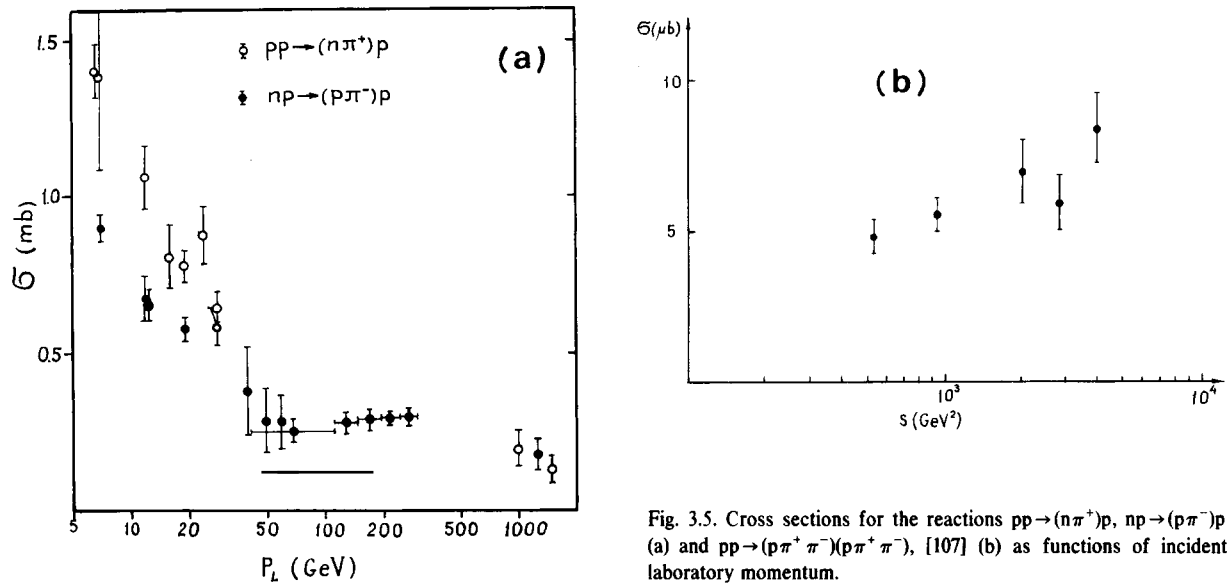

Fig. 3.5. Cross sections for the reactions $pp \to (n\pi^+)p$, $np \to (p\pi^-)p$ (a) and $pp \to (p\pi^+\pi^-)(p\pi^+\pi^-)$, [107] (b) as functions of incident laboratory momentum.

information on the character of the asymptotic behaviour of the theory. The abovementioned rise of the cross sections for inelastic diffractive reaction in most of the cases will probably take place, at higher energies than for elastic reactions. This is due to the large contributions of secondary exchanges. Nevertheless, it is possible to point out some reactions, where an early rise of the cross sections (at $E_L \geq 30$ GeV) can be expected. For example the reaction $K^+p \to K^+(n\pi^+)$ is described in the DHD-models by the diagrams shown in fig. 3.7, which are determined by the amplitudes for elastic $K^+\pi^+$ and K^+p-scattering. Both of them have exotic quantum numbers in the s-channel. So the contribution of secondary exchange is expected to be small. The same arguments can be applied to the reaction $pp \to (p\pi^+\pi^-)$ $(p\pi^+\pi^-) \to (\Delta^{++}\pi^-)$ $(\Delta^{++}\pi^-)$ and the experimental data [107] indicate a substantial increase of the cross section for this process in the ISR energy range, fig. 3.5b.

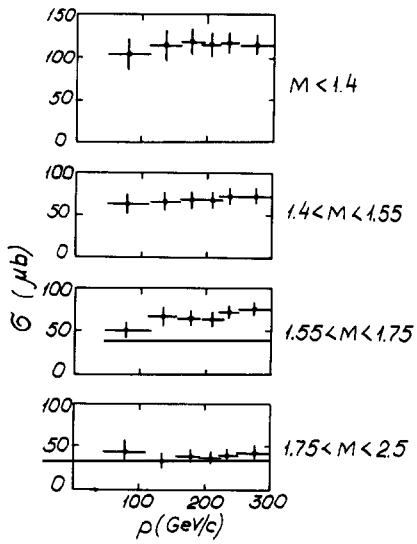

Fig. 3.6. Energy dependence of differential cross sections for the reaction $np \to (p\pi^-)p$ for different mass intervals of the $(p\pi^-)$-system [104, 105].

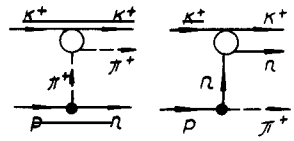

Fig. 3.7. Diagrams of the DHD-model for the reaction $K^+p \to K^+(n\pi^+)$.

b) The mass spectra of diffractively produced systems are concentrated in a region of rather small masses, i.e. $M \leqslant 2\,\text{GeV}$ (see figs. 3.8, 3.9). At higher masses the differential cross sections decrease rapidly with M (fig. 3.10). The form of the mass spectra depends weakly on the initial energy and on the type of colliding particles (figs. 3.8, 3.9). In the threshold region $d^2\sigma/dt\, dM^2$ has a maximum, which is in agreement with the predictions of the DHD-model. The structures, corresponding to the production of resonances with the same isospin (or G-parity for the nonstrange bosonic systems) as the initial particle, are seen, as well, in the mass spectra of diffractively produced systems. For example the nucleon resonances with $I = \frac{1}{2}$, N*(1520) $J^P = \frac{3^-}{2}$, N*(1688) $\frac{5^+}{2}$ and N*(2100) are produced in the nucleon diffractions dissociation $N \to N\pi$. The amplitude analysis of the diffractively produced systems [108–110] allows one to study the properties of diffraction dissociation in more detail. It has been found that the threshold enhancements in $(\rho\pi)$, $(f\pi)$, $(N\pi)$, $(\Delta\pi)$ systems have mainly non-resonance character (the phase of the corresponding partial wave amplitude has a slow variation in the region of the maximum). This is in agreement with the explanation of these enhancements in the DHD-model. In most of the cases the quantum numbers of the diffractively produced systems satisfy

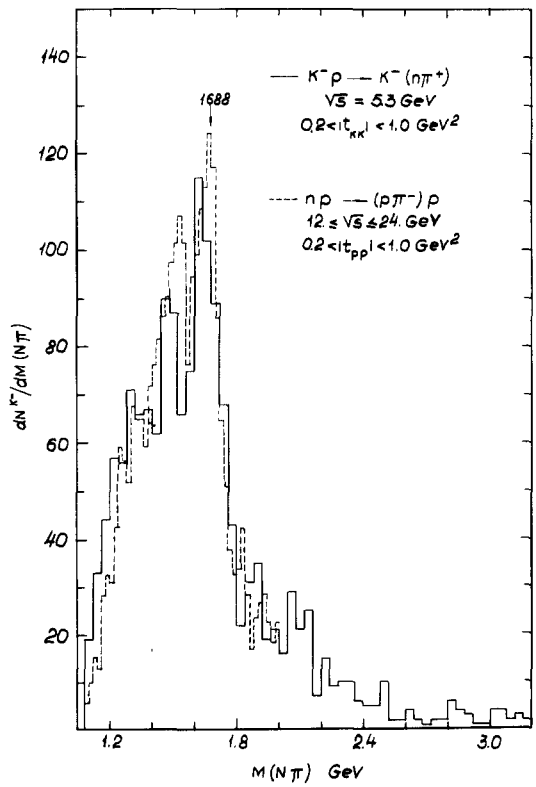

Fig. 3.8. Mass spectra of the $N\pi$-system for the reactions $np \to (p\pi^-)p$, [104] and $K^-p \to K^-(n\pi^+)$, [106].

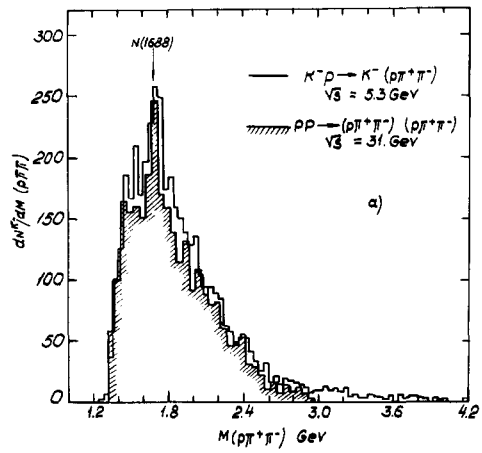

Fig. 3.9. Mass spectra of the $p\pi^+\pi^-$ system for the reactions $pp \to (p\pi^+\pi^-)(p\pi^+\pi^-)$, [107] and $K^-p \to K^-(p\pi^+\pi^-)$, [106].

the relation $\Delta P \cdot (-1)^{\Delta J} = +1$, where ΔP and ΔJ are the changes of parity and of angular momentum in the diffractive transitions $a \to a^*$ (the Morrison rule [111]). It should be pointed out however that there are some diffractive transitions which do not satisfy this rule. For example the transitions $\pi \to A_2(1310)$ (quantum numbers of A_2 $J^P = 2^+$) or the s-wave amplitude ($J^P = \frac{1}{2}^-$) in the $N\pi$-system diffractively produced in the reaction $\pi N \to \pi(N\pi)$, [109].

c) The momentum transfer t distributions depend strongly on the mass of the produced system. The slope B of the differential cross section rapidly decreases as the mass M increases (slope-mass correlation), fig. 3.11a. The strongest dependence of B on M is observed in a threshold region. The amplitude analysis shows [110], that this correlation takes place also for final states with definite quantum numbers.

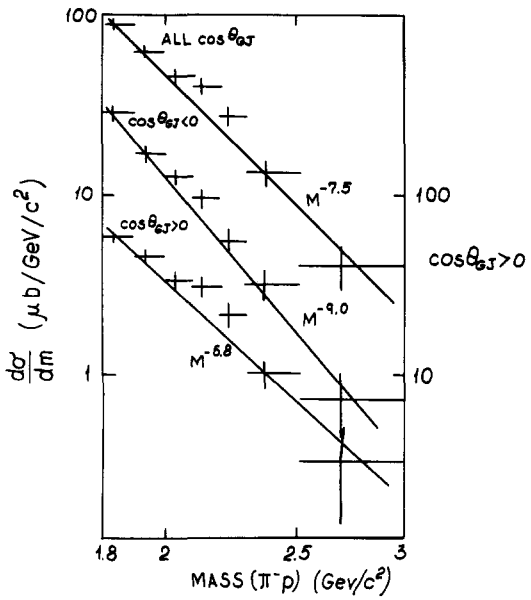

Fig. 3.10. Mass dependence of the cross section for the process $np \to (p\pi^-)p$ in the region $M_{\pi^-p} > 1.8$ GeV, [104].

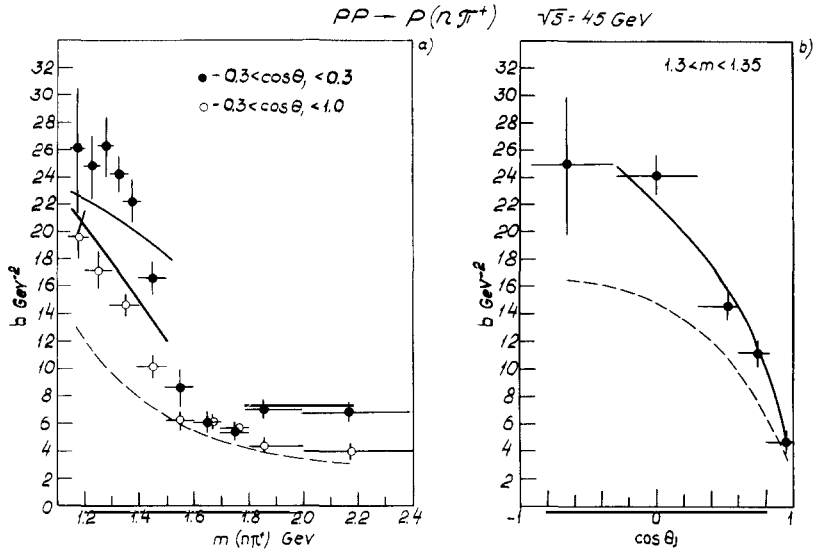

Fig. 3.11. Dependence of the slope B on $M_{n\pi^+}$ and $\cos\theta_J$ for the reaction $pp \to p(n\pi^+)$, [112]. Dashed curves are the results of calculations, based on the pion Deck model (fig. 2.5a). Full curves are obtained taking into account all the diagrams of fig. 2.5 and the effects of absorption (fig. 2.36), [74].

d) The slope B depends not only on the mass M, but also (at fixed value of M) on the $\cos\theta_J$ of the diffractively produced particle in the c.m. of the produced system (θ_J is the polar angle in the Gottfried–Jackson system). This interesting effect means that there is a correlation between the production and the decay of the hadronic system. It has been observed in the reactions $NN \to N(N\pi)$, $\pi N \to \pi(N\pi)$ [104, 112, 113], fig. 3.11.

e) There are dips and breaks in the t-distributions for the diffractive production of $N\pi$ and $N\pi\pi$ systems with small masses [112, 104, 106]. These structures depend both on the mass and the value of $\cos\theta_J$ and are closely correlated to the dependence of the slope B on M and $\cos\theta_J$. The differential cross sections $d\sigma/dt\, dM^2$ have dips at $|t| \approx (0.2\text{–}0.3)$ GeV^2, which are most clearly seen in the region $M \leqslant 1.35$ GeV and $\cos\theta_J \approx 0$. This is shown in fig. 3.12.

From the impact parameter space point of view the t-distribution of the type, shown in fig. 3.12a can arise, if $f(b)$ has a peripheral form (fig. 1.4) with $R \approx 1$ fermi. The simplest model based on the assumption that b-space distributions for inelastic diffractive processes have a universal peripheral character has been proposed in ref. [19]. In the framework of this model the dependence of the slope B on M is connected with the increase of the angular momentum of the produced system and growth of the number of helicity amplitudes with $\Delta\lambda \neq 0$ as M increases. The contributions of these helicity amplitudes to $d\sigma/dt$ have diffraction minima at higher values of $|t|$, so at $M > 1.4$ the minimum in $d\sigma/dt$ practically disappears and the slope decreases. However, the dependence of B on M for a state with definite J and the correlations between t and $\cos\theta_J$ distributions contradict this simple model.

Let us now discuss an interesting question: whether the properties c)–e) of inelastic diffractive processes correspond to the one Pomeron exchange and are connected with the structure of the vertex ($N \to N\pi$) or the peripheral character of the b-space distributions points out to the important role of absorptive effects (moving cuts)? In the framework of the DHD-model, which takes into account only the pole graphs of fig. 2.6, it is possible to explain qualitatively the properties c)–e) [74, 114–116]. In this model the minima in the differential cross sections at t-values which depend on M

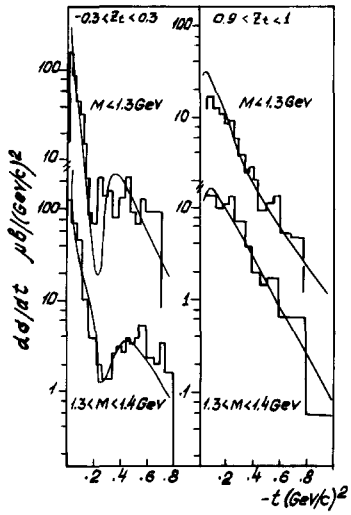

Fig. 3.12. Momentum transfer distributions for the reaction $np \to (p\pi^-)p$ for various ranges of the $p\pi^-$-mass and $\cos\theta_J$, [104]. Full curves are the predictions of the DHD -model with absorption [74].

and $\cos\theta_J$ are connected with the mutual cancellation of the graphs of fig. 2.6 in the corresponding point of phase space [114, 115] (the graphs a), b) and c) have different signs). The sharp backward peak, observed in the $\cos\theta_J$ distribution of the reaction $NN \to N(\pi N)$, [116] in the region of small masses for the $N\pi$-system (the established resonances do not contribute to this region of M), indicates the important role of baryon exchange (diagram 2.6b). It is also possible to describe qualitatively the dependence of the slope B on M in the DHD-model. An interesting dual generalization of the DHD-model, which provides the possibility to include in an economic way into the scheme production of nucleon resonances has been proposed in ref. [115]. This model reproduces the structure with minima of the differential cross section for the reaction $NN \to N(N\pi)$. However a good quantitative description of the experimental data (including normalization) for the reactions $NN \to N(N\pi)$ in the region $M < 1.4\,\text{GeV}$ (full curves in figs. 3.11, 3.12) can only be obtained [74] if rescattering effects to the pole diagrams of fig. 2.6 are taken into account. Thus the analysis of experimental data for some exclusive diffractive processes indicates that: i) the DHD-model is a good first approximation for the amplitudes of these reactions and ii) both P-pole exchange and many Pomeron cuts should be taken into account.

If the moving branch points give an important contribution to the cross sections, then the factorization property, generally speaking, does not take place. However the data on exclusive diffractive processes show that:

e) An approximate factorization of the differential cross sections is observed in diffractive reactions.

The experimental observation of independence of the M and t-distributions on the type of colliding particles in the reactions $ab \to ab^*$ (figs. 3.8, 3.9) points to the factorization of amplitudes. More complete tests of factorization in single diffraction dissociation processes can be carried out using the following relation

$$\frac{d\sigma}{dt}(ab \to ab^*) \Big/ \frac{d\sigma}{dt}(a'b \to a'b^*) = \frac{d\sigma}{dt}(ap \to ap) \Big/ \frac{d\sigma}{dt}(a'p \to a'p). \tag{3.5}$$

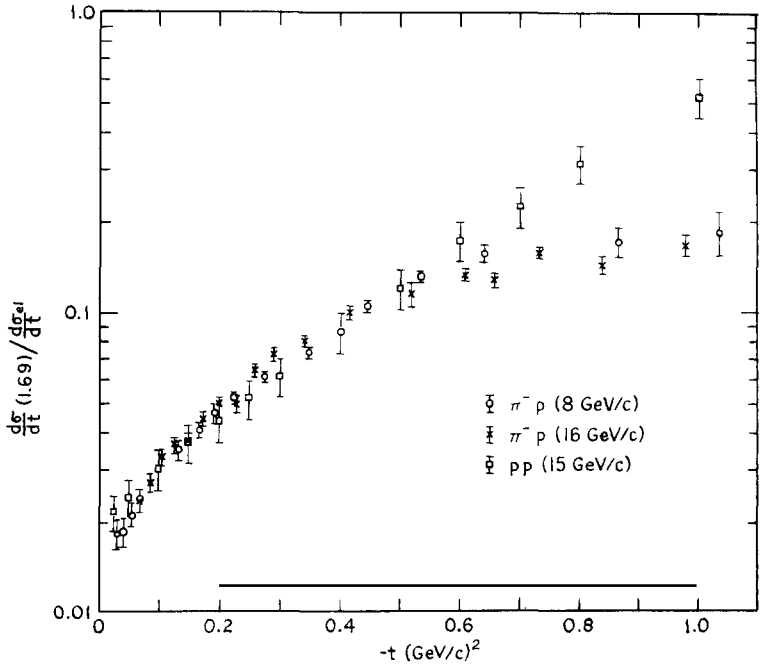

Fig. 3.13. Comparison of the experimental data on N* (1688) production in pp and πp-collisions with the factorisation relation (3.5).

For all studied reactions this relation is approximately satisfied at $|t| \lesssim 0.6\,\mathrm{GeV}^2$ (see for example fig. 3.13). Deviations from factorization in this region do not exceed usually $\approx 20\%$.

Another test of factorization, which is more sensitive to the contribution of rescattering, is the comparison of the differential cross sections for double and single diffractive dissociation (2.19). Because of the low statistics of present experiments for double diffraction dissociation processes (which have very small cross sections) a relation between the cross sections integrated over M and t is usually used

$$\sigma_{ab\to a^*b^*} = \frac{\sigma_{ab\to a^*b}\cdot\sigma_{ab\to ab^*}}{\sigma_{ab\to ab}}\cdot\frac{B_{ab\to a^*b}\cdot B_{ab\to ab^*}}{B_{ab\to a^*b^*}\cdot B_{ab\to ab}}. \tag{3.6}$$

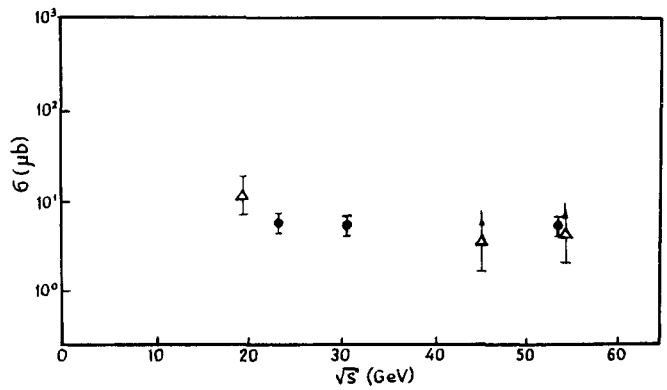

Fig. 3.14. Cross sections for the double diffraction dissociation reaction $pp\to(p\pi^+\pi^-)(p\pi^+\pi^-)$: ♦, [107] and the factorisation predictions: ⧫.

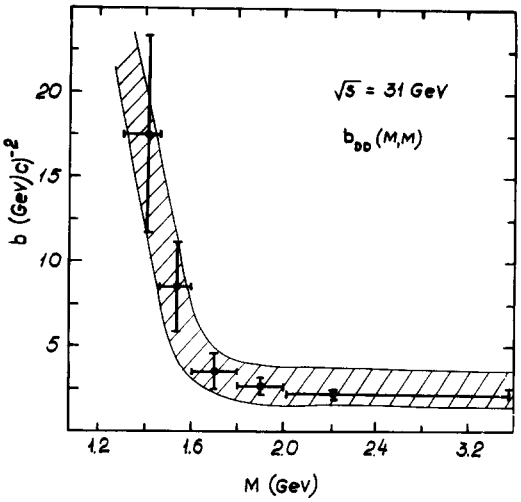

Fig. 3.15. Slope for the reaction $pp \to (p\pi^+\pi^-)\,(p\pi^+\pi^-)$, [107] versus mass of the $p\pi^+\pi^-$-system and the factorization prediction (shaded area).

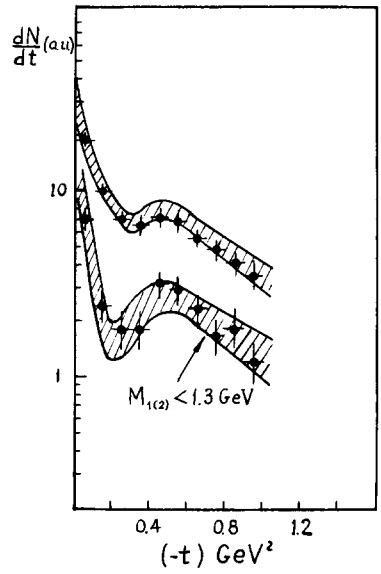

Fig. 3.16. Differential cross section for the reaction $nn \to (p\pi^-)\,(p\pi^-)$, [119]. Shaded areas are the factorization predictions, calculated from the data on the reaction $np \to (p\pi^-)p$, [104], [118] and elastic NN-scattering.

Within rather big experimental errors eq. (3.6) is in an agreement with the data, see fig. 3.14. It should be noted, that the differential cross sections are much more sensitive to deviations from factorization predictions than the integrated quantities.

If the factorization relation (2.19) is valid, then the slopes measured in different diffractive processes are related namely:

$$B_{ab\to a^*b^*} + B_{ab\to ab} = B_{ab\to a^*b} + B_{ab\to ab^*}. \tag{3.7}$$

This relation is in an agreement with experimental data on the reactions $pp \to (p\pi^+\pi^-)\,(p\pi^+\pi^-)$, $pp \to (p\pi^+\pi^-)p$ and $pp \to pp$, fig. 3.15.

A comparison of the factorization relation (2.19) with experimental data at the ISR [118, 119] on differential cross sections for the processes $np \to (p\pi^-)p$ and $nn \to (p\pi^-)(p\pi^-)$ is shown in fig. 3.16. Factorization is satisfied up to $|t| \sim 1\ \mathrm{GeV}^2$.

In subsection 3.4 we shall see, that factorization also takes place for inclusive diffractive processes.

Thus factorization is approximately satisfied for inelastic diffractive processes at $|t| \leqslant 0.5\ \mathrm{GeV}^2$. It should be noted however that, up to now, a detailed test of the factorization relations (3.5), (2.19) for different M, $\cos\theta_J$ and t-intervals has not been carried out. In particular it would be very interesting to study the dependence of the value t_0, the position of the dip of the $d\sigma/dt\ dM\ d\cos\theta_J$ differential cross section in the reactions $aN \to a(N\pi)$, $NN \to (N\pi)(N\pi)$, on the type of colliding particles. If the minimum is connected with rescattering effects the value of t_0 should differ for different reactions.

3.3. Inclusive diffractive production of particles and the Pomeron–proton total cross sections

Investigation of exclusive diffractive channels allows one to obtain complete information on the properties of inelastic diffraction. However it is more convenient to study some important charac-

teristics of diffraction using the inclusive approach to the diffractive production of particles. This approach is especially suitable for the production of large mass states, which decay into many particles. In the past few years many interesting experimental results have been obtained in this field [120–135].

The study of the inclusive spectra of particles in the reaction $a+b\to a'+X$ near the kinematical boundary $x\to 1$ (or $s_1\equiv M_X^2\ll s$) gives the possibility to determine (according to 2.14) the total cross section for Pomeron–particle interaction. In the case of the reaction $pp\to pX$ at $s\to\infty$

$$\frac{d^2\sigma}{ds_1\,dt}=\frac{(g^P_{pp}(t))^2}{2s_1}\left(\frac{s}{s_1}\right)^{2(\alpha_P(t)-1)}\cdot\sigma^{(tot)}_{Pp}(s_1,t). \tag{3.8}$$

The contributions of secondary exchanges (with $\alpha_i(0)<1$) at fixed values of s_1 decrease as some powers of s. So, if the differential cross section at $t\approx 0$ is parametrized in the form

$$\frac{d^2\sigma}{ds_1\,dt}=A(s_1)+\sum_i B_i(s_1)/s^{\gamma_i}. \tag{3.9}$$

Then the quantity $A(s_1)=(g^P_{pp}(0))^2\sigma^{(tot)}_{P_p}(s_1,0)/2s_1$ is the P-pole contribution and the parameters B_i are connected with secondary Regge-exchanges (for the π-pole $\gamma=2(1-\alpha_\pi(0))\approx 2$ for P', ω, ρ, A_2 $\gamma=2(1-\alpha_R(0))\approx 1$, the interference term PR gives $\gamma=\alpha_P(0)+\alpha_R(0)-2\approx 0.5$).

The results of the analysis of experimental data, based on this procedure [41, 70] are shown in fig. 3.17. The value of the parameter γ is found to be ≈ 1 for all masses (except the region $s_1\approx M^2_{\Delta_{33}}$, where the π-pole contribution is important). This points to the smallness of the interference (RP) term. The following parameters for the P-pole contribution to elastic pp-scattering have been used in the calculations of $\sigma^{(tot)}_{Pp}$ at $t\neq 0$,: $\alpha'_P=0.3\,\mathrm{GeV}^{-2}$, $(g^P_{pp}(t))^2=(g^P_{pp}(0))^2\exp(R^2_{pp}t)$; $(g^P_{pp}(0))^2=4\,\mathrm{GeV}^{-2}$; $R^2_{pp}=4\,\mathrm{GeV}^{-2}$. The total cross section for the Pomeron–proton interaction has maxima in the small

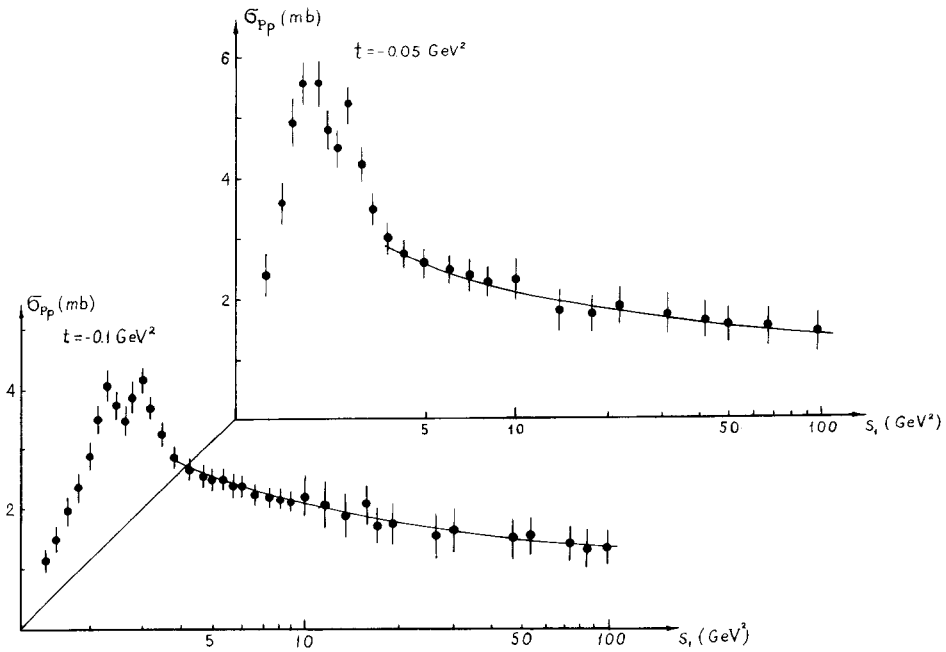

Fig. 3.17. The Pomeron–proton total cross section.

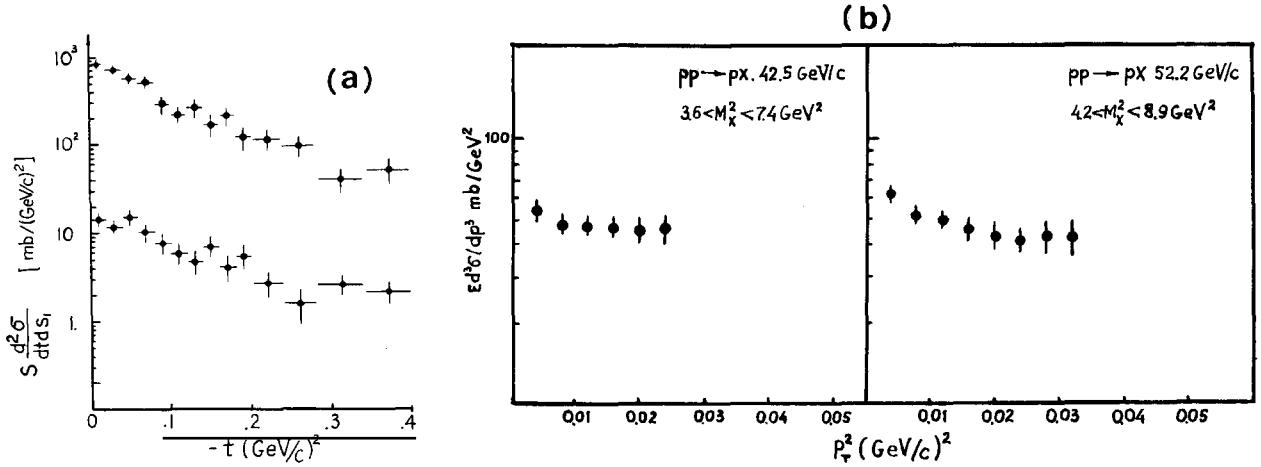

Fig. 3.18. Momentum transfer dependence of the cross sections for the reaction pp→pX (a) at incident momentum 205 GeV/c, $s_1 < 5$ GeV^2 – upper points, $10 < s_1 < 25$ GeV^2 – lower points (multiplied by 1/10) [122] and (b) at incident momentum 42.5 and 52.5 GeV/c [133].

mass region (due to resonances at $M = 1.4$ to 1.5 GeV and $M = 1.7$ GeV) and a smooth Regge behaviour for $M > (2$ to $3)$ GeV,

$$\sigma_{Pp}^{(tot)}(s_1, t) = 8\pi(g_{pp}^{P}(0)\, r_{PP}^{P}(t) + g_{pp}^{R}(0)\, r_{PP}^{R}(t)\ \sqrt{s_0/s_1}).$$

The asymptotic value of $\sigma_{Pp}^{(tot)}(s_1, t) = 8\pi g_{pp}^{P}(0)\, r_{PP}^{P}$ is close to 1 mb and is practically independent on t. Experimental data on the behaviour of diffractive production cross sections $d^2\sigma/dt\, ds_1$ in the small t-region (see for example fig. 3.18) show no evidence for a minimum in the forward direction (as can be expected in the weak coupling theory). We shall therefore assume in the following that $r_{PP}^{P}(0) \neq 0$. We thus have for the triple-Pomeron coupling $r_{PP}^{P}(t) \approx r_{PP}^{P}(0) = \sigma_{Pp}^{(tot)}/8\pi g_{pp}^{P}(0) = (0.05 \pm 0.01)\,\text{GeV}^{-1}$. In order to determine the parameters of Pomeron interactions and the value of the nondiffractive "background" for the large mass region of inclusive processes it is convenient to use the triple Regge model (2.17)

$$f = E\frac{d^3\sigma}{d^3p} = \sum_{ijk} G_{ijk}(t)\,(1-x)^{\alpha_k(0)-\alpha_i(t)-\alpha_j(t)}\left(\frac{s}{s_0}\right)^{\alpha_k(0)-1}.$$

At very high energies ($s \gtrsim 10^3$ GeV) scaling terms with $\alpha_k(0) = 1$ are the only important ones in this sum.

Experimental data on inclusive cross section

$$\frac{1}{\pi}\frac{d^2\sigma}{dt\, d(M^2/s)} = E\frac{d^3\sigma}{d^3p}$$

for the reaction pp→pX at ISR energies [121] are shown in fig. 3.19. It can be seen from this figure that:

a) The function $f = E\, d^3\sigma/d^3p$ does not depend on energy for fixed values of $M^2/s \simeq 1 - x$; within the errors of 5–10% scaling takes place at $s > 500$ GeV^2.

b) In the triple Regge region $x \to 1$ the spectra have a pronounced peak, which is consistent with the behaviour $f \sim 1/(1-x)$, expected for the triple-Pomeron interaction (see table 1).

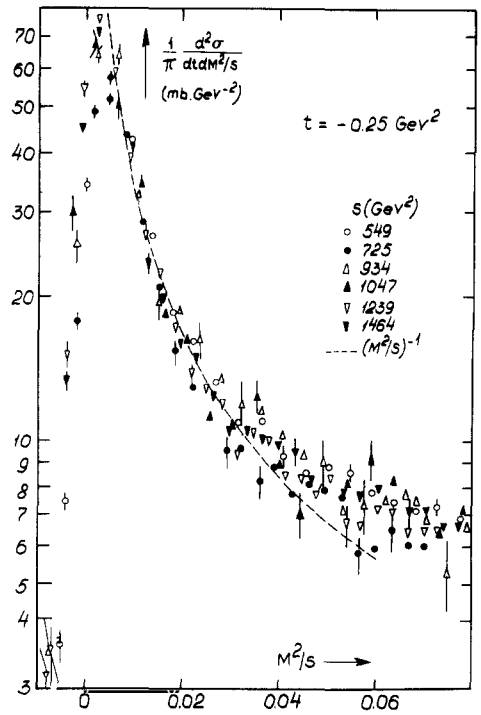

Fig. 3.19. Inclusive cross sections for the reaction pp→pX at ISR [121].

c) The function f decreases with $(1-x)$ less rapidly in the region $(1-x)>0.05$ and for $(1-x)\geq 0.1$ the spectra are practically x-independent. From the point of view of the triple-Regge model this is connected with the important role of the secondary exchanges RRP, $\pi\pi$P etc. in this region of x.

Triple-Regge analysis of experimental data on inclusive reactions have been carried out by many authors [136–141, 41, 46, 124, 131]. The Pomeron terms PPP, PPR and the secondary Regge-terms RRP, RRR, $\pi\pi$P, $\pi\pi$R are usually taken into account (sometimes the interference terms PRP, PRR are also included in the analysis). The π-exchange contribution ($\pi\pi$P and $\pi\pi$R-terms) to the reaction NN→NX can be expressed in terms of the total cross section for πN-scattering

$$\left(E\frac{d^3\sigma}{d^3p}\right)_\pi = \frac{G^2_{NN\pi}}{4\pi}\frac{(-t)}{4\pi^2(t-\mu^2)^2}(1-x)^{1-2\alpha_\pi(t)}\,\sigma^{(tot)}_{\pi N}(s(1-x))\,F^2(t). \tag{3.10}$$

The t-dependence of the form-factor $F(t)$ is determined from the analysis of exclusive processes or from the inclusive reaction pp→nX, where π-exchange dominates in the region $0.4<1-x<0.95$, [142, 38].

The triple Regge-model allows one to obtain a good description of inclusive spectra at high energies in the region $1-x<0.2$. The parameters of the model (triple-Regge vertices) are determined from fits to experimental data. The PPP-contribution, which is the most interesting one from the theoretical point of view, is reliably determined from this analysis and the value of $r^P_{PP}(0)$ is found to be $(0.05\pm 0.01)\,\mathrm{GeV}^{-1}$. This value is in an agreement with the prediction of the OPE-model, based on the diagram of fig. 2.14a [38, 45]. Let us note that secondary exchanges are usually important in the region of not too small $(1-x)$ and may describe for $(1-x)\geq 0.1$ the average effect of other mechanisms as for example the production and decay of resonances. For small values of $1-x$ ($(1-x)<0.05$) the

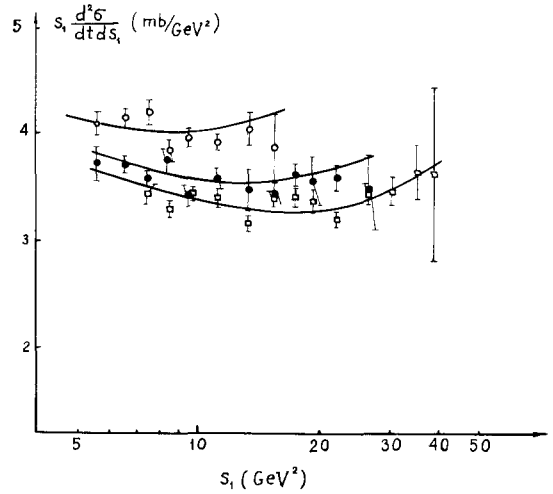

Fig. 3.20. Triple -Regge description for the reaction pp→pX. PPP, PPR and RRP terms are taken into account. Parameters of the model are given in table 2. (Cross sections, obtained from the data on the reaction pd→Xd under the assumption of factorisation [124], were multiplied by the normalization factor 1.2, which takes into account shadow corrections in deuteron [124].) ⚲ - $E = 150$ GeV, ⚲ - $E = 275$ GeV, ⚲ - $E = 385$ GeV; $t = -0.05\ \text{GeV}^2/c^2$.

nondiffractive "background" due to RRP, RRR, $\pi\pi$P-terms should be taken into account in order to extract from the data the diffractive PPP and PPR-contributions. The condition, that $s_1\,\mathrm{d}^2\sigma/\mathrm{d}s_1\,\mathrm{d}t \approx$ const for $s_1 \gg m^2$ and a fixed energy (or a narrow energy interval), which is often used as a signature for the dominance of the PPP-term, is insufficient in order to determine reliably the PPP-contribution. An energy extrapolation of the data (as given by eq. (3.9)) should be carried out for this purpose. This is connected with the fact that at the energies $E \sim 100$ GeV and $s_1 \sim 10\ \text{GeV}^2$ the RRP, RRR terms give a significant contribution to $s_1\,\mathrm{d}^2\sigma/\mathrm{d}t\,\mathrm{d}s_1$, which increases with s_1. These terms plus PPR contribution to $s_1\,\mathrm{d}^2\sigma/\mathrm{d}t\,\mathrm{d}s_1$ (which decreases with s_1) imitate the approximate constancy of the differential cross section in some interval of s_1 (the minimum of $s_1\,\mathrm{d}^2\sigma/\mathrm{d}t\,\mathrm{d}s_1$ moves to larger values of s_1 as E increases). In this case the differential cross section at fixed s_1 decreases with energy to it's asymptotic value (see fig. 3.20). Quite contradictory results can be obtained if the triple-Regge analysis is carried out in a limited range of kinematical variables E and s_1. For example in ref. [131] the PPP

Table 2

The parameters of the triple Regge description of the inclusive proton spectra. Functions $G_{iik}(t)$ are parametrized in the form $G_{iik}(t) = G_{iik}(0)\exp(R^2_{iik}t)$. This parametrization is valid in the small t-region, $|t| \leq 0.2\ \text{GeV}^2$. The RRP-term also takes into account effectively RRR-contribution, a good description of the data can be obtained for a large enough RRR-term if the value of $G_{\text{RRP}}(0)$ is decreased and $\alpha_R(0) \approx 0.4$. The π-exchange contribution ($\pi\pi$P, $\pi\pi$R) has been chosen in agreement with eq. (3.10)

	$G_{iik}(0)$ (mb/GeV²)	R^2_{iik} (GeV⁻²)	α'_i (GeV⁻²)
PPP	0.67	4	0.3
PPR	2.2	4	0.3
RRP	10.8	2	0.75

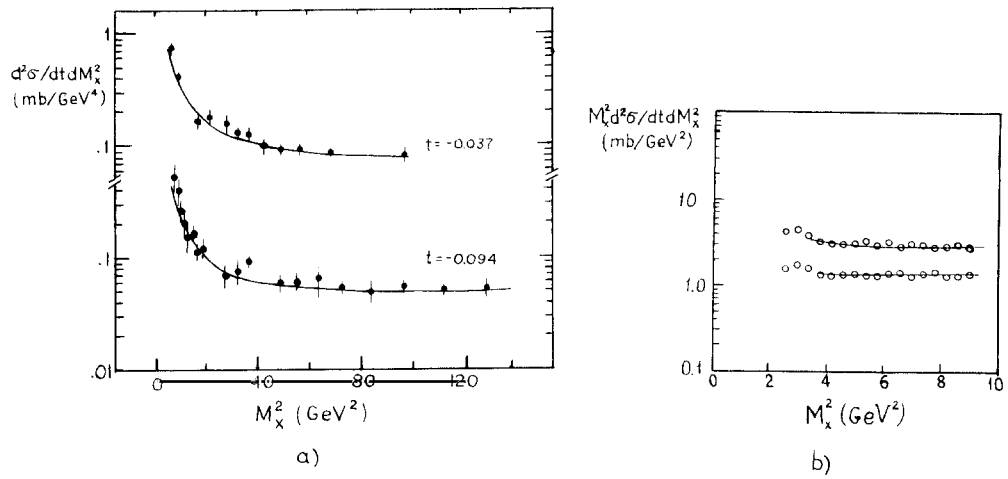

Fig. 3.21. Triple-Regge description of the data on the reaction $pp \to pX$ at energies 500 GeV (a) [128] and 140–175 GeV (b) [131], the upper curve for $\langle -t \rangle = 0.1$ (GeV/c)^2, the lower one for $\langle -t \rangle = 0.225$ (GeV/c)^2.

contribution is overestimated ($r^{\mathrm{P}}_{\mathrm{PP}}(0) = 0.15\ \mathrm{GeV}^{-1}$) on the contrary it is claimed in ref. [128] that the triple Pomeron contribution is negligible. The data of the both groups can be successfully described with $r^{\mathrm{P}}_{\mathrm{PP}}(0) = 0.05\ \mathrm{GeV}^{-1}$ taking into account the effects discussed above (fig. 3.21).

The relatively small value of the triple-Pomeron constant has important implications for the structure of Regge-theory at present energies. The dimensionless constant $(r^{\mathrm{P}}_{\mathrm{PP}}(0))^2/4\alpha'_{\mathrm{P}}(0)$ which enters the loop diagrams of Reggeon calculus (of the type shown in fig. 2.28), turns out to be very small $\sim 10^{-2}$. The characteristic expansion parameter of the theory is $\{(r^{\mathrm{P}}_{\mathrm{PP}}(0))^2/4\alpha'_{\mathrm{P}}\} \ln(s/s_0)$, so for present energies (and all practically accessible energies) the triple Pomeron interaction is small and can be taken into account. using a perturbation expansion.

It should be noted however that the value of $r^{\mathrm{P}}_{\mathrm{PP}}(0)$ has been obtained from experimental data in the pure Regge pole model, without absorption corrections. The accuracy of the data on inclusive spectra does not allow one to separate the pole and cuts contributions and the value of the $r^{\mathrm{P}}_{\mathrm{PP}}$ should be considered as an "effective" one, which also takes into account rescattering effects. The estimates of these effects in the eikonal model (fig. 3.22a) shows that the "effective" value of $r^{\mathrm{P}}_{\mathrm{PP}}(0)$ can be 2 to 3 times less than the true value of $r^{\mathrm{P}}_{\mathrm{PP}}(0)$, [143]. The graphs of fig. 3.22b (in the eikonal approximation) lead to an extra increase of $r^{\mathrm{P}}_{\mathrm{PP}}(0)$ by a factor of two to three. In this case the value of $(r^{\mathrm{P}}_{\mathrm{PP}}(0))^2/4\alpha'_{\mathrm{P}}$ becomes so large that all the diagrams with triple Pomeron interaction should be taken into account at present energies. The eikonal model probably overestimates the many Pomeron amplitudes in inelastic diffractive reaction. So we must understand better the role of Pomeron rescattering in inclusive diffractive processes

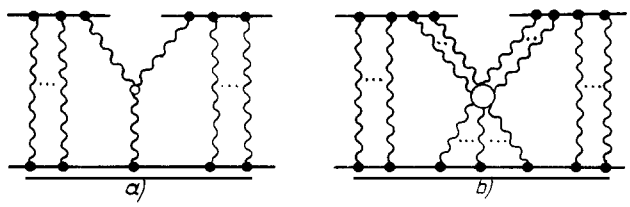

Fig. 3.22. Graphs, corresponding to absorption in the triple-Regge limit.

in order to decide whether the "bare" triple-Pomeron coupling is really small and the perturbation expansion in $r_{PP}^{P}(0)$ is valid or the strong coupling solution should be used.

3.4. Factorization and inclusive diffractive processes

Tests of the factorization relations in inclusive diffractive reactions allows one to estimate the effects of absorption for these processes. The factorization relations of the type of eq. (3.5) exist for the diffractive excitation of the shower of particles due to P-pole exchange

$$\frac{f(ab\to aX)}{f(a'b\to a'X)}=\frac{d^2\sigma}{dt\,ds_1}(ab\to aX)\Big/\frac{d^2\sigma}{dt\,ds_1}(a'b\to a'X)=\frac{d\sigma}{dt}(ab\to ab)\Big/\frac{d\sigma}{dt}(a'b\to a'b). \tag{3.11}$$

These relations are valid for arbitrary masses $\sqrt{s_1}$ of the excited system ($s_1 \ll s$). It has been shown in subsection 3.2, that the factorization relations (3.11) are in agreement with experiment in the small mass region and for $|t| \leq 0.5\ \mathrm{GeV}^2$. These relations have been checked also in the triple-Regge region $s_1 \gg m^2$. It has been shown in ref. [131] that the function $s_1\{d^2\sigma(ap\to aX)/dt\,ds_1\}/\{d\sigma(ap\to ap)/dt\}$ at energies $E \approx 150\ \mathrm{GeV}$ does not depend within errors on the type of particle a ($a = \pi^{\pm}, K^{+}, p, \bar{p}$) in the region $2.4\ \mathrm{GeV}^2 \leq s_1 \leq 9\ \mathrm{GeV}^2$ and $0.05\ \mathrm{GeV}^2 < |t| < 0.6\ \mathrm{GeV}^2$. Thus factorization is approximately satisfied even for large masses of the excited system. It should be noted however that nonfactorizable contributions due to Regge cuts and secondary exchanges can cancel to a large degree in the ratios of cross sections (3.11).

If the total cross sections for reggeons-particles interactions in the large mass region $s_1 \gg m^2$ are determined by P-pole exchange the following factorization relations should take place

$$\frac{f(ab\to aX)}{f(ab'\to aX)}=\frac{\sigma_{(ab)}^{(tot)}}{\sigma_{(ab')}^{(tot)}}. \tag{3.12}$$

In particular

$$\frac{f(\pi p\to pX)}{f(pp\to pX)}=\frac{\sigma_{(\pi p)}^{(tot)}}{\sigma_{(pp)}^{(tot)}},\qquad \frac{f(Kp\to pX)}{f(pp\to pX)}=\frac{\sigma_{(Kp)}^{(tot)}}{\sigma_{(pp)}^{(tot)}}. \tag{3.13}$$

The functions $f(\pi p\to pX)(f(Kp\to pX))$ describe the diffractive dissociation of π(K)-mesons into large mass states. These reactions correspond to protons with $x \approx -1$ in the c.m. system (slow p in the lab. system). The relations (3.12), (3.13) also agree with experiment (with an accuracy~20%).

It has been already emphasized in subsection 3.2, that the double diffraction dissociation processes are especially suitable for factorization tests. If factorization is valid, the differential cross section for the inclusive diffractive production of two showers in pp-collisions can be written in the form

$$\frac{d\sigma_{DD}}{ds_1\,ds_2\,dt}=\frac{1}{16\pi}\,\sigma_{Pp}^{(tot)}(s_1,t)\,\sigma_{Pp}^{(tot)}(s_2,t)\left(\frac{s\cdot m^2}{s_1\cdot s_2}\right)^{2(\alpha_P(t)-1)}. \tag{3.14}$$

The analysis of inclusive single diffraction dissociation shows that $\sigma_{Pp}^{(tot)}(s_1,t)$ practically does not depend on t for $s_1 \geq 3\ \mathrm{GeV}^2$. This means that the differential cross section for double diffractive production of two large mass states must have a weak t-dependence with a slope $B = 2\alpha_P' \ln(s\cdot m^2/s_1\cdot s_2)$ (for $s\cdot m^2/s_1\cdot s_2 \approx 20$, $B \approx 2$).

The investigation of the double diffraction dissociation of large masses states ($\xi_1, \xi_2 > \xi_0$) is very difficult at present energies. This is due to kinematical limitations ($\xi > 2\xi_0 + \Delta_0$) and to the smallness of

the diffractive contribution, which should be separated from a large nondiffractive background. This cross section in pp-collisions, calculated according to eq. (2.21) with $r^{P}_{PP}(0) = 0.05\,\mathrm{GeV}^{-1}$ is only ~ 0.1 mb at $s \sim 10^3\,\mathrm{GeV}^2$ while it reaches the value of 1 mb at $s \sim 10^6$ GeV.

Double diffraction dissociation is now studied in the processes $pp \to (p\pi^+\pi^-)X$, $pp \to (\Lambda^0 K^+)X$ [135] for not too large masses of one of the showers ($p\pi^+\pi^-$ and $\Lambda^0 K^+$ systems are mainly concentrated in the region $s_1 \approx (2 \text{ to } 4)\,\mathrm{GeV}^2$). Inclusive distributions as functions of $x = 2p_i/\sqrt{s}$, where p_i is the total momentum of the $p\pi^+\pi^-$ or $\Lambda^0 K^+$ system, have a pronounced peak at $x \to 1$, which can be interpreted as a manifestation of the diffraction excitation of the systems $p\pi^+\pi^-(\Lambda^0 K^+)$ and X. In agreement with the factorization prediction, the mean value of the slope in the process $pp \to (p\pi^+\pi^-)X$ is small $B = (2.2 \pm 0.2)\,\mathrm{GeV}^{-2}$[135]. More detailed comparison with factorization has been carried out in ref. [135]. If factorization is valid then all ratios $R_i = \{d\sigma(pp \to ip)/dt\}/\{d\sigma(pp \to iX)/dt\}$, where i is any hadronic system ($i = p$, $p\pi^+\pi^-$, $\Lambda^0 K^+$), should be equal. The comparison of this factorization prediction with experimental data is shown in fig. 3.23. Factorization is satisfied in the region $0.15 < |t| < 0.5\,\mathrm{GeV}^2$. There is an apparent violation of the factorization relation $R_p = R_{p\pi^+\pi^-}$ for $|t| > 0.5\,\mathrm{GeV}^2$. It is mainly connected with a fast decrease of $d\sigma(pp \to pp)/dt$ in this t-region.

The agreement of the factorization relations with experimental data on inelastic diffractive processes indicates that the cut contributions are possibly less important in the region $|t| < 0.5\,\mathrm{GeV}^2$, than predicted by the eikonal model. However more detailed tests of factorization for different mass intervals of the excited systems are needed before a final conclusion can be reached. It is also interesting to study from this point of view the region of very small t ($|t| \lesssim 0.1\,\mathrm{GeV}^2$).

3.5. Energy dependence of the total inelastic diffractive cross section

The total cross section for diffractive production of large mass states increases with energy and it is interesting to face the question, – whether the rise of $\sigma_D^{(in)}$ can explain the rise of the total cross sections at high energies? Consider the case of pp-interaction which is studied in the largest energy range. For pp-collisions the cross section for the diffractive excitation of low mass systems has a weak energy dependence and is equal to (2.5 to 3) mb*. The cross section for the diffractive

*Here and in the following the numbers correspond to the diffractive production of particles in both hemispheres in the center of mass system.

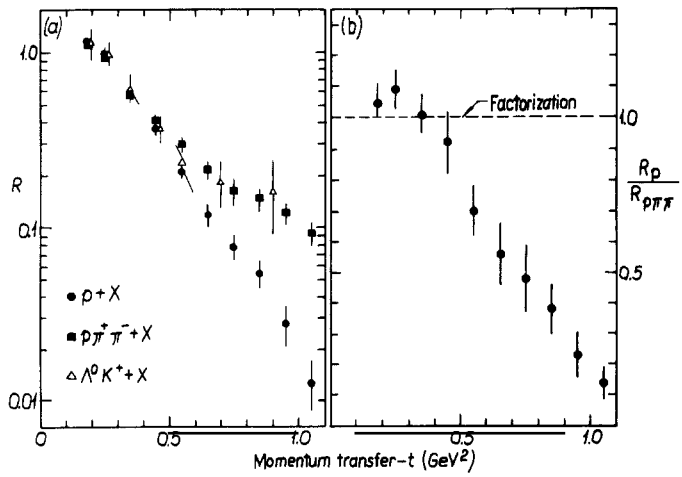

Fig. 3.23. Test of factorization in the inclusive processes of double diffractive dissociation [135].

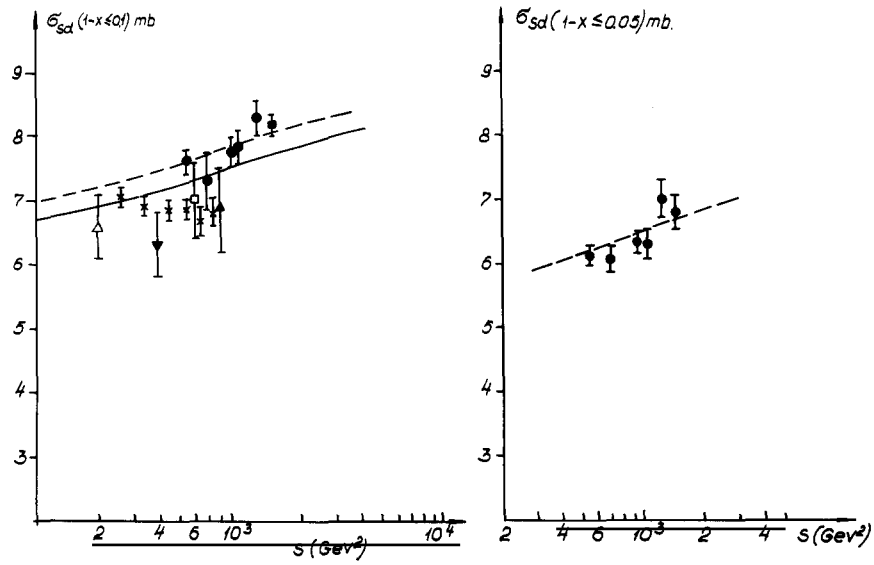

Fig. 3.24. Energy dependence of the cross section in the diffractive region [121]. The curvature in the t-dependence of diffractive production of high masses [121] is taken into account in theoretical calculation (full curve). The same curvature is assumed for low masses ($M^2 \leq 4\,\mathrm{GeV}^2$), dashed curve.

production of a shower with large mass $5\,\mathrm{GeV}^2 < s_1 < 0.1\,s - \sigma_{PP}^{P}$ increases by ≈ 3 mb as the energy changes from $E_L = 30\,\mathrm{GeV}$ to $E_L = 2 \times 10^3\,\mathrm{GeV}$ and it seems at first sight that the rise of σ_{PP}^{P} can explain nearly all the increase of $\sigma_{in}^{(tot)}(pp)$, which rises by 3.3 mb in the ISR energy range. However the main part of the increase of σ_{PP}^{P} comes from the energy range $E_L < 200\,\mathrm{GeV}$; over the ISR energy range the rise of this cross section is relatively small ≈ 1.3 mb. Moreover there are background contributions in the "diffractive" part of the inclusive spectra ($x \geq 0.9$), which decrease with energy (for example RRR and $\pi\pi R$-terms). So the rise of the inelastic cross section in the region $|x| > 0.9$ is about 1 mb in the ISR energy range. A calculation based on triple Regge phenomenology is compared with the data of FNAL and ISR in fig. 3.24. The curve reproduces the absolute value and the energy dependence of the single shower production cross section (the theoretical predictions have a scale error $\approx 10\%$).

The total double diffractive cross section can be calculated from the data on single diffraction excitation using the factorization relation (2.19). It is found to be $\approx$ (1.8 to 2) mb at $s \sim 3 \times 10^3\,\mathrm{GeV}^2$*. It rises by ≈ 0.7 mb over the ISR energy range. Thus the total increase of the cross section for inelastic diffraction from $s = 5 \times 10^2\ \mathrm{GeV}^2$ to $s = 3 \times 10^3\,\mathrm{GeV}^2$ is equal to (1.5 to 2) mb.

3.6. *Properties of diffractively produced systems of particles*

Consider now the characteristics of the particles, produced in diffraction dissociation processes. In the framework of the multiperipheral approach the shower of particles with a large invariant mass $s_1 \gg m^2$ which is produced in a P-particle collision, must have the same structure as

*The value $\sigma_{DD} = (5.0 \pm 0.8)$ mb, which has been found in ref. [135] seems to be overestimated because: a) non-diffractive background has not been separated out, b) factorization relation for cross sections integrated over masses of showers, which is not valid for large masses of the produced states, has been used in ref. [135].

the usual multiperipheral configuration in hadronic collisions (small means transverse momenta, flat rapidity distributions in the rapidity interval of the shower, i.e. $\ln(s_1/m_b\bar{\mu}_T)$). In this model such characteristics of the diffractively produced shower as $\langle n_{ch}\rangle$, σ_n, f_2 and so on do not depend on s. They are determined only by the value of s_1 and are analogous to the corresponding quantities for particle collisions at $s = s_1$, [144–146]. In particular the mean multiplicity of particles logarithmically depends on s_1 at large s_1

$$\langle n\rangle_{s_1} = a \ln(s_1/s_0) + b \tag{3.15}$$

and the coefficient a must be equal to that found for πp (pp) collisions. This should be compared with the predictions of models, where diffractively produced clusters of particles decay isotropically according to the statistical mechanism and $\langle n\rangle_{s_1} \sim \sqrt{s_1/s_0}$.

Experimental information on the mean multiplicity of charged particles produced in the inclusive reactions pp→pX as a function of the mass of the system X [34] is shown in fig. 3.25. It follows from this figure that $\langle n\rangle$ increases with s_1 approximately logarithmically (dependence of the type $\langle n\rangle_{s_1} \sim \sqrt{s_1/s_0}$ is excluded by the data) and practically does not depend on the initial energy. The full curve in fig. 3.25 is the prediction of the pion-exchange model (OPER) [38].

Thus the behaviour of the mean multiplicity of the shower is a strong argument in favour of it's multiperipheral structure. The analysis of experimental data on inclusive processes [146] shows that not only $\langle n\rangle_{s_1}$ but also other characteristics of the shower, such as multiplicity distributions σ_n, correlation parameters, rapidity (or x) distributions are analogous to the corresponding characteristics of the final states observed in standard particle collisions. The properties of particles produced in Pomeron–proton collisions are in particular similar to those found for γp-interaction (see fig. 3.26). This observation points out to an analogy between the Pomeron and photon interactions [145]. The following experimental facts also show that the interactions for these two objects of a completely different origin may be very similar:

a) The dependence of the Pomeron residues on t in pp-elastic scattering is close to the behaviour of the electromagnetic form-factors of the proton.

b) Weak t dependence of $\sigma_{Pp}^{(tot)}$ for $s_1 \geq 3\,\text{GeV}^2$. This is similar to that observed in the process of electroproduction. These two facts can be qualitatively understood in the framework of the quark–parton model.

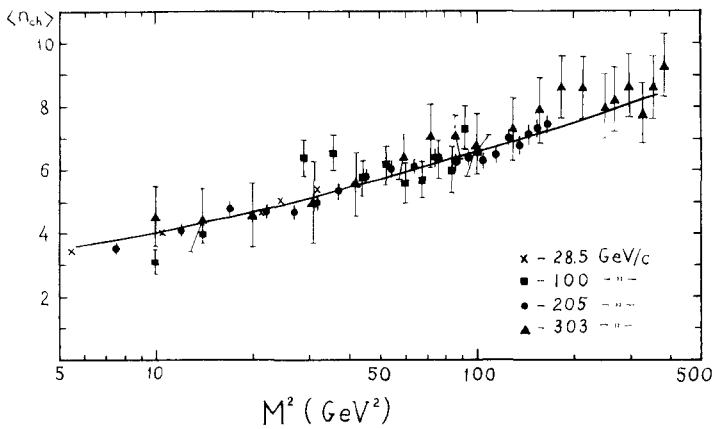

Fig. 3.25. Mass dependence of the mean multiplicity of charged particles in the process pp→pX. The full curve is the prediction of the OPER-model [38].

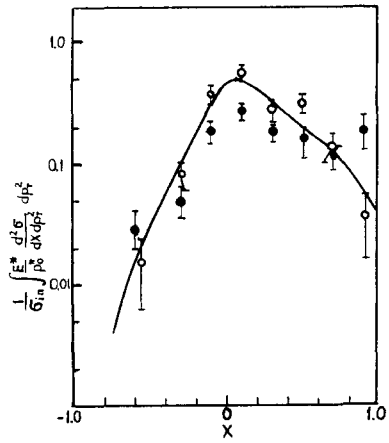

Fig. 3.26. Comparison of inclusive π^- spectra in the reactions $pp \to p\pi^- X$: ⊻, $20 < M_X^2 < 50\,\text{GeV}^2$; ⧫, $11 < M_X^2 < 20\,\text{GeV}^2$ and $\gamma p \to \pi^- X$ (full curve) [146].

Interesting data on the characteristics of the particles of the diffractively excited shower have been obtained at the ISR [147]. The rapidity distribution of charged particles for large values of s_1 (in the diffractive region $s_1/s \ll 1$) has a central plateau, which is practically intependent on t. This fact indicates that the mechanism of diffractive production does not change appreciably up to $|t| \approx 1\,\text{GeV}^2$. As the relative contributions of the many Pomeron exchange amplitudes increase with $|t|$ and each P-pole can produce particles, we would expect that the mean multiplicity and the height of the plateau for the excited cluster should increase with $|t|$, if the many Pomeron cuts were important. Thus present experimental observation points to a dominance of the P-pole contribution up to $|t| \sim 1\,\text{GeV}^2$.

Investigation of the azimuthal distribution of particles for the diffractively excited system shows an approximate t-channel helicity conservation.

3.7. Double Pomeron exchange

In the preceding subsections we have considered experimental information on single Pomeron exchange processes. One of the main results, which has been obtained in this field, is the experimental discovery of the triple-Pomeron interaction. The very high energies available now at ISR, FNAL, SPS make possible the experimental investigation of a completely new class of diffractive reactions, namely double Pomeron exchange reactions. It has been already pointed out in section 2, that the question of the existence of the DPE-mechanism is very important from the theoretical point of view. Experimental study of the DPE-mechanism (if it will be firmly established) would help to clarify many properties of the Pomeranchuk singularity.

In order to separate the DPE contribution from a nondiffractive background one should study final state configurations with two large rapidity gaps Δ_1, $\Delta_2 \gg 1$ (fig. 2.20). We have seen already that a clear separation of the diffractive mechanism is rather difficult even for the case of single Pomeron exchange (one large rapidity gap). For the DPE process the kinematical limitations (the total rapidity interval at present energies is less then 8) make this problem more difficult. It should also be kept in mind that the experimental cuts, which are imposed in order to separate the DPE-mechanism (Δ_1, $\Delta_2 > \Delta_0$ or Δ_1, $\Delta_2 = \frac{1}{2}(\xi - \xi_0)$) not only reduce the nondiffractive background, but somewhat distort the rapidity distributions and strongly influence the value of the cross section arrived at for the DPE-events.

It is convenient to describe inclusive double-Pomeron exchange in terms of the variables $\xi_1' = \ln 1/(1-x_{a'})$, $\xi_2' = \ln 1/(1-x_{b'})$ [148]. The boundary of the physical region on the ξ_1', ξ_2'-plot (the line FG in fig. 3.27) moves to the right as ξ increases because $\xi_1' + \xi_2' = \xi + \xi_M$. The kinematical region, where DPE is valid is shown by a hatched area in fig. 3.27 ($\xi_i' > \Delta_0$, $\xi - \xi_i' > \xi_0$)*. Lines of constant $M_\perp^2$ are parallel to the line FG.

In order to exclude the ξ_M dependence of the amplitudes it is convenient to introduce the new variables $\xi_M = \xi - \xi_1' - \xi_2'$ and $Y = \frac{1}{2}(\xi_2' - \xi_1')$ and to consider cross sections at fixed ξ_M. Then in the process $pp \to pXp$ the differential cross section for the production of a central cluster with "center" Y and "dimension" ξ_M has the form (at $q_1 \approx q_2 \approx 0$)

$$\frac{d\sigma}{dY\, d\xi_M\, d^2q_1\, d^2q_2} = \frac{1}{(2\pi)^2}\Big\{(g^P_{pp}(0))^4 \sigma^{(tot)}_{PP}(\xi_M) + (g^P_{pp}(0)\, g^R_{pp}(0))^2\, \sigma^{(tot)}_{PR}(\xi_M) 2\mathrm{ch}\, Y \exp\Big[-\frac{(\xi-\xi_M)}{2}\Big] + (g^R_{pp}(0))^4\, \sigma^{(tot)}_{RR}(\xi_M) \exp[-(\xi-\xi_M)]\Big\}. \quad (3.16)$$

The PP, PR and RR-interactions are taken into account in eq. (3.16). At fixed values of ξ_M and Y the PR and RR terms decrease as $1/\sqrt{s}$ and $1/s$ correspondingly as the energy increases. The terms, which are due to an interference between P and R-exchanges, can also contribute to the differential cross section†. These terms decrease with energy (at fixed ξ_M, Y) as $s^{-1/4}$.

It is clear from eq. (3.16) that in order to determine the DPE-contribution it is necessary to study the energy dependence of the differential cross section at fixed value of ξ_M. The only contribution which does not depend on energy is the DPE-term. Note that the PR-term, contrary to the DPE, leads to a strong Y-dependence of the cross section. The PR and RR-contributions to eq. (3.16) can be estimated for large M^2 in the framework of the triple Regge model (fig. 2.23), using the vertices determined from the analysis of the single-particle inclusive spectra. These estimates show (see for example [149, 150]) that up to the highest ISR-energies the background contribution, connected with PR and RR-terms is rather substantial. Nevertheless careful experimental analysis of the s and Y dependences of the differential cross sections allows one to separate different terms and to determine the value of the DPE-contribution.

The DPE has been studied at very high energies by several experimental groups [151–156]. The results depend strongly on the experimental cuts, imposed on data in order to separate the DPE. Note

*The conditions $\xi - \xi_i' > \xi_0$ are automatically satisfied if Δ_0 is chosen to be sufficiently large. However in practice $\Delta_0 \approx 2$ and it is necessary to impose the conditions $\xi - \xi_i > \xi_0$ in order to exclude the non-Regge region.

†The analysis of single diffraction dissociation shows that the interference terms are not very important. An estimate of the P–P′-interference terms for the DPE-processes can be carried out using the OPE-model (fig. 2.21). The calculation [55] points out that these terms are essential up to ISR-energies.

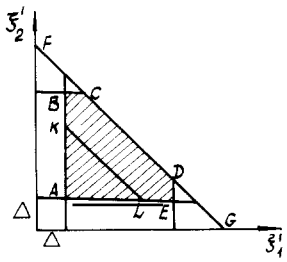

Fig. 3.27. Kinematical region of DPE (shaded area) on the ξ_1', ξ_2'-plot.

that if the condition $\Delta_1, \Delta_2 > \Delta_0$ is used, then the DPE cross section must increase with s (at present energies) due to the increase of the available phase space (hatched area in fig. 3.27). On the other hand if the final pions are measured in a limited rapidity interval in the c.m. system ($\Delta_{1(2)} \geqslant \frac{1}{2}\xi - a$, a is fixed) the behaviour of the cross section is then determined by the energy dependence of the matrix element (does not depend on s for DPE) [13, 149, 157]. The results of the experiments performed at ISR, where the DPE mechanism has been studied in the reaction $pp \to pp\pi^+\pi^-$ are shown in fig. 3.28 together with the theoretical predictions. Experimental data show that events of the reaction $pp \to pp\pi^+\pi^-$ in the region $|x_{ip}| > 0.9$ and $|y_{\pi i}| < 1$ satisfy to the criteria for DPE, i.e. a weak energy dependence and a flat Y-distributions. It has been also observed, that: a) the momentum transfer $t_1 = -q_1^2$ and $t_2 = -q_2^2$ distributions are factorized and have a slope $B = (6 \text{ to } 7)\ \text{GeV}^{-2}$, b) there are no correlations between the transverse momenta of the final protons, c) the mass distributions of the $\pi^+\pi^-$-system have a threshold maximum at $M \approx 0.5$ GeV in agreement with the OPE-prediction, d) the angular distributions of pions in their rest frame are approximately isotropic.

Thus the experimental data strongly indicate the existence of the DPE-mechanism with a cross section which is close to the theoretical estimates. However a more detailed investigation of the energy dependence of the differential cross sections at fixed values of M^2, q_1 and q_2 is needed for a final conclusion.

If the existence of the DPE would be firmly established it would then be very interesting to study the following properties of the PP-interection.

a) The total cross section of PP-interaction $\sigma_{PP}^{(tot)}(\xi_M)$ and different exclusive channels, $-\pi^+\pi^-$, $\pi^0\pi^0$, $K\bar{K}$, $p\bar{p}$ etc.

b) The behaviour of the DPE at small values of t_i.

c) The factorization relations (2.34) in the large M^2 region. These relations are sensitive to Regge-cut contributions.

d) The properties of the particles, produced in PP-interaction namely $\langle n \rangle_{M^2}$, $\sigma_n(M^2)$, $d\sigma_i/dy$ and so on.

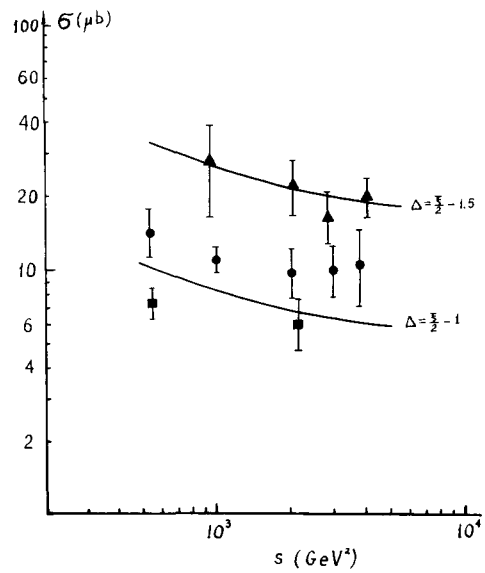

Fig. 3.28. Cross section for the reaction $pp \to pp\pi^+\pi^-$ in the DPE-region. Theoretical calculation (curves) takes into account the "background" contribution and kinematical cuts of the experiments: ▲ [154], $\Delta_1 = \Delta_2 = \frac{1}{2}\xi - 1.5$; ◆ [156] and ◆ [155], $\Delta_1 = \Delta_2 = \frac{1}{2}\xi - 1$.

e) The phase shifts for the partial waves of the $\pi\pi(K\bar{K})$ system. The phase-shift analysis would allow one to clarify the structure of the amplitude $PP \to \pi\pi(K\bar{K})$.

3.8. Summary and conclusions

In this article some of the recent experimental results in the field of inelastic diffraction, which have important implications for the nature of the Pomeranchuk singularity, have been discussed. We have considered theoretical approaches to the problem of diffractive scattering. Special attention has been paid to Reggeon theory which provides a unified framework for the description of a large class of low p_T phenomena at high energies. One of the main problems of this approach is connected with the role of Regge-cuts in the amplitudes for diffractive processes. The present situation is very peculiar, some experimental facts (such as the "geometrical" character of diffractive scattering, structures in the momentum transfer distributions etc.) point out to an important role of Regge cuts; on the other hand an approximate factorization takes place. Thus the detailed test of the factorization relations is one of the main experimental problems in this field. Investigation of the energy behaviour of the differential cross section for inelastic diffractive reactions with a good accuracy (in order to establish reliably the rise of these cross sections with energy at $s \sim 10^3\,\mathrm{GeV}^2$) and clear experimental separation of the DPE-mechanism are also important issues for the theoretical understanding of diffractive scattering.

Gribov's Reggeon calculus method allows one to study the properties of many-Pomeron exchange amplitudes and to establish their connection with t-channel and s-channel unitarity. However many important parameters (Regge trajectories, residues, reggeon vertices etc.) are not fixed by the theory and a new method for reliable estimates of the unknown parameters of the Reggeon theory is needed. This question is also closely related to the problem of the asymptotic behaviour of the theory. It is possible that the solution of these problems will follow from the future development of quantum field theory. The best candidate for the underlying theory of strong interactions is the quantum chromodynamics: the non-Abelian gauge theory of quarks and gluons. In this theory the Pomeron can be closely related to the gluon structure of hadrons and the character of the gluon–gluon interaction.

Acknowledgements

I would like to acknowledge valuable conversations with K.G. Boreskov, V.N. Gribov, E.M. Levin, L.A. Ponomarev, K.A. Ter-Martirosyan and V.A. Khoze.

References

[1] E.L. Feinberg and I.Ya. Pomeranchuk, Suppl. Nuovo Cim. 3 (1956) 652.
[2] M.L. Good and W.D. Walker, Phys. Rev. 120 (1960) 1854.
[3] J. Pumplin, Phys. Rev. D8 (1973) 2899.
[4] L. Caneschi, P. Grassberger, H.I. Miettinen and F. Henyey, Phys. Lett. 56B (1975) 359.
[5] U.P. Sukhatme and F.S. Henyey, Nucl. Phys. B108 (1976) 317.
[6] K. Fialkowski and H.I. Miettinen, Nucl. Phys. B103 (1976) 247.
[7] M. Baker and K.A. Ter-Martirosyan, Phys. Reports 28C (1976) 3.
[8] K.A. Ter-Martirosyan, Preprints ITEP No. 70, 71 (1975); No. 7, 11, 133, 134, 135, 158 (1976).
[9] K. Gottfried, Preprint CERN TH 1564 (1973);
H. Bingham, Acta Phys. Polon. B3 (1972) 31;

H.J. Lubatti, Acta Phys. Polon. B3 (1972) 721;
G. Grammer Jr. and J.D. Sullivan, Preprint ILL-(TH)-77-20.
[10] H.I. Miettinen, Plenary Session Talk at the EPS Intern. Conf. on High energy physics, Palermo, 1975, Preprint CERN TH. 2072 (1975).
[11] M. Derrick, ANL-HEP-CP-75-52.
[12] D.W.S. Leith, SLAC-PUB-1646 (1975).
[13] A.B. Kaidalov, Proc. XVIII Intern. Conf. on High energy physics, Tbilisi (1976) vol. 1, A1-27.
[14] U. Amaldi et al., Annual Reviews of Nuclear Sciences 26 (1976) 385.
[15] H.I. Miettinen, Preprint CERN TH. 1906 (1974).
[16] T.T. Chou and C.N. Yang, Phys. Rev. 170 (1968) 1591; Phys. Rev. Lett. 20 (1968) 1213.
[17] L. Durand III and R. Lipes, Phys. Rev. Lett. 20 (1968) 637.
[18] G.L. Kane, Acta Phys. Polon. B3 (1973) 845.
[19] S. Humble, Nucl. Phys. B76 (1974) 137; B86 (1975) 285.
[20] M. Froissart, Phys. Rev. 123 (1961) 1053.
[21] B. Knapp et al., Phys. Rev. Lett. 34 (1975) 1040;
T. Nash et al. Phys. Rev. Lett. 36 (1976) 1233.
[22] R.L. Anderson et al., Phys. Rev. Lett. 37 (1977) 263.
[23] E.M. Levin and L.L. Frankfurt, Pisma JETP 2 (1965) 105;
H.J. Lipkin and F. Scheck, Phys. Rev. Lett. 16 (1966) 71;
J.J.K. Kakkedee and L. Van Hove, Nuovo Cim. 42A (1966) 711.
[24] E.M. Levin and V.M. Schechter, Proc. IX Winter School on Nucl. and elementary particles, Phys. LIYF, vol. 3 (1974) 28;
V.M. Schechter, Proc. IV School of Phys. ITEP, Moscow, Atomisdat, vol. 4 (1976).
[25] S. Pokorski and L. Van Hove, Acta Phys. Polon. B5 (1974) 229;
L. Van Hove and S. Pokorski, Nucl. Phys. B86 (1975) 243;
L. Van Hove, Acta Phys. Pol. B7 (1976) 339.
[26] L. Van Hove and K. Fialkowski, Nucl. Phys. B107 (1976) 211.
[27] L. Van Hove, Nucl. Phys. B122 (1977) 525.
[28] F.E. Low, Phys. Rev. D12 (1975) 163.
[29] S. Nussinov, Phys. Rev. D14 (1976) 246.
[30] G.L. Kane and York-Peng Yao, Preprint UM HE 77-44;
G.L. Kane, Preprint UM HE 77-45.
[31] VN. Gribov, Sov. Phys. JETP 14 (1962) 478, 1395:
G.F. Chew and S. Frautschi, Phys. Rev. Lett. 7 (1961) 394;
R. Blankenbecler and M.L. Goldberger, Phys. Rev. 126 (1962) 766.
[32] T. Regge, Nuovo Cimento 14 (1959) 951.
[33] D. Amati, A. Stanghellini and S. Fubini, Nuovo Cimento 26 (1962) 896.
[34] E.M. Levin and M.G. Ryskin, Proc. 1 School of Physics ITEP, Moscow, Atomisdat (1973) vol. 2, p. 42;
L. Foa, Physics Reports 22 (1975) 1;
A.B. Kaidalov, Proc. 2 School of Physics ITEP, Moscow, Atomisdat (1975) vol. 3, p. 5;
P.V. Chliapnikov, Proc. XVIII Intern. Conf. on High energy physics, Tbilisi (1976) vol. A2-42.
[35] G. Goebel, Phys. Rev. Lett. 1 (1958) 337;
G.F. Chew and F.E. Low, Phys. Rev. 113 (1959) 1640;
V.B. Berestetsky and I.Ya. Pomeranchuk, JETP 39 (1960) 1078;
S.D. Drell, Rev. Mod. Phys. 33 (1961) 458.
[36] E. Ferrari and F. Selleri, Phys. Rev. Lett. 7 (1961) 387;
H.P. Dürr and H. Pilkuhn, Nuovo Cim. 40 (1965) 899;
G. Wolf, Phys. Rev. 182 (1969) 1538.
[37] E.L. Berger, Phys. Rev. Lett. 21 (1968) 701.
[38] K.G. Boreskov et al., Yad. Fiz. 15 (1972) 351;
K.G. Boreskov et al., Yad. Fiz. 15 (1972) 557;
K.G. Boreskov, A.B. Kaidalov and L.A. Ponomarev, Preprints ITEP No. 950 (1972), No. 43 (1973), No. 16 (1974); Yad. Fiz. 17 (1973) 1285; 19 (1974) 1103;
L.A. Ponomarev, Physics of elementary particles and atomic nucleus 7 (1976) 186.
[39] J.W. Dash et al., Phys. Rev. D9 (1974) 1404;
J.W. Dash and S.T. Jones, Argonne Reports ANL/HEP 7371, 7422, 7429 (1974).
[40] S.D. Drell and K. Hiida, Phys. Rev. Lett. 7 (1961) 199;
R.T. Deck, Phys. Rev. Lett. 13 (1964) 169.
[41] A.B. Kaidalov and K.A. Ter-Martirosyan, Nucl. Phys. B75 (1974) 471.
[42] L. Caneschi and A. Pignotti, Phys. Rev. Lett. 22 (1969) 1219.

[43] O.V. Kancheli, JETP Lett. 11 (1970) 267.
[44] P.D. Ting and H.J. Yessian, Phys. Lett. 35B (1971) 321;
C.E. de Tar et al., Phys. Rev. Lett. 26 (1971) 675.
[45] C. Sorenson, Phys. Rev. D6 (1972) 2554.
[46] A.B. Kaidalov, V.A. Khoze, Yu.F. Pirogov and N.L. Ter-Isaakyan, Phys. Lett. 45B (1973) 493.
[47] K.A. Ter-Martirosyan, Sov. Phys. JETP 17 (1963) 233; Nucl. Phys. 68 (1964) 591.
[48] I.A. Verdiev, O.V. Kancheli, S.G. Matinyan, A.M. Popova and K.A. Ter-Martirosyan, Sov. Phys. JETP 19 (1964) 1148.
[49] J. Finkelstein and K. Kajantie, Phys. Lett. 26B (1968) 305; Nuovo Cimento 56A (1968) 658.
[50] D.Z. Freedman, C.E. Jones, F.E. Low and J.R. Young, Phys. Rev. Lett. 26 (1971) 1197.
[51] C. Jen, K. Kang, P. Shen and C.I. Tan, Phys. Rev. Lett. 27 (1971) 458.
[52] K.A. Ter-Martirosyan and Yu.M. Shabelski, Pisma JETP 15 (1972) 164.
[53] R. Shankar, Nucl. Phys. B70 (1974) 168.
[54] Ya.I. Azimov, E.M. Levin, M.G. Ryskin and V.A. Khoze, Yad. Fiz. 21 (1975) 413.
[55] L.A. Ponomarev, Paper No. 33/A1-33, submitted to the XVIII Intern. Conf. on High energy physics, Tbilisi (1976).
[56] J. Pumplin and F. Henyey, Nucl. Phys. B117 (1976) 377.
[57] V.N. Gribov and A.A. Migdal, Sov. J. Nucl. Phys. 8 (1969) 583.
[58] V.N. Gribov, Yad. Fiz. 17 (1973) 603; Proc. of the 8 Winter School on Nuclear and elementary particle physics LIYF 11 (1973) 5.
[59] R.C. Brower and J.H. Weis, Rev. Mod. Phys. 47 (1975) 605;
R.C. Brower, C.E. De Tar and J.H. Weis, Phys. Reports 14C (1974) 257.
[60] I.Ya. Azimov, E.M. Levin, M.G. Ryskin and V.A. Khoze, Nucl. Phys. B89 (1975) 508.
[61] S. Mandelstam, Nuovo Cimento 30 (1963) 1127; 1148.
[62] V.N. Gribov, I.Ya. Pomeranchuk and K.A. Ter-Martirosyan, Phys. Rev. B139 (1965) 184.
[63] V.N. Gribov, Sov. Phys. JETP 26 (1968) 414.
[64] R.C. Arnold, Phys. Rev. 153 (1967) 1523.
[65] G. Cohen-Tannoudji, A. Morel and Ph. Salin, Nuovo Cimento 55A (1968) 412.
[66] F.S. Henyey, G.L. Kane, J. Pumplin and M.H. Ross, Phys. Rev. 182 (1969) 1579.
[67] K.A. Ter-Martorosyan, Yad. Fiz. 10 (1969) 1047.
[68] V.A. Abramovskii, V.N. Gribov and O.V. Kancheli, Sov. J. Nucl. Phys. 18 (1974) 308.
[69] K.G. Boreskov, A.M. Lapidus, S.T. Sukhorukov and K.A. Ter-Martirosyan, Yad. Fiz. 16 (1972) 389.
[70] A.B. Kaidalov, Yad. Fiz. 13 (1971) 401; 16 (1972) 389.
[71] J. Pumplin and G.L. Kane, Phys. Rev. Lett. 32 (1974) 963.
[72] V. Tsarev, Phys. Rev. D11 (1975) 1864; 1875.
[73] E.L. Berger and P. Pirila, Phys. Rev. D12 (1975) 3448.
[74] L.A. Ponomarev, Proc. XVIII Intern. Conf. on High energy physics, Tbilisi (1976) vol. I, A1-24; Preprint ITEP-96 (1977).
[75] H.D.I. Abarbanel, J.B. Bronzan, R.L. Sugar and A.R. White, Phys. Reports 21C (1975) 119.
[76] M. Moshe, Preprint UCSC 77/118.
[77] A.A. Migdal, A.M. Polyakov and K.A. Ter-Martirosyan, Phys. Lett. 48B (1974) 239; JETP 67 (1974) 84.
[78] H.D.I. Abarbanel and J.B. Bronzan, Phys. Lett. 48B (1974) 345; Phys. Rev. D9 (1974) 2397.
[79] J. Bartels and E. Rabinovici, Phys. Rev. D12 (1975) 3938.
[80] H.D.I. Abarbanel, J. Bartels, J.B. Bronzan and D. Sidhy, Phys. Rev. D12 (1975) 2459; 2798.
[81] J.L. Cardy, Nucl. Phys. B75 (1974) 413.
[82] D. Amati and R. Jengo, Phys. Lett. 56B (1975) 465;
D. Amati, L. Caneschi and R. Jengo, Nucl. Phys. B101 (1975) 397;
D. Amati, M. Ciafalloni, M. LeBellac and G. Marchesini, Nucl. Phys. B112 (1976) 107;
D. Amati, G. Marchesini, M. Ciafalloni and G. Parisi, Nucl. Phys. B114 (1976) 483.
[83] A. Czechowski, Nucl. Phys. B113 (1976) 323.
[84] M.S. Dubovikov and K.A. Ter-Martirosyan, Preprint ITEP-37, Moscow (1976);
B.Z. Kopeliovich and L.I. Lapidus, Preprint JINR, E2-9537, Dubna (1976);
M.S. Dubovikov, L.I. Lapidus, B.Z. Kopeliovich and K.A. Ter-Martirosyan, Nucl. Phys. B123 (1977) 147.
[85] M.S. Dubovikov and K.A. Ter-Martirosyan, Nucl. Phys. B124 (1977) 163.
[86] G. Marchesini and E. Rabinovici, Preprint FERMILAB-Pub-76/74-THY (1976).
[87] E.M. Levin and M.G. Ryskin, Yad. Fiz. 25 (1977) 849; Preprint LIYF 370 (1977).
[88] A. Capella and J. Kaplan, Phys. Lett. 52B (1974) 448;
A. Capella, J. Kaplan and J. Tranh Thanh Van, Nucl. Phys. B97 (1975) 493.
[89] A. Capella and A. Kaidalov, Nucl. Phys. B111 (1976) 477.
[90] H. Cheng and T.T.Wu, Phys. Rev. Lett. 24 (1970) 1456;
H. Cheng, J.K. Walker and T.T.Wu, Phys. Lett. 44B (1973) 97.
[91] V.N. Gribov, Proc. 10 Winter School on Nucl. and elementary particles phys. LIYF vol. 1 (1975) 6; Nucl. Phys. B106 (1976) 189.

[92] W. Galbraith et al. Phys. Rev. B138 (1965) 913;
K.J. Foley et al., Phys. Rev. Lett. 19 (1967) 330;
S.P. Denisov et al., Phys. Lett. B36 (1971) 415, 528; Nucl. Phys. 65B (1973) 1;
U. Amaldi et al., Phys. Lett. B44 (1973) 112;
S.R. Amendolia et al., Phys. Lett. B44 (1973) 119;
CERN–Pisa–Rome–Stony Brook Collab., Phys. Lett. 62B (1976) 460;
A.S. Carrol et al., Phys. Lett. 61B (1976) 303.
[93] G.G. Beznogikh et al., Phys. Lett. B30 (1969) 274;
V. Bartenev et al., Phys. Rev. Lett. 31 (1973) 1367;
K.J. Foley et al., Phys. Rev. 181 (1969) 1775;
U. Amaldi et al., Phys. Lett. B43 (1973) 231.
[94] U. Amaldi, Phys. Lett. 66B (1977) 390.
[95] G.G. Beznogikh et al., Yad. Fiz. 10 (1969) 12;
L.F. Kirillova et al., Yad. Fiz. 1 (1965) 533;
U. Amaldi et al., Phys. Lett. B36 (1971) 504;
G. Barbiellini et al., Phys. Lett. B39 (1972) 663.
[96] V. Bartenev et al., Phys. Rev. Lett. 31 (1973) 1088.
[97] Yu. M. Antipov et al., Paper No.40/A1–40 submitted to the XVIII Intern. Conf. on High energy physics, Tbilisi (1976).
[98] J. Dias de Deus, Nucl. Phys. B59 (1973) 231;
A.J. Buras and J. Dias de Deus, Nucl. Phys. B71 (1974) 481.
[99] W. Grein and P. Kroll, Phys. Lett. 58B (1975) 79.
[100] V. Barger, J. Luthe and R.J.N. Phillips, Nucl. Phys. B88 (1975) 237.
[101] V. Barger and R.J.N. Phillips, Phys. Lett. 60B (1976) 358.
[102] P.D. Collins et al., Phys. Lett. 47B (1973) 171; Nucl. Phys. B80 (1974) 135; B83 (1974) 241.
[103] A.M. Lapidus, V.I. Lisin, K.A. Ter-Martirosyan and P.E. Volkovitsky, Preprint ITEP-115 (1976).
[104] J. Biel et al., Phys. Rev. Lett. 36 (1976) 504, 507; Phys. Lett. 65B (1976) 291 and papers No. 909/A1-8, 69/A1–69 submitted to the XVIII Intern. Conf. on High energy physics, Tbilisi (1976).
[105] T. Ferbel, Preprint UR–587, COO–3065–152 (1976).
[106] D. Denegri et al., Nucl. Phys. B114 (1976) 413;
T. Pons et al., Nucl. Phys. B123 (1977) 349.
[107] M. Cavalli-Sforza et al., Nuovo Cim. Letters 14 (1975) 345, 353, 359;
G. Goggi et al., Phys. Lett. 72B (1977) 261.
[108] G. Ascoli et al., Phys. Rev. Lett. 25 (1971) 962; 26 (1971) 929; Phys. Rev. D7 (1973) 669; D8 (1973) 3894; D9 (1974) 1963;
Yu. M. Antipov et al., Nucl. Phys. B63 (1973) 141, 153;
M. Deutschmann et al., Phys. Lett. 49B (1974) 388;
G. Otter et al., Nucl. Phys. B96 (1975) 365; B106 (1976) 77.
[109] W. Ochs et al., Nucl. Phys. B86 (1975) 253;
Aachen–Berlin–Bonn–CERN Collab. Paper No. 52/A1-52, submitted to the Intern. Conf. on High energy physics, Tbilisi (1976).
[110] G.W. Brandenburg et al., Phys. Rev. Lett. 36 (1976) 703, 706, 1239;
R.K. Carnegie et al., Phys. Lett. B63 (1976) 235.
[111] D.R.O. Morrison, Phys. Rev. 165 (1968) 1699.
[112] H. de Kerret et al., Phys. Lett. B55 (1975) 331; Phys. Lett. B63 (1976) 477, 483.
[113] J. Ballam et al., Paper submitted to the Intern. Conf. on High energy physics, Tbilisi (1976).
[114] F. Hayot, A. Morel, A. Santoro and M. Souza, Nuovo Cim. Lett. 18 (1977) 185.
[115] G. Cohen-Tannoudji, A. Santoro and M. Souza, Nucl. Phys. B125 (1977) 445.
[116] A.I. Babaev et al. Nucl. Phys. B116 (1976) 28;
Yu. Kamushkov, Proc. of the XVIII Intern. Conf. on High energy physics, Tbilisi (1976) vol I, A1–7.
[117] R. Webb et al., Phys. Lett. 55B (1975) 331, 336.
[118] G.C. Mantovani et al., Phys. Lett. B64 (1976) 471.
[119] G.C. Mantovani et al., Phys. Lett. B65 (1976) 401.
[120] E.W. Anderson et al., Phys. Rev. Lett. 16 (1966) 855;
R.M. Edelstein et al., Phys. Rev. D5 (1972) 1073.
[121] M.G. Albrow et al., Nucl. Phys. B51 (1973) 388; B54 (1973) 6; B72 (1974) 376; B108 (1976) 1.
[122] S.J. Barish et al., Phys. Rev. Lett. 31 (1973) 1080; Phys. Rev. D9 (1974) 1171, 2689.
[123] J.M. Chapmen et al., Phys. Rev. Lett. 32 (1974) 257.
[124] Yu. Akimov et al., Phys. Rev. Lett. 35 (1975) 763, 866;
Yu. Akimov et al., Phys. Rev. D14, (1976) 3148;
S.V. Mukhin, Proc. XVIII Intern. Conf. on High energy physics, Tbilisi (1976) vol. I, A1–3;
Yu. Akimov et al., Phys. Rev. Lett. 39 (1977) 1432.

[125] H. Bialkowska et al., Nucl. Phys. B116 (1976) 77;
V.V. Ammosov et al., Nuovo Cimento 40A (1977) 237.
[126] F.T. Dao et al., Phys. Lett. 45B (1973) 399, 402.
[127] S. Childress et al., Phys. Rev. Lett. 32 (1974) 389;
R.D. Schamberger et al., Phys. Rev. Lett. 34 (1975) 1121.
[128] S.P. Childress et al., Phys. Lett. 65B (1976) 177.
[129] F. Sannes et al., Phys. Rev. Lett. 30 (1973) 766; 31 (1973) 1527, 1530.
[130] F.C. Winkelman et al., Phys. Rev. Lett. 32 (1974) 121; Phys. Lett. 48B (1974) 273.
[131] D.S. Ayres et al., Phys. Rev. Lett. 37 (1976) 1724.
[132] R.L. Anderson et al., Phys. Rev. Lett. 38 (1977) 880.
[133] V.D. Apokin et al., Preprints IHEP OEF77-34, OEF77-118.
[134] L. Baksay et al., Phys. Lett. 53B (1975) 484; 55B (1975) 491.
[135] W. Lockman et al., Paper No. 1210/A1-163, submitted to the XVII Intern. Conf. on High energy physics, Tbilisi (1976).
[136] A.B. Kaidalov et al., Pisma v JETP 17 (1973) 626.
[137] A. Capella, Phys. Rev. D8 (1973) 2047.
[138] R.D. Field and G.C. Fox, Nucl. Phys. B80 (1974) 367.
[139] D.P. Roy and R.G. Roberts, Nucl. Phys. B77 (1974) 240.
[140] Yu. M. Kazarinov et al., JETP 70 (1976) 1152.
[141] T. Inami and R.G. Roberts, Preprint RL-75-025.
[142] M. Bishari, Phys. Lett. 38B (1972) 510.
[143] A. Capella, J. Kaplan and J. Tran Thanh Van, Nucl. Phys. B105 (1976) 333;
V.A. Abramovskii, Pisma JETP 23 (1976) 228.
[144] A.B. Kaidalov and V.A. Khoze, Proc. Intern. Seminar on Deep Inelastic and Many-Body Processes at High Engeries, June 1973, Dubna, p. 450, Preprint LIYF No. 652 (1973).
[145] A.B. Kaidalov and V.A. Khoze, Preprint LIYE No. 193 (1975).
[146] J. Whitmore and M. Derrick, Phys. Lett. 50B (1974) 280.
[147] M.G. Albrow et al., Nucl. Phys. B102 (1976) 275.
[148] D.M. Chew and G.F. Chew, Phys. Lett. 53B (1974) 191.
[149] A.B. Kaidalov, Theoretical Introduction to Double Pomeron Exchange, in: Summary of the 18-th ISR Discussion Meeting between Experimentalists and Theorists, CERN/TH (1976).
[150] R.G. Roberts, Preprint RL-75-164.
[151] M. Derrick et al., Phys. Rev. Lett. 32 (1974) 80.
[152] B. Musgrave, ANL-HEP-CP-75-31.
[153] D. Denegri et al., Nucl. Phys. B98 (1975) 189.
[154] L. Baksay et al., Phys. Lett. 61B (1976) 89.
[155] H. de Kerret et al., Phys. Lett. 68B (1977) 385.
[156] M. Della Negra et al., Phys. Lett. 65B (1976) 394.
[157] D.M. Chew, Phys. Lett. 65B (1976) 367.